Dynamic Characteristics of Multi-Bladed S-Shaped Vane Type Rotor

by

Zakia Afroz

A thesis
Submitted to the Department of Mechanical Engineering in partial fulfillment of the requirements for the degree
of

MASTER OF SCIENCE
IN MECHANICAL ENGINEERING

DEPARTMENT OF MECHANICAL ENGINEERING
BANGLADESH UNIVERSITY OF ENGINEERING AND TECHNOLOGY
DHAKA-1000, BANGLADESH
March 2011

RECOMMENDATION OF THE BOARD OF EXAMINERS

The board of Examiners hereby recommends to the Department of Mechanical Engineering, Bangladesh University of Engineering and Technology, Dhaka, the acceptance of the thesis titled "Dynamic Characteristics of Multi-Bladed S-Shaped Rotor", submitted by Zakia Afroz, Roll No: 100710022F, Session: October 2007, in partial fulfillment of the requirements for the degree of Master of Science in Mechanical Engineering on March 22, 2011.

1. _____

Dr. Md. Quamrul Islam (Supervisor) Chairman
Professor
Department of Mechanical Engineering
BUET, Dhaka – 1000

2. _____

Dr. M. Mahbubul Alam (Ex-Officio) Member
Professor & Head
Department of Mechanical Engineering
BUET, Dhaka – 1000

3. _____

Dr. Mohammad Ali Member
Professor
Department of Mechanical Engineering
BUET, Dhaka – 1000

4. _____

Dr. Mohammad Mamun Member
Associate Professor
Department of Mechanical Engineering
BUET, Dhaka – 1000

5. _____

Dr. A.K.M. Sadrul Islam Member
Professor (External)
MCE Department, IUT

ABSTRACT

The present research work concerns with the dynamic conditions of Multi-bladed rotor at different Reynolds number. The investigation on wind loading and aerodynamic effects on the four, five and six bladed S-shaped vertical axis vane type rotor have been conducted with the help of a subsonic wind tunnel together with the experiment set-up of the vane type rotor and a spring balance. The experiment was carried out in the open circuit subsonic wind tunnel by placing the rotor at its exit section. For different bladed rotor the flow velocities were varied from 5m/s to 9m/s covering the Reynolds numbers up to 1.35×10^5.

For the purpose of analyzing the dynamic conditions of rotor, the rpm of multi-bladed rotor at different loading conditions and the difference in tensions between two ends of the friction belt for different Reynolds number were measured. Finally from these data, the changes in Tip Speed Ratio, Power co-efficient and Torque coefficient with the increase in load in the load carrying plate were determined at different Reynolds number of multi-bladed rotor.

The nature of predicted dynamic aerodynamic characteristics has been analyzed by comparing them with existing research works. For comparison power coefficient versus tip speed ratio of the present measurement and previous researcher's works has been plotted on the same graph. It is seen that there is a close correlation between the values predicted by the present method and those obtained from the existing research works and the nature of all compared curves are similar to previous measurements.

CERTIFICATE OF RESEARCH

This is to certify that the work presented in this thesis is an outcome of the investigation carried out by the author under the supervision of Dr. Md. Quamrul Islam, Professor, Department of Mechanical Engineering, Bangladesh University of Engineering and Technology (BUET), Dhaka.

Dr. Md. Quamrul Islam	Zakia Afroz
Supervisor	Author

ACKNOWLEDGEMENT

I wish to express my sincerest gratitude and indebtedness to Dr. Md. Quamrul Islam for his guidance and supervision throughout the entire period of the experimental investigation. His encouragement and invaluable suggestions are gratefully acknowledged.

I am also grateful to Professor Dr. M. Mahbubul Alam, Head of the Department of Mechanical Engineering for his encouragement in completing this work in time.

Sincere thanks are offered to Superintendent and Chief Instructors and Technicians of Machine Shop, Carpentry Shop, BUET for their co-operation in fabricating and assembling different parts and components of the experimental set-up. Thanks are also due to Lab Instructors and Technicians of SM Laboratory of Mechanical Engineering Department for their co-operation at different stages of the work.

Lastly, I would like to thank my father, mother, younger brother and husband for their inspiration to complete this work in proper time.

CONTENTS

Chapter-3

THEORIES OF WIND TURBINE

Chapter-4

DESIGN AND FABRICATION

Chapter-5

EXPERIMENTAL SETUP AND PROCEDURE

Chapter-6

RESULTS AND DISCUSSIONS

Chapter-7

CONCLUSIONS AND RECOMMENDATIONS

LIST OF FIGURES

LIST OF TABLES

Page

LIST OF SYMBOLS

C_P	Power Coefficient, $C_p = \frac{P_t}{\frac{1}{2}\rho V^3 A}$
P_t	Power developed by the turbine
A	Rotor cross-sectional area, HD
D	Diameter of the rotor
H	Height of the rotor
V	Free stream wind speed
C_Q	Torque Coefficient, $C_T = \frac{T_t}{\frac{1}{2}\rho V^2 AR}$
T_t	Actual torque the shaft can develop
R	Radius of the turbine rotor
d	Diameter of the blade
F_L	Lift force acting on a blade
F_D	Drag force acting on a blade
F_N	Normal force acting on a blade
F_T	Tangential force acting on a blade
V_{rel}	Relative velocity
R	Reynolds number, VD/ν

Greek Symbols:

ρ	Air density
λ	Tip speed ratio, $D\omega/2V$
ω	Angular speed of the rotor
ν	Kinematics viscosity of air
δ	Blade solidity

1. CONVERGING MOUTH ENTRY
2. PERSPEX SECTION
3. RECTANGULAR DIVERGING SECTION
4. FAN SECTION
5. BUTTERFLY SECTION
6. SILENCER WITH HONEYCOMB SECTION
7. DIVERGING SECTION
8. CONVERGING SECTION
9. RECTANGULAR SECTION
10. FLOW STRAIGHTNER SECTION
11. RECTANGULAR EXIT SECTION

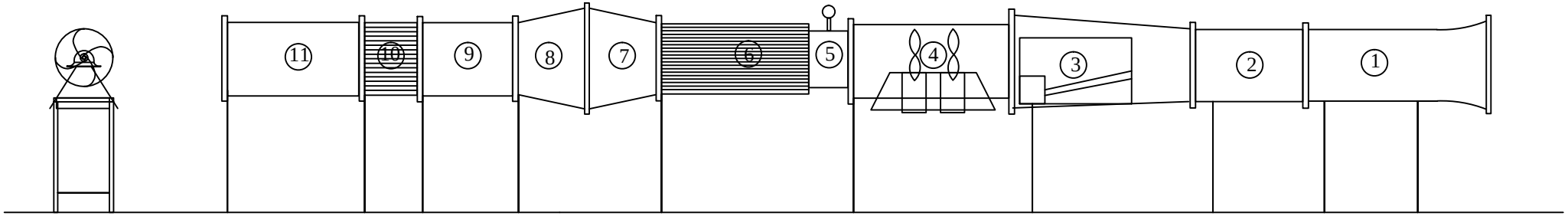

Figure 5.2.1: Schematic diagram of wind tunnel

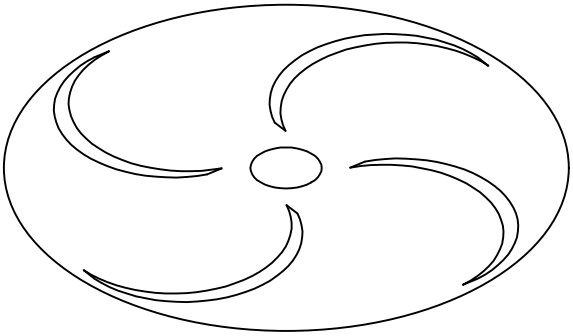

Section A-A

Figure 5.4.2 (a): Cross Sectional View of Four Bladed S-shaped Vane Type Rotor

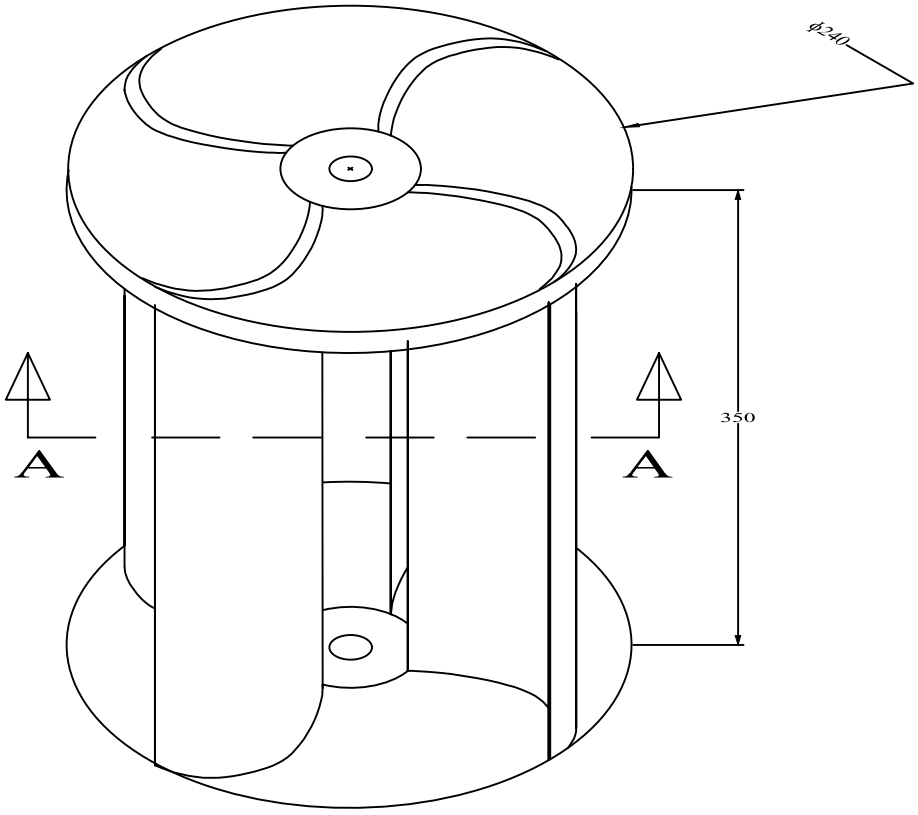

Figure 5.4.2 (b): Three Dimensional View of Four Bladed S-shaped Vane Type Rotor

All dimensions are in mm

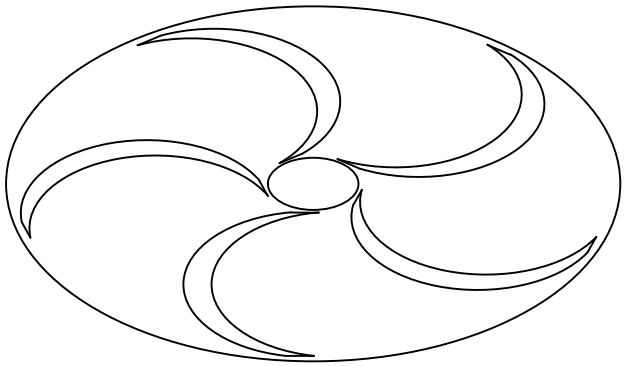

Figure 5.4.3 (a): Cross Sectional View of Five Bladed Vertical Axis Vane Type Rotor

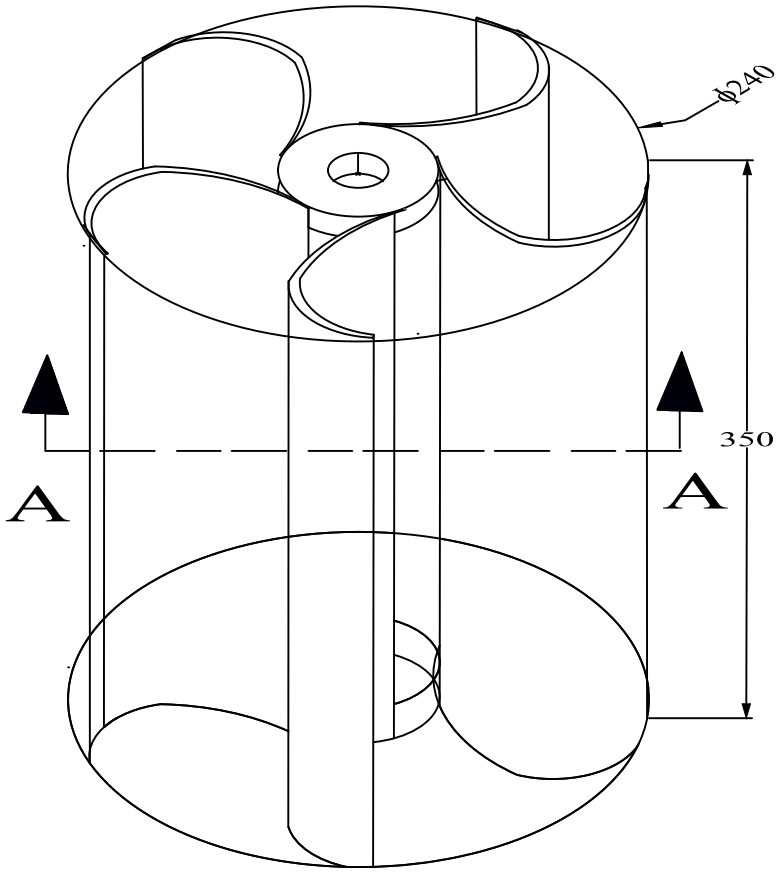

Figure 5.4.3 (b): Three Dimensional View of Five Bladed Vertical Axis Vane Type Rotor

All dimensions are in mm

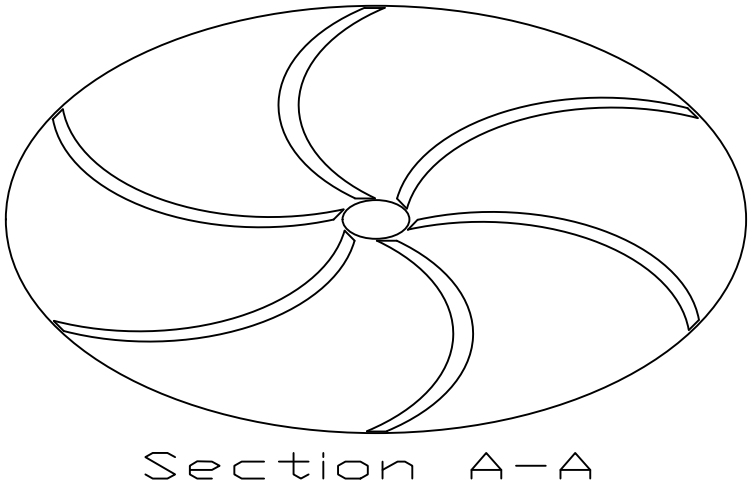

Figure 5.4.4 (a):Cross Sectional View of Six Bladed Vertical Axis Vane Type Rotor

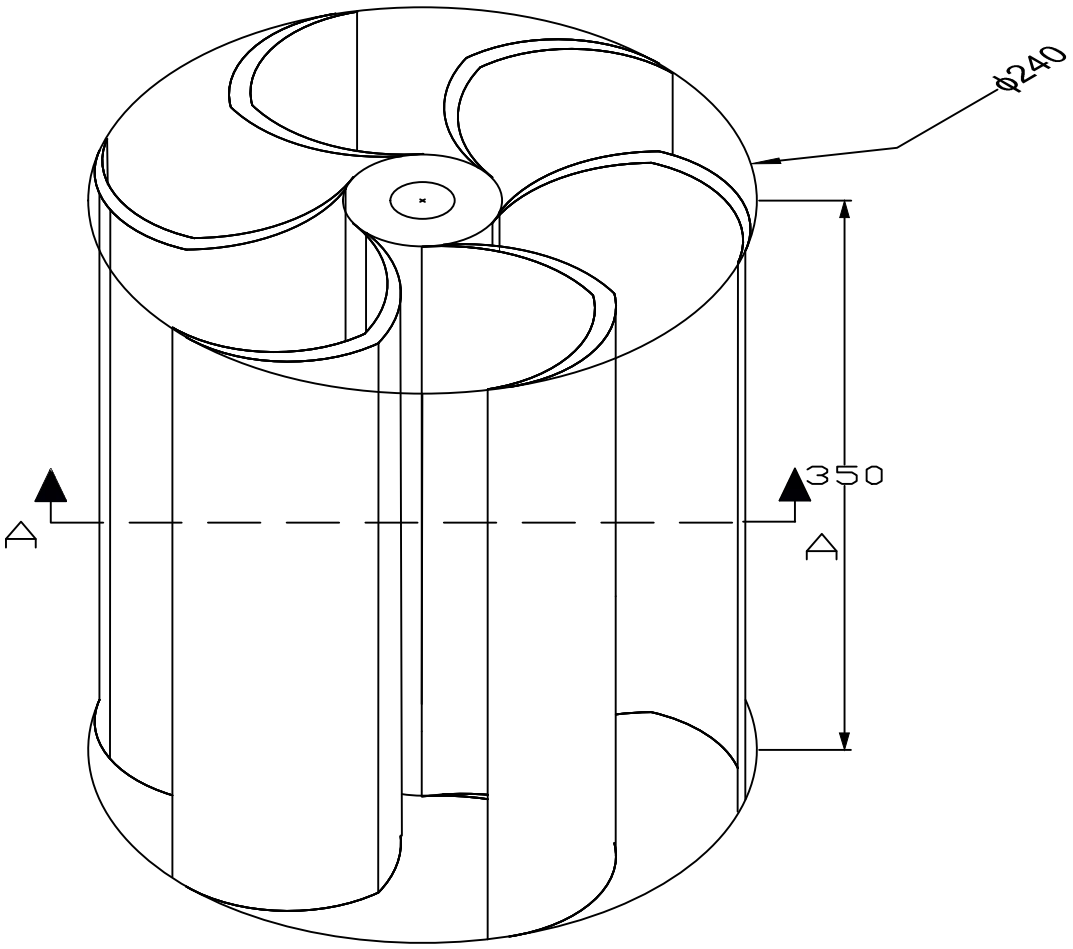

Figure 5.4.4 (b): Three Dimensional View of Six Bladed Vertical Axis Vane Type Rotor

All dimensions are in mm

Chapter-1

INTRODUCTION

1.1 General

Energy is the prime mover of modern civilization. Due to rapid development, the need of energy is increasing day by day. As a result, all non-renewable energy is diminishing in an alarming way. With the increasing prices of fuel, depletion of commercial energy sources, frequent failures in power supply and pollution, attention is being drawn on utilizing renewable sources of energy. Wind energy, as an environment friendly renewable energy, holds good prospect. The European Wind Energy Association (EWEA) estimates that between 20 GW and 40 GW of offshore wind energy capacity will be operating in the European Union by 2020. A fully developed European offshore wind resource could deliver a capacity of several hundred GW to supply our future energy demands. According to World Wind Energy Association (WWEA), 73,904 MW capacity wind turbine has been installed worldwide, in which Europe and US have installed 62,991 MW, Asia have 8,675 MW and other 2,238 MW. According to projection by World Wind Energy Association (WWEA), wind turbine installation in the world through the end of 2010 will be 160 GW. Over the years people are extracting wind energy in various ways. One of the means for converting the wind energy to a more useful form is through the use of windmills.

Humans have been using wind power for at least 5,500 years to propel sailboats and sailing ships, and architects have used wind-driven natural ventilation in buildings since similarly ancient times. Windmills have been used for irrigation pumping and for milling grain since the 7th century AD.

There are various types of windmills. The most common one having the blades of airfoil shape is the horizontal axis turbine. Another type is the vertical-axis wind turbine. The primary attraction of the vertical-axis wind turbine is the simplicity of its manufacture compared to that of horizontal axis wind turbine. Among the different vertical axis wind turbines, the vertical axis vane type wind turbine is a slow running wind machine and has a relatively lower efficiency. Still it is being used in the developing countries because of its simple design, easy and cheap technology for construction and having a good starting torque at low wind speeds [3,11,14]. Rigorous studies on the performance characteristics of the horizontal axis wind rotor are found in the literature and these enable the identification of an optimum geometrical configuration for practical design [9,12,18].

1.2 Source of Wind Energy

Wind energy is an indirect form of solar energy. The sun radiates 1014 kJ/sec of energy to the earth. Sufficient amount of energy is continuously transferred from the sun to the air of earth. Some of the sun's energy is absorbed directly by air. Most of the energy of the sun is first absorbed by the surface of the earth and then transferred to air by convection. Between 1-2% of the solar radiation that reaches the earth is converted into wind energy. Global wind pattern depends mainly on the earth's rotation around its own axis, ocean current and cosmic gravitational pulls. However, the prime cause of local wind is different. The Earth is unevenly heated by the sun, such that the poles receive less energy from the sun than the equator; along with this, dry land heats up (and cools down) more quickly than the seas do. Cold air over the sea then replaces the rising air. The diagram below shows how this 'system' works. The differential heating drives a global atmospheric convection system reaching from the Earth's surface to the stratosphere which acts as a virtual ceiling. Most of the energy stored in these wind movements can be found at high altitudes where continuous wind speeds of over 160 km/h (99 mph) occur. Eventually, the wind energy is converted through friction into diffuse heat throughout the Earth's surface and the atmosphere.

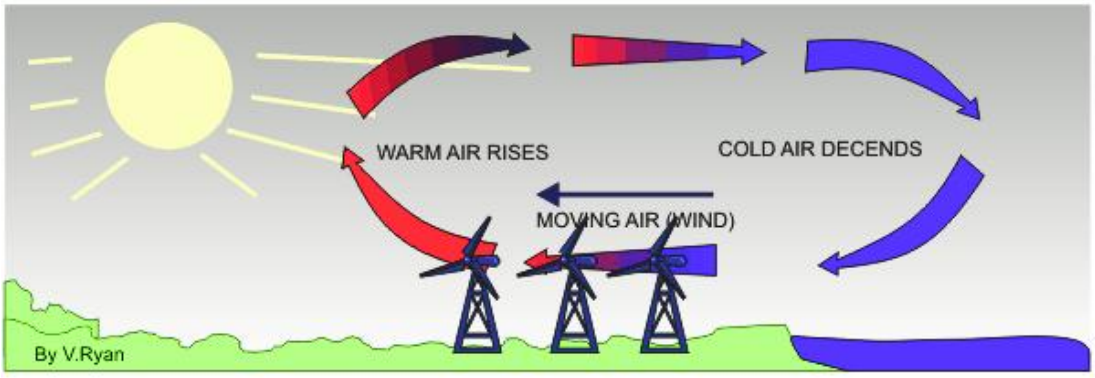

Figure 1.2.1: How wind turbine works

1.3 Nature of Wind Energy

Wind energy is the kinetic energy that is present in moving air; this kinetic energy in turn derives from the heating of the atmosphere, earth and oceans by the sun. The amount of energy in the wind depends mainly on wind speed, but is also affected slightly by the density of the air, which is determined by the air temperature, barometric pressure and altitude.

For any wind turbine, the power and energy output increases dramatically as the wind speed increases. Therefore, the most cost-effective wind turbines are located in the windiest areas. Wind speed is affected by the local terrain and increases with height above the ground, so wind turbines are usually mounted on tall towers.

1.4 Wind as a Source of Energy

From a long time people have been extracting energy mainly from the fossil fuel in almost all the countries. In some of the countries, they are also utilizing uranium fuel, which is a source of nuclear energy. With the rising demand of energy and for many other reasons, prices of these fuels are increasing day by day. So the scientists and engineers are trying to find the alternative sources of energy to exploit them at the cheap rate. Wind energy is a kind of energy source that will never be diminished. It is available almost all the times, at all places and in large quantities all over the world. The total amount of economically extractable power available from the wind is considerably more than present human power use from all sources. An estimated 72 terawatt (TW) of wind power on the Earth potentially can be commercially viable, compared to about 15 TW average global power consumption from all sources in 2005.

Fossil and uranium fuel will be completely depleted someday. Moreover, these are not available in all countries. Besides these, every nation is interested to be self-dependent; they do not like to rely on imported fuel that requires huge amount of foreign currency. As a result in different parts of the world, scientists are taking keen interest to develop efficient and economic devices to collect energy from the wind. Recently, the utilization of wind power is increasing in many developed as well as under developed countries.

Wind and hydroelectric power generation have negligible fuel costs and relatively low maintenance costs. Its marginal cost is also very low.

1.5 Costs of Wind Energy

The cost of wind energy is determined by:

- the initial cost for installation of wind turbine
- the interest rate on the money invested
- the maintenance cost of wind turbine
- the amount of output energy per unit time

The cost of wind energy depends mainly on site where wind turbine has been installed. So, it’s very important to assess the wind at the potential site.

Modern wind turbine generators cost about $1500 per kilowatt for wind farms that use multiple-unit arrays of large machines. Smaller individual units cost up to $3000 per kilowatt. In proper wind areas, the costs of generating electricity lie between five to ten cents per kilowatt hour. That cost is somewhat higher than the costs associated with an electrical facility, but wind energy cost is decreasing every year, whereas most conventional energy costs are increasing day by day.

In remote areas where generating electricity by diesel generator can cost more than $ 0.25 per kilowatt hour, there generating electricity by wind energy can be cost effective and also competitive.

1.6 Environmental effect

Compared to the environmental effects of traditional energy sources, the environmental effects of wind power are relatively minor. Wind power consumes no fuel, and emits no air pollution, unlike fossil fuel power sources. The energy consumed to manufacture and transport the materials used to build a wind power plant is equal to the new energy produced by the plant within a few months of operation. Garrett Gross, a scientist from UMKC in Kansas City, Missouri states, "The impact made on the environment is very little when compared to what is gained." The initial carbon dioxide emission from energy used in the installation is "paid back" within about 9 months of operation for offshore turbines. Each megawatt-hour of electricity generated by wind energy helps to reduce 0.8 to 0.9 tones of greenhouse gas emissions as compared to electricity generation by coal or diesel fuel.

1.7 Global Wind Energy Utilization Scenario

Wind energy "penetration" refers to the fraction of energy produced by wind compared with the total available generation capacity. At present, a few grid systems have penetration of wind energy above 5%: Denmark (values over 19%), Spain and Portugal (values over 11%), Germany and the Republic of Ireland (values over 6%). For instance, in the morning hours of 8 November 2009, wind energy produced covered more than half the electricity demand in Spain, setting a new record, and without problems for the network.

The Danish grid is heavily interconnected to the European electrical grid, and it has solved grid management problems by exporting almost half of its wind power to Norway. The correlation between electricity export and wind power production is very strong.

There are now many thousands of wind turbines operating, with a total capacity of 157,899 MW of which wind power in Europe accounts for 48% (2009). World wind generation capacity more than quadrupled between 2000 and 2006, doubling about every three years. 81% of wind power installations are in the US and Europe. The share of the top five countries in terms of new installations fell from 71% in 2004 to 62% in 2006, but climbed to 73% by 2008 as those countries—the United States, Germany, Spain, China, and India—have seen substantial capacity growth in the past two years.

By 2010, the World Wind Energy Association expects 160 GW of capacity to be installed worldwide, up from 73.9 GW at the end of 2006, implying an anticipated net growth rate of more than 21% per year.

Denmark generates nearly one-fifth of its electricity with wind turbines—the highest percentage of any country—and is ninth in the world in total wind power generation. Denmark is prominent in the manufacturing and use of wind turbines, with a commitment made in the 1970s to eventually produce half of the country's power by wind.

In recent years, the US has added more wind energy to its grid than any other country, with a growth in power capacity of 45% to 16.8 GW in 2007. Wind power generation in the U.S. was up 31.8% in February, 2007 from February, 2006. The average output of one MW of wind power is equivalent to the average electricity consumption of about 250 American households. According to the American Wind Energy Association, wind will generate enough electricity in 2008 to power just over 1% (equivalent to 4.5 million households) of total electricity in U.S., up from less than 0.1% in 1999.

China had originally set a generating target of 30,000 MW by 2020 from renewable energy sources, but reached 22,500 MW by end of 2009 and could easily surpass 30,000 MW by end of 2010. Indigenous wind power could generate up to 253,000 MW. By 2008, wind power was growing faster in China than the government had planned, and indeed faster in percentage terms than in any other large country, having more than doubled each year since 2005. Policymakers doubled their wind power prediction for 2010, after the wind industry reached the original goal of 5 GW three years ahead of schedule. Current trends suggest an actual installed capacity near 20 GW by 2010, with China shortly thereafter pursuing the United States for the world wind power lead.

India ranks 5th in the world with a total wind power capacity of 9,587 MW in 2008, or 3% of all electricity produced in India.

Mexico recently opened La Vento II wind power project as an important step in reducing Mexico's consumption of fossil fuels. The 88 MW project is the first of its kind in

Mexico, and will provide 13 percent of the electricity needs of the state of Oaxaca. By 2012 the project will have a capacity of 3500 MW.

Another growing market is Brazil, with a wind potential of 143 GW. The federal government has created an incentive program, called Proinfa, to build production capacity of 3300 MW of renewable energy for 2008, of which 1422 MW through wind energy. The program seeks to produce 10% of Brazilian electricity through renewable sources.

South Africa has a proposed station situated on the West Coast north of the Olifants River mouth near the town of Koekenaap, east of Vredendal in the Western Cape Province. The station is proposed to have a total output of 100 MW although there are negotiations to double this capacity. The plant could be operational by 2010.

France has announced a target of 12,500 MW installed by 2010, though their installation trends over the past few years suggest they'll fall well short of their goal.

Canada experienced rapid growth of wind capacity between 2000 and 2006, with total installed capacity increasing from 137 MW to 1,451 MW, and showing an annual growth rate of 38%. Particularly rapid growth was seen in 2006, with total capacity doubling from the 684 MW at end-2005. By 2025, Canada will reach its capacity of 55,000 MW of wind energy, or 20% of the country's energy needs.

1.8 Prospects of Wind Energy in Bangladesh

Wind can be a vital source of energy if properly utilized and exploited. But before high-end projects are implemented, adequate research should be done to study the feasibility and determine a suitable type of project to implement. The primary parameter needed is wind speed and direction. Bangladesh is situated between 20.30 – 26.38 degrees North latitude and 88.04 – 92.44 degrees East.

In Bangladesh, some early studies on wind energy prospects were made by Professor Muhtasham Hussain of Dhaka University and his colleagues [Hussain et. al 1986], as well as some enthusiasts from Bangladesh University of Engineering and Technologies (BUET). The Bangladesh Meteorological department has wind speed measuring stations in towns and cities. Data from earlier measurements and analysis of upper air data by CWET India show that wind energy resource of Bangladesh is not good enough (>7 m/s) for grid connected wind parks [GEF 2001].

Over the past years, many organizations have made many attempts to collect data on wind resources in Bangladesh. Wind speed has been measured in Patenga, Cox's Bazar, Kuakata, Moheshkhali, and Noakhali by the computerized anemometers. The wind computers have been installed at 20 meters height. According to this study annual average wind speeds in the coastal regions of Bangladesh are greater than 6.5 m/s at the height of 20 meters. It has been observed that during day times (8 a.m. to 7 p.m.) wind speeds are about 30 to 40% higher than the average values. The value of the power exponent α has been determined in the above sites and it is 0,139. So, at 40 meters height the annual average wind speed is about 7.15 m/s. So, wind speeds in the coastal regions of Bangladesh are suitable for both water pumping and electricity generation.

Based on this collected data, many small wind energy projects have been undertaken. At present, several wind resource assessment program (WERM, SWERA, WRAP OF BPDB) is ongoing in the country.

The first-ever generation of electricity from wind at the 0.9 Mw (900 kilowatt) plant near the Muhuri Dam in Sonagazi upazila under Feni district has ushered in new hopes for generation of power with minimum cost in the country, report BSS. The power plant having separate wind turbines of 225 kw each, established at a cost of Tk 90 million including Tk 19.3 million for feasibility study, is now ready to generate electricity from wind and supply to the Muhuri Irrigation Project and the national grid.

1.9 Aim of the Present Work

Due to the simplicity of S-shaped vane type rotor in design and also for its low cost, further studies are required for the efficient use of S-shaped vane type rotor. In the present analysis, detailed investigation on four/ five/ six bladed S-shaped vane type rotors will be carried out in the subsonic wind tunnel. The present research work consists of determining dynamic power co-efficient, dynamic torque co-efficient etc. at different tip speed ratios of four, five and six bladed vane type rotor. Finally a comparison may be made between the results of the present rotor with other existing experimental and theoretical works for predicting the performance of four, five and six bladed vane type rotor.

1.10 Objectives with Specific Aims and Possible Outcome:

The objectives of the present study are as follows:

a) To determine the dynamic characteristics (i.e. tip speed ratios, power coefficient, torque coefficient etc. at different Tip speed ratios) of multi bladed S-shaped vane type rotor at different loading conditions.

b) To study the effect of number of blades of S-shaped vane type rotor.

c) To study the effect of change of Reynolds number on its dynamic characteristics.

d) To analyze the present research works by comparing them with other existing experimental and theoretical research works.

1.11 Scope of the thesis

The study covers only the experimental investigation of multi bladed Savonius rotor.

The prime objective of the investigation is to observe the effects of multi bladed S-Shaped Savonius rotors in place of Semi-cylindrical bladed rotors on the dynamic characteristics of a vertical axis wind turbine.

The present research programme covers only the experimental investigation of the r.p.m. of the rotor at its dynamic condition at different loading condition for different free stream velocity ranging from 5m/s to 9m/s. The several phases of the entire investigation are described in this thesis.

Chapter 2 provides a brief description of findings of several researches in the field of wind energy with special emphasis to rotor design and its performance depending on its type. Notable contributions were made by R.J. Templin [1], R.E. Wilson, P.B.S. Lissaman [2], J. Park [3], J.H. Strickland [4], R.D. Littler [5], N.V.C. Swamy, A.A. Fritzsche [6], J.B. Fanucci, R.E. Watters [7], O. Holme [8], W.A.M. Jansen, P.T. Smulders [9], R.E. Sheldahi, B.F. Blackwell and L.V. Feltz [10], H.G. Bos, E.H. Cordes [11], H.J.M. Beurskens [12, 14], R.B. Noll, N.D. Ham [15], J.P. Baird and S.F. Pender [16], G. Bergeles and N. Athanassiadis [17], E.H. Lysen [18,11], I. Paraschivoiu [19, 22], F. Delclaux [19], S. Sivasegaram and S. Sivapalan [20], G.J. Bowden, S.A. McAleese [21], P. Fraunic, C. Beguier [22], A.C. Mandal [23, 29], T. Sawada, M. Nakamura, S. Kamada [24], T. Ogawa and H. Yoshida [25], T.K. Aldos, K.M. Obeidat [26], J. Gavalda, J. Massons, F. Diaz [27], M.D. Huda, M.A. Selim [28], A.K.M.S. Islam [28, 29, 30],

M.Q. Islam [28,29, 30, 44, 49], M.M. Razzaque, [29, 30], R. Ashraf [30], J.D. Burton, M. Hijazin, S. Rizvi [31], N. Fujisawa [32], F. Rasmussen, J.T. Petersen, P. Volund, P. Leconte, E. Szechenyi, C. Westergaard [33], D.A. Spera [34], M.R. Patel [35], M. Rahman [36], I. Ammara, L. Leclerc, C. Masson [37], H.K. Bhuiyan [38], A. Iida, A. Mizuno, K. Fukudome [39], S. Hyosung, L. Soogab [40], P. Cooper, O. Kennedy [41], S.H. Song, B.C. Jeong, H.I. Lee, G. Venkataramanan [42], M.J. Rajkumar [43], M.N. Hasan, S. Saha [44], T. Maeda, H. Kawabuchi [45], R. Gupta, A. Biswas, K.K. Sharma [46], U.K. Saha [47,43], D. Maity [47], J.O. Ajedegba [48], F.M. Kamal [49].

Chapter 3 deals with details description of the aerodynamics theory and blade element momentum theory together with the performance characteristics of vertical axis wind turbine. Rotor performance parameters are also examined in this chapter.

Chapter 4 presents detailed description of design and fabrication of vertical axis wind turbine. Specific application of S-shaped multi-bladed vane type rotor of vertical axis wind turbine, choice of rotor blade material and selection of blade design parameters have been presented in this chapter.

In Chapter 5 mainly an account of the experimental arrangement and procedure adopted for the investigation are presented. It includes the description of the wind tunnel, the constructional details of the test section and the four, five and six bladed S-shaped Vane type rotor that are used for the study. This chapter includes the experimental procedure of the research work.

Chapter 6 presents the analysis concerning the results and discussions of the present experimental results, which are presented in graphical form. The nature of torque and power co-efficients at different Reynolds number of different bladed rotors is analyzed in this chapter. In few cases the existing experimental results of different researchers are correlated with the present one.

Finally, the conclusions, which are drawn from the present investigation, are given in Chapter 7. This chapter also includes an outline regarding further research in this field.

Chapter-2

REVIEW OF LITERATURE

2.1 Introduction

The utilization of wind energy is not a new technology but draws on the rediscovery of a long tradition of wind power technology. However, expected developments have not been achieved in wind driven machines to cope with the characteristics of wind turbines. Conventional machines are being used now a day even though they are not always suitable from the operational point of view. Arising from the increasing practical importance of wind turbine aerodynamics, there have been, over the past few decades, enormous increases in research works concerning laboratory simulations, full-scale measurements and more recently, numerical calculations and theoretical predictions of flows over a wide variety of vane type wind turbine. Researchers in different countries have been contributing greatly to the knowledge of analytical prediction methods of wind turbines, but the major part of the reported works have been of fundamental nature involving the flow over horizontal axis wind turbine and vertical axis Darrieus rotor. Most of the researchers have conducted research works on either two/ three semi cylindrical bladed savonius rotor or S-shaped rotor with various flow parameters. A brief of some of the papers related to the present work is given in this chapter. A historical background of wind power starting from the ancient time to modern age is also presented in this chapter.

2.2 Historical Background

The history of wind power shows a general evolution from the use of simple, light devices driven by aerodynamic drag forces; to heavy, material-intensive drag devices; to the increased use of light, material-efficient aerodynamic lift devices in the modern era. However aerodynamic lift (the force that makes airplanes fly) is not a modern concept as it was known to the ancients. The earliest known use of wind power is the sail boat, and this technology had an important impact on the later development of sail-type windmills. Ancient sailors understood lift and used it every day, even though they didn't have the physics to explain how or why it worked.

The first windmills were developed to automate the tasks of grain-grinding and water-pumping and the earliest-known design is the vertical axis system developed in Persia about 500-900 A.D. The first use was apparently water pumping, but the exact method of water transport is not known because no drawings or designs -- only verbal accounts -- are available. The first known documented design is also of a Persian windmill, this one

with vertical sails made of bundles of reeds or wood which were attached to the central vertical shaft by horizontal struts (Figure 2.2.1).

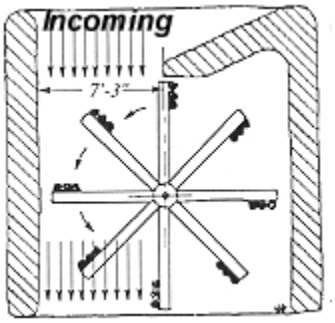

Figure 2.2.1: Perison Windmill of vertical axis type

In this Persian panemone design, the rotor can only harvest half of the wind striking the collection area. The panemone is one of the least efficient, but most commonly reinvented (and patented) wind turbine concepts.

Vertical-axis windmills were also used in China, which is often claimed as their birthplace. While the belief that the windmill was invented in China more than 2000 years ago is widespread and may be accurate, the earliest actual documentation of a Chinese windmill was in 1219 A.D. by the Chinese statesman Yehlu Chhu-Tshai. Here also, the primary applications were apparently grain grinding and water pumping.

The first windmills to appear in Western Europe were of the horizontal-axis configuration. The reason for the sudden evolution from the vertical-axis Persian design approach is unknown, but the fact that European water wheels also had a horizontal-axis configuration and apparently served as the technological model for the early windmills. Another reason may have been the higher structural efficiency of drag-type horizontal machines over drag-type vertical machines, which (remember) lose up to half of their rotor collection area due to shielding requirements. The first illustrations (1270 A.D.) show a four- bladed mill mounted on a central post (thus, a "**postmill**") which was already fairly technologically advanced relative to the Persian mills. These mills used wooden cog-and-ring gears to translate the motion of the horizontal shaft to vertical movement to turn a grindstone.

As early as 1390, the Dutch set out to refine the **tower mill** design, which had appeared somewhat earlier along the Mediterranean Sea. The Dutch essentially affixed the standard post mill to the top of a multi-story tower, with separate floors devoted to grinding grain,

removing chaff, storing grain, and (on the bottom) living quarters for the wind smith and his family.

By the 14th century, Dutch windmills were in use to drain areas of the Rhine River delta. In Denmark by 1900, there were about 2500 windmills for mechanical loads such as pumps and mills, producing an estimated combined peak power of about 30 MW. The first known electricity generating windmill operated was a battery charging machine installed in 1887 by James Blyth in Scotland. The first windmill for electricity production in the United States was built in Cleveland, Ohio by Charles F Brush in 1888 (Figure 2.2.2), and in 1908 there were 72 wind-driven electric generators from 5 kW to 25 kW. The largest machines were on 24 m (79 ft) towers with four-bladed 23 m (75 ft) diameter rotors. Around the time of World War I, American windmill makers were producing 100,000 farm windmills each year, mostly for water-pumping. By the 1930s, windmills for electricity were common on farms, mostly in the United States where distribution systems had not yet been installed. In this period, high-tensile steel was cheap, and windmills were placed a top prefabricated open steel lattice towers.

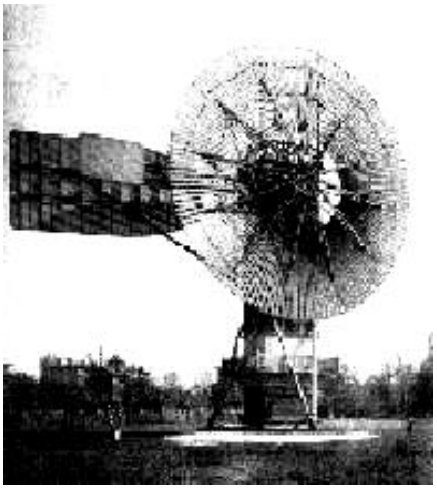

Figure 2.2.2: The Brush windmill (the first use of a large windmill to generate electricity.) in Cleveland, Ohio, 1888.

A forerunner of modern horizontal-axis wind generators was in service at Yalta, USSR in 1931. This was a 100 kW generator on a 30 m (100 ft) tower, connected to the local 6.3 kV distribution system. It was reported to have an annual capacity factor of 32 per cent, not much different from current wind machines. In the fall of 1941, the first megawatt-class wind turbine was synchronized to a utility grid in Vermont. The Smith-Putnam wind turbine only ran for 1100 hours. Due to war time material shortages the unit was not repaired.

The first utility grid-connected wind turbine operated in the UK was built by John Brown & Company in 1954 in the Orkney Islands. It had an 18 meter diameter, three-bladed rotor and a rated output of 100 kW.

A primary improvement of the European mills was their designer's use of sails that generated aerodynamic lift. This feature provided improved rotor efficiency compared with the Persian mills by allowing an increase in rotor speed, which also allowed for superior grinding and pumping action.

The process of perfecting the windmill sail, making incremental improvements in efficiency, took 500 years. By the time the process was completed, windmill sails had all the major features recognized by modern designers as being crucial to the performance of modern wind turbine blades, including 1) camber along the leading edge, 2) placement of the blade spar at the quarter chord position (25% of the way back from the leading edge toward the trailing edge), 3) center of gravity at the same 1/4 chord position, and 4) nonlinear twist of the blade from root to tip (Drees, 1977).

These mills were the "electrical motor" of pre-industrial Europe. Applications were diverse, ranging from the common water well, irrigation, or drainage pumping using a scoop wheel (single or tandem), grain-grinding (again, using single or multiple stones), saw-milling of timber, and the processing of other commodities such as spices, cocoa, paints and dyes, and tobacco.

While continuing well into the 19th century, the use of large tower mills declined with the increased use of steam engines. The next spurt of wind power development occurred many thousands of miles to the west.

2.3 Review of Existing Prediction Methods

Over the past few decades, extensive research works of wind turbines have been performed. Among them wind tunnel test, full-scale measurements, theoretical predictions may be mentioned. Researchers in the different parts of the world have developed different types of prediction methods so far. A brief description of some of the research papers related to the present work is given below:

Bowden, G.J. and McAleese, S.A. [21] made some measurements on the Queensland optimum S-shaped rotor to examine the properties of isolated and coupled S-shaped rotor. In particular it is shown that the efficiency of the turbine is around 18%, which is lower than the figure of 23% given by earlier workers. In the experimental setup the open jet air-stream, diameter 0.76m, was used to produce wind speeds in the range 0 to

30m/sec. The turbulence ($\sqrt{u^2}/V_\alpha$) in the jet stream was low. Wind flow measurements were investigated using 'tell-tales' (light pieces of cotton attached to a probe) and a stroboscope. In this way it was possible to detect the direction of the air-flow relative to the angular position of the rotor blades. Many photographs were taken and later used to construct a visual air-flow pattern around the rotor. The linearized hot-wire anemometer, on the other hand, enabled measurements to be made of velocity magnitudes and fluctuations to an upper frequency limit of 5 kHz. It cannot however, be used to measure direction. Hot-wire anemometer linearizer was based on a design of the Institute of Sound and Vibration Research (ISVR), Southampton University, U.K. In general, a storage oscilloscope was used to record the data, particularly from the more structured turbulent regions. However, measurements of turbulence intensity were also made by connecting an rms voltmeter to the output of the hot-wire linearizer. The results of this research were subsequently used to suggest that some form of active coupling between Savonius rotors might be possible. In particular, it has been shown that if two counter-rotating rotor are placed side by side, a natural phase locking occurs between the two turbines.

Huda et al. [28] analyzed the performance of S-shaped rotor by placing a flat plate in front of the returning blade. They found that the power coefficient of a S-shaped rotor is dependent on the Reynolds number and the value of Cp (power coefficient) is increased with Reynolds number in the range of the Reynolds number studied and maximum 20% of power coefficient can be increased by using the deflecting plate which occurs at a deflecting angle of 35^0 for b=0.5D, where b=distance between plate and rotor center and D=diameter of the rotor.

Islam et al. [30] investigated the aerodynamic forces acting on a stationary S-shaped rotor and made an attempt to predict the dynamic performance from these forces. The work was done by measuring the pressure distribution over the surface of the blades. The measurements were carried out in a uniform flow jet produced by an open circuit wind tunnel and at a constant wind speed of 8.9 m/s, which corresponds, to a Reynolds number ($R_e = \rho U_0 D / \mu$) of 1.1 x 10^5. The results indicate that flow separates over the front and back surfaces of the blades and the point of separation depends on the rotor angle. The pressure difference was observed between the convex and concave surfaces of each blade, which in turn, gave drag coefficients. The drag and hence, the torque of each blade varies with rotor angle and was found to be maximum at $\alpha = 45^0$ for the advancing blade and at $\alpha = 105^0$ for the returning blade. The maximum net torque was obtained at $\alpha = 45^0$ and became negative in the range of rotor angle between 135^0 to 165^0.

Ammara, Leclerc and Masson [37] for the aerodynamic analysis of wind farms used various CFD techniques to simulate turbine performance, such as the viscous three

dimensional differential/actuator disk method. In order to improve vertical axis wind turbine performance, CFD can be used to predict flow fields around a vertical axis wind turbine. The flow field around a vertical axis wind turbine is complicated, because of interactions between the large separated flow and wake itself.

Akiyoshi et al. [39] simulated flow around a vertical axis wind turbine and estimated its aerodynamic performance. The sub-grid scale turbulence model was developed to simulate the separated flow from the turbine blades. A sliding mesh technique was introduced to simulate flow through the rotational blades. Numerical results were compared with predictions based on momentum theory.

Saha et al. [43] aimed at exploring the feasibility of S-shaped bladed Savonius rotor for power generation. The S-shaped blade in a three-bladed rotor system has been tested in a low speed wind tunnel, and its performance has been compared with conventional semicircular blades (with twist angle of 01). Performance analysis has been made on the basis of starting characteristics, static torque and rotational speed. Experimental evidence shows the potential of the S-shaped bladed rotor in terms of smooth running, higher efficiency and self-starting capability as compared to that of the conventional bladed rotor. Further experiments have been conducted in the same setup to optimize the twist angle.

Islam et al. [44] made an investigation on variation of static torque and drag coefficient of an S-Shaped Savonius rotor for different number of rotor blades. This has been done by measuring the pressure distribution on the blade surfaces for different rotor angles. All the experiments have been carried out at Reynolds number $1.07*10^5$ in a uniform flow jet produced by an open circuit wind tunnel. Experimental results indicate that both of the drag force and hence the torque change frequently with rotor angle. It is also found that as the number of rotor blade increases, the starting torque of rotor increases but there is no significant increase in net torque output. It is observed that, torque distribution becomes more uniform as the number of blade of rotor increases.

Ajedegba, J.O. [48] in this thesis analyzed the performance of a vertical axis wind turbine for applications in urban areas. Numerical simulations with FLUENT software are presented to predict the fluid flow through a novel Zephyr vertical axis wind turbine (VAWT). Simulations of air flow through the turbine rotor were performed to analyze the performance characteristics of the device. Major blade geometries were examined. A multiple reference frame (MRF) model capability of FLUENT was used to express the dimensionless form of power output of the wind turbine as a function of the wind free stream velocity and the rotor's rotational speed. A sliding mesh model was used to

examine the transient effects arising from flow interaction between the stationary components and the rotating blades. The simulation results exhibit close agreement with a stream-tube momentum model.

The simplest prediction method for the calculation of performance characteristics of a Darrieus wind turbine is the single stream tube mode. It has been introduced first by Templin [1] in 1974. In this method, the whole turbine is assumed to be enclosed within the single stream tube. Templin first incorporated the concept of the windmill actuator disc theories into the analytical model of a Darrieus wind turbine. In the actuator disc theory the induced velocity (rotor axial flow velocity) is assumed to be constant through the disc and is obtained by equating the stream-wise drag with the change in axial momentum. According to the assumption of Templin, the actuator disc is considered as the surface of the imaginary body of revolution. It is assumed that the flow velocity is constant. This theory presented by Templin was the first approach to permit the numerical design calculation for a vertical-axis Darrieus wind turbine.

An improvement to the above method was the multiple stream tube model induced by Wilson and Lissaman [2]. In this model, the swept volume of the turbine was divided into a series of adjacent, aerodynamically independent stream tubes. Blade element and momentum theories were then employed for each stream tube. In their method they considered the flow as inviscid and incompressible for the calculation of induced velocity through the stream tube. As a result, there appeared only the lift force in the calculation of induced velocity through the stream tube. Wilson et al. considered the theoretical lift for their calculation. This induced velocity was varied over the frontal disc area both in the vertical and the horizontal directions. Atmospheric wind shear was included in the multiple stream tube models. Multiple stream tube model was inadequate in its description of the flow field. Wilson's model could be applied only for a fast running lightly loaded wind turbine.

Strickland [4] in his paper presented a multiple stream tube model for a vertical axis Darrieus turbine. He found the induced velocity by equating the blade element forces (including the airfoil drag) and the changes of momentum along each stream tube. The basic difference between the Wilson's and Strickland's models was that Wilson used the lift force (theoretical) only in the calculation of theoretical velocity while Stickland added the effect of drag force as well for the similar calculation. Wilson's model gave fast convergence while Stickland's model gave slow convergence.

Swamy and Fritzsche [6] investigated with the objective to improve the Darrieus type of motor. The conventional cross section of the blade for the Darrieus motor is that of a

symmetrical airfoil section. Mathematical relations describing the blade geometry were presented and the behavior of the blade in a centrifugal force field was investigated, taking into account a comparison of the actual shape of the rotor blades with a quadratic parabola and catenaries for different rotor height-diameter ratios. The contribution to the torque provided by the various segments of the rotor was determined. There appeared to be a distinct advantage in using a straight cylindrical section instead of curved blades. This hypothesis is to be investigated with the aid of a small model.

Fanacci and Walters [7] presented a two dimensional vortex model applicable to a straight-bladed wind turbine. In their analysis they considered a very small angle of attack thereby eliminating the stall effect.

Holme [8] presented a vortex model for a fast running vertical axis wind turbine having a large number of straight, very narrow blades and a high height diameter ratio (in order to make two dimensional flow assumption). The analysis was valid for a lightly loaded wind tribune only.

An analytical method using single stream tube model was presented by Noll and Ham [15] for the performance prediction of a vertical-axis wind turbine with straight blades, which were cyclically pitched. They added the effect of strut drag, turbulence wake state and dynamic stall to their analytical method.

In the paper presented by Paraschivoiu and Delelaux [19], improvements were made in the double multiple stream tube model. They considered the induced velocity variation as a function of the azimuth angle for each stream-tube. They added a new formulation for an approximate Troposkien shape by considering the effect of gravitational field and a semi-empirical dynamic stall model.

Paraschivoiu, Fraunie and Beguier [22] introduced in their paper the expansion effects of the stream tubes through the rotor and these were included with the double multiple stream tube model. With the measured and predicted data they observed that stream tube expansion effects were relatively significant at high tip speed ratio.

Gupta et al. [46] made a comparative study of a three-bucket Savonius rotor with a combined three-bucket Savonius–three-bladed Darrieus rotor. A combined Savonius–Darrieus type vertical axis wind rotor has got many advantages over individual Savonius or individual Darrieus wind rotor, such as better efficiency than Savonius rotor and high starting torque than Darrieus rotor. But works on the combined Savonius–Darrieus wind rotor are very scare. In view of the above, two types of models, one simple Savonius and the other combined Savonius–Darrieus wind rotors were designed and fabricated. The

Savonius rotor was a three-bucket system having provisions for overlap variations. The Savonius–Darrieus rotor was a combination of three-bucket Savonius and three-bladed Darrieus rotors with the Savonius placed on top of the Darrieus rotor. The overlap variation was made in the upper part, i.e. the Savonius rotor only. These were tested in a subsonic wind tunnel available in the department. The various parameters namely, power coefficients and torque coefficients were calculated for both overlap and without overlap conditions. From the present investigation, it is seen that with the increase of overlap, the power coefficients start decreasing. The maximum power coefficient of 51% is obtained at no overlap condition. However, while comparing the power coefficients (C_p) for simple Savonius-rotor with that of the combined configuration of Savonius–Darrieus rotor, it is observed that there is a definite improvement in the power coefficient for the combined Savonius–Darrieus rotor without overlap condition. Combined rotor without overlap condition provided an efficiency of 0.51, which is higher than the efficiency of the Savonius rotor at any overlap positions under the same test conditions.

Islam et al. [49] investigated the drag and torque coefficients of a stationary five bladed vane type rotor by measuring the pressure distribution on the blade surfaces at various rotor angles. The experimental investigation has been performed at Reynolds number 1.65×10^5 in a uniform flow jet produced by an open circuit wind tunnel. It has been observed that the total static torque coefficient increases from 0^0 to 10^0, and reaches its maximum value and then decreases up to 300. From this point, the total static torque increases up to 72°. Total static torque coefficient at different rotor angles curve repeats from 72^0 to 144^0, 144^0 to 216^0, 216^0 to 288^0, and 288^0 to 360^0 angle of rotation. A quasi steady approach has been applied for the prediction of dynamic performance of the rotor using the static drag and torque coefficients. This method results in a fair agreement with the measured power coefficient.

Sawada, et al. [24] experimentally studied the mechanism of rotation of Savonius rotor which have two semi-cylindrical blades. The force acting on a blade is measured in a water tank for both cases, rotor at rest and is rotated. A flow around the rotor is observed by using aluminum powder floating on the water surface. Although the Savonius rotor is classified as a resistance type, the lift produces a torque in a pretty wide range of blade angles relative to the flow. The researchers concluded that

- The rotor is at rest, the rotor with overlap ratio (ratio between overlap distance and cylinder diameter) a/d = 0.21 produces a positive torque at any rotor angle (α).
- The lift ($\alpha = 240^0 \sim 330^0$) contributes a lot to the torque occurring when the rotor is rotated. Although, the Savonius rotor is classified as a resistance type, the lift produces a torque in a pretty wide range of angles relative to the flow.

- When the rotor is rotated, the effect of the pressure recovery by the flow through the overlap portion on the lift is little for the rotor of a/d = 0.21. For the rotor of a/d = 0.51, the existence of a flow through the center of the rotor contributes to the production of a negative torque opposing the clockwise rotation.

Diaz et al. [27] analyzed the drag and lift coefficients of Savonius wind machine, in order to obtain quantitative information about the aerodynamic performance of the Savonius rotor. The experiments were carried out in a low turbulence open jet of 300 mm x 500 mm section outlet, which provides an air speed adjustable between o to 30 m/sec. The results of this work showed that for e/d = 1/6, at which the rotor generated the optimum power, the drag and lift coefficients were little dependent on the operating conditions (Reynolds number Re, tip speed ratio λ) if λ was near the optimum value $\lambda = 1$. There were three findings of this work: (a) the maximum efficiency of the Savonius rotor, in terms of power coefficient, took place for $\lambda \approx 1$, and that C_D decreased sharply when λ increased or decreased from the value, (b) for a given Reynolds number, as the tip speed ratio increased from zero, the drag values were maintained practically constant, $C_D \approx 1.5$ in the interval ranging from $\lambda = 0$ to $\lambda = 1.25$. The most interesting zone for power extraction was located near $\lambda \approx 1$, where C_D showed minimal values. For tip speed ratios greater than 1.25, the drag coefficient increased, (c) in a wide interval around $\lambda = 1$ (the most important region of operation of the Savonius rotor) the lift coefficient remained practically constant and the value was $C_L = 0.5$.

Islam et al. [29] investigated Aerodynamic characteristics of a stationary Savonius rotor of two semi cylindrical blades. The test was carried out in a uniform flow jet produced by an open circuit wind tunnel. The exit of the wind tunnel consisted of a square section nozzle with a side length of 500 mm. The rotor was placed at the jet axis and at 750 mm downstream of the nozzle exit. This study was carried out at constant wind speed of U_0 = 13.3 m/sec i.e., at Reynolds number, Re = 2 x 10^5. The results of this work showed that flow separated over the convex surface of the blades and the separation point moved towards the leading and trailing edges of the advancing and returning blades respectively as the rotor angle increased from 0^0 to 90^0. Beyond $\alpha = 90^0$, flow separated over the convex surface of the returning blade only. They also found that the difference in pressure on the convex and concave surfaces, produced drag coefficients, C_n and C_t in the normal and tangential direction of the chord. Drag coefficient C_n and C_t were a function of rotor angle and their resultant reached a maximum value at $\alpha = 120^0$ and a minimum value at $\alpha = 0^0$.

Aldoss and Obeidat [26] analyzed the performance of two Savonius rotor running side by side at different separations using the discrete vortex method. Two configurations were

considered. The torque and power coefficients were computed and compared with the available experimental results presented by Aldoss and Najjar in an earlier paper.

Fujisawa [32] analyzed the power mechanism of a Savonius rotor by pressure measurements on the blade surface and by a flow visualization experiment. It was found that a low pressure region was formed on the convex side of the advancing blade contributing to the power production of the rotating rotor. This phenomenon was observed as a Coanda-like flow pattern in the flow visualization experiment, which controlled the flow separation on the convex side. It was also noticed that the flow field near the rotor was effectively two-dimensional as the torque and the power coefficients evaluated from the pressure measurements at the middle plane agreed closely with the results by total torque measurement.

Saha and Maity [47] experimented for augmenting the energy-harnessing effectiveness. The proposal given by them was to employ a V-shaped deflector mounted upstream of the rotor, apex into the wind, so that the air-flow resistance encountered by the half of the wind-turbine blade advancing (i.e. moving) into the wind was reduced. By (i) carrying out experimental tests with the deflector in different positions relative to the rotor, and (ii) varying the wedge angle between the deflector blades, an optimal configuration for the particular system tested was determined. With the optimally pitched deflector set at its optimal location, the rotor harnessed about 20% more power, compared with the unblocked (i.e. standard) rotor both for an approximate wind speed of 4 ms^{-1}. Such a significant improvement, achieved by this simple cheap means, suggests that the use of the partially blocking wedge is highly desirable.

Chapter-3

THEORIES OF WIND TURBINE

3.1 General

Accurate models of the aerodynamic aspects of wind turbines are essential to successfully design and analyze wind energy systems. Wind turbine aerodynamic models are used to relate wind inflow conditions to loads applied on the turbine. One must enter the field of wind turbine aerodynamics analysis with an appreciation for the complexity of the subject. However, after years of investigation and testing, researchers throughout Europe and the United States have concluded that the typical atmospheric conditions under which a wind turbine operates are incredibly complex. The underlying flow physics of wind turbine operation are also much more complex than originally thought.

The true fluid flow passing around and through a wind turbine is governed by the first principles based Navier-Stokes equations. Unfortunately, these equations are so complex that analytical solutions have been found for only a few simple cases. Although numerical solutions may be found via a computer, most first-principles-based solutions are computationally intense and the cost of such detailed simulations prohibits their use in the design and analysis environment. As an alternative, most wind turbine designers and analysts have opted to develop models that incorporate two-dimensional airfoil analysis techniques and quasi-steady flow fields and this theory is known as classical theory. This theory is often called the strip theory or modified blade element theory. It is the combination of momentum theory and blade element theory.

3.2 S-shaped Vane type Rotor

Vane type wind turbines are drag based vertical axis wind turbine that operate on the theory and principle of a paddle propelling a boat through water. If no slip exists between the paddle and water, the maximum speed attained will be the same as the tangential speed of the paddle. Similarly, in a drag based vertical axis wind turbine, the speed at the tip of the blade can seldom exceed the speed of the wind. In order words, the drag can also be described as the pressure force or the thrust on the blades created by the wind as it passes through it.

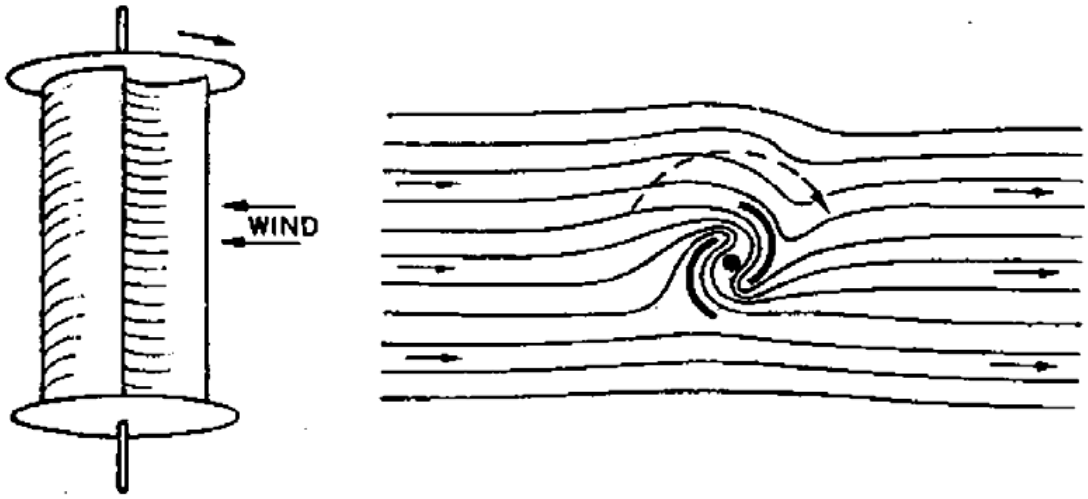

Figure 3.2.1: Vane Type S-shaped rotor

The Vane type rotor of S-shaped cross section (fig. 3.2.1) is predominantly drag based, but also uses a certain amount of aerodynamic lift. Drag based vertical axis wind turbines have relatively higher starting torque and less rotational speed than their lift based counterparts. Furthermore, their power output to weight ratio is also less. Because of the low speed, these are generally considered unsuitable for producing electricity, although it is possible by selecting proper gear trains. Drag based windmills are useful for other applications such as grinding grain, pumping water and a small output of electricity. A major advantage of drag based vertical axis wind turbines lies in their self–starting capacity, unlike the Darrieus lift–based vertical axis wind turbines.

3.3 Computational Fluid Dynamic Technique

Computational Fluid Dynamics is an important tool for the analysis, development, and optimization of wind power systems. Various CFD techniques have been used to simulate turbine performance, such as the viscous three-dimensional differential/actuator disk method, adapted by Ammara, Leclerc and Masson [37] for the aerodynamic analysis of wind farms. In order to improve vertical axis wind turbine performance, CFD can be used to predict flow fields around a vertical axis wind turbine. The flow field around a vertical axis wind turbine is complicated, because of interactions between the large separated flow and wake itself. The flow field through a vertical axis wind turbine is essentially unsteady, turbulent and separated flow. Akiyoshi et al. [39] simulated flow around a vertical axis wind turbine and estimated its aerodynamic performance. The sub-grid scale turbulence model was developed to simulate the separated flow from the turbine blades.

A sliding mesh technique was introduced to simulate flow through the rotational blades. Numerical results were compared with predictions based on momentum theory.

CFD numerical techniques are useful in various flow aspects of turbine performance. The viscous three-dimensional differential/actuator disk method has been used for the aerodynamic analysis of wind turbine. In this approach, the rotor is modeled as a permeable surface from which the time-averaged mechanical work is extracted by the rotor from the air.

The torque and pressure on the rotors of a vertical axis wind turbine are important parameters for a design. With many vertical axis wind turbines, especially designs with high rotor-stator interaction, the power output of the turbine can be rapidly changing and diverse throughout each rotation. For such applications, an unsteady time-dependant CFD simulation can offer a useful and straightforward method for determining a turbine's power output throughout each cycle. This technique is effective even for power curves with a high level of fluctuation. This is an important benefit of the moving mesh model, as it is the only method available to produce reliable time-dependent results.

3.4 Aerodynamics Theory and Performance Characteristics

The aerodynamic analysis of vertical axis wind turbines is complicated due to their orientation in the oncoming wind. The vertical axis wind turbines have a rotational axis perpendicular to the oncoming airflow. This accounts for aerodynamics that is more complicated than a conventional horizontal axis wind turbine. However, the configuration has an independence of wind direction. The main shortfalls are the high local angles of attack and the wake coming from the blades in the upwind part and axis. Understanding the aerodynamics of the pure drag type of vertical axis wind turbine will give important insight for improving the lift coefficient, and designing this turbine for better and more efficient harnessing of the wind energy.

3.4.1 Lift Force

The lift force, L, is one of the major force components exerted on an airfoil section inserted in a moving fluid. It acts normal to the fluid flow direction. This force is a consequence of the uneven pressure distribution between the upper and lower blade surfaces (fig. 3.4.1), and can be expressed as follows:

$$L = 0.5 C_l \rho V^2 A \tag{3.4.1}$$

where ρ is the air density, C_l is the lift coefficient and A is the blade airfoil area.

3.4.2 Drag force

The drag force, D acts in the direction of the fluid flow. Drag occurs due to the viscous friction forces on the airfoil surfaces, and the unequal pressure on surfaces of the airfoil. Drag is a function of the relative wind velocity at the rotor surface, which is the difference between the wind speed and the speed of the surface, and can be expressed as

$$D = 0.5C_d \rho(U - \Omega r)^2 A \tag{3.4.2}$$

where Ωr is the speed of the surface at the blade, C_d is drag coefficient and V is the wind speed.

The lift and drag coefficient values are usually obtained experimentally and correlated against the Reynolds number. A section of a blade at radius r is illustrated in Fig. 3.4.1, with the associated velocities, forces and angles shown. The relative wind vector at radius r, is denoted by V_{rel}, and the angle of the relative wind speed to the plane of rotation, by φ. The resultant lift and drag forces are represented by L and D, which are directly perpendicular and parallel to the relative wind as shown

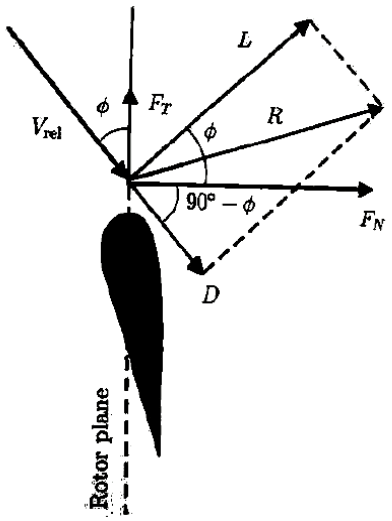

Figure 3.4.1: Local forces on a blade [34]

A careful choice of the rotor blades geometry and shape modification is crucial for maximum efficiency. Wind turbines have typically used airfoils based on the wings of airplanes, although new airfoils are specially designed for use on rotors. Airfoils use the concept of lift, as opposed to drag, to harness the wind's energy. Blades that operate with lift (forces perpendicular to the direction of flow) are more efficient than a drag machine. Certain curved and rounded shapes have resulted most efficient in employing lift. When the edge of the airfoil is angled slightly out of the direction of the wind, the air moves

more quickly on the downstream (upper) side creating a low pressure. On the upstream side of airfoil, the pressure is high. Essentially, this pressure differential lifts the airfoil upward. (Fig.3.4.2). In the case of a wind turbine, the lift creates a turning effect. An operating conditions with a low blade angle of attack, α, thus favors the lift force.

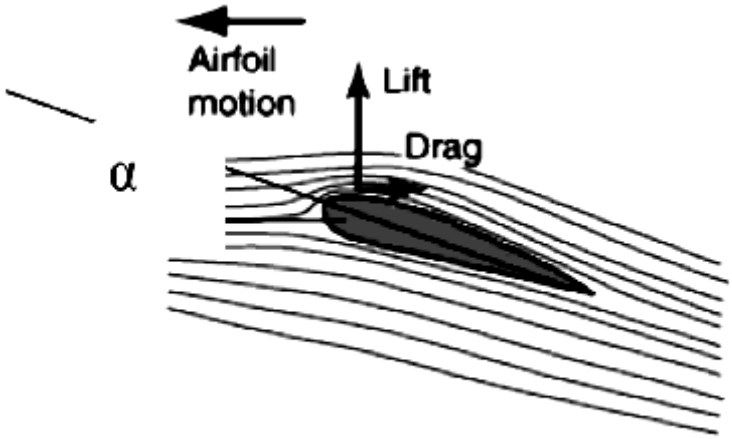

Figure 3.4.2: Airflow around an airfoil

Bernoulli's principle indicates how faster flow implies lower pressure on the airfoil:

$$P + \frac{1}{2}\rho v = \text{constant} \tag{3.4.3}$$

The first term in equation (3.4.3) is the static pressure and the second term is the dynamic pressure. An increase in velocity leads to a corresponding decrease in the static pressure to maintain a constant, and vice versa. The equation can be understood through a conservation of energy as pressure work is converted to / from kinetic energy in the flow field.

3.4.3 Reynolds number

The Reynolds number Re is the ratio of the inertia forces to the viscous forces. It is a non-dimensional parameter that defines the characteristics of the fluid flow conditions. It is used when calibrating the lift and drag coefficients of an airfoil. For a high speed rotor,

$$\text{Re} = \frac{UL}{\nu} = \frac{\rho UL}{\mu} = \frac{\rho V_\theta c}{\mu} \quad , \tag{3.4.4}$$

where μ is the fluid viscosity, $\upsilon = \frac{\rho}{\mu}$ is the kinematics viscosity, L is the characteristics length scale, c is the blade chord length, and V_θ is the blade tip velocity

3.4.4 Blade Solidity

Solidity is usually defined as the percentage of the circumference of the rotor which contains material rather than air. Savonius is a high solidity machine. It generates much higher starting torque than low-solidity machines, like Darrieus for example, but is inherently less efficient than low-solidity machines.

Another advantage of high-solidity machines is that they do not need to be made with as much precision as low-solidity ones. This type of turbine is self-starting and provides high torque at low speeds.

The blade solidity,δ , is the ratio of the blade area compared with the swept area. For a vertical axis wind turbine, the solidity is defined as

$$\delta = \frac{Bc}{2\pi r} \tag{3.4.5}$$

where B is the number of blades. Changing the number of blades or the blade chord dimensions will alter the vertical axis wind turbine solidity. An increase in the chord results in a large aerodynamics force and consequently in high power.

3.4.5 Tip speed ratio

The tip speed ratio λ, is defined as the velocity at the tip of the blade, to the free stream velocity. It is given by

$$\lambda = \frac{R\omega}{V} \tag{3.4.6}$$

3.4.6 Betz number

The Betz number or Betz limit is a useful performance indicator of wind turbines. It is the maximum amount of power that can be extracted by a wind generator from the available wind kinetic energy. This maximum turbine power is the difference between the upstream and downstream wind powers.

$$P_t = \frac{1}{2} * \frac{dm}{dt} * (V^2 - V_0^2) \tag{3.4.7}$$

where

P_t = turbine output power (watts),

V = upstream wind velocity (m/s) and

V_0 = downstream wind velocity (m/s)

The mass of air flowing through the turbine rotor area is a function of the air density and velocity (upstream and downstream average),

$$\frac{dm}{dt} = \rho_{air} A * \frac{1}{2}(V + V_0) \tag{3.4.8}$$

Substituting equation (3.2.8) into equation (3.2.6), the turbine power becomes

$$P_t = \frac{1}{2}\left[\rho_{air} * A * \frac{(V + V_0)}{2}\right] * \{V^2 - V_0^2\} \tag{3.4.9}$$

Equation (3.2.9) is rearranged to give the following expression:

$$P_t = \frac{1}{2} * \rho_{air} * A * V^3 * \frac{\left(1 + \frac{V_0}{V}\right) * \left[1 - \left(\frac{V_0}{V}\right)^2\right]}{2} \tag{3.4.10}$$

This power from the turbine rotor can be expressed as a fraction of the upstream wind power, i.e.,

$$P_t = \frac{1}{2} * \rho_{air} * A * V^3 * C_p \tag{3.4.11}$$

where Cp is the fraction of power captured by the rotor blades also called power coefficient or rotor efficiency.

Re-arranging the previous results, it can be shown that

$$C_p = \frac{\left(1 + \frac{V_0}{V}\right) * \left[1 - \left(\frac{V_0}{V}\right)^2\right]}{2} \tag{3.4.12}$$

Figure 3.4.3 shows the variation of C_p with downstream to upstream wind speed ratio, V_0/V. The theoretical maximum rotor power coefficient is C_p = 16/27 (= 0.59), when the downstream to upstream wind speed ratio is V_0/V = 0.33, called the *Betz limit* after the first analysis carried out by Betz (1926). However, the practical limits for C_p are typically

0.46 for high speed two-blade system and 0.50 for three-blade turbines. The drag turbine operates at about 1/3 of the 0.59 Betz limit.

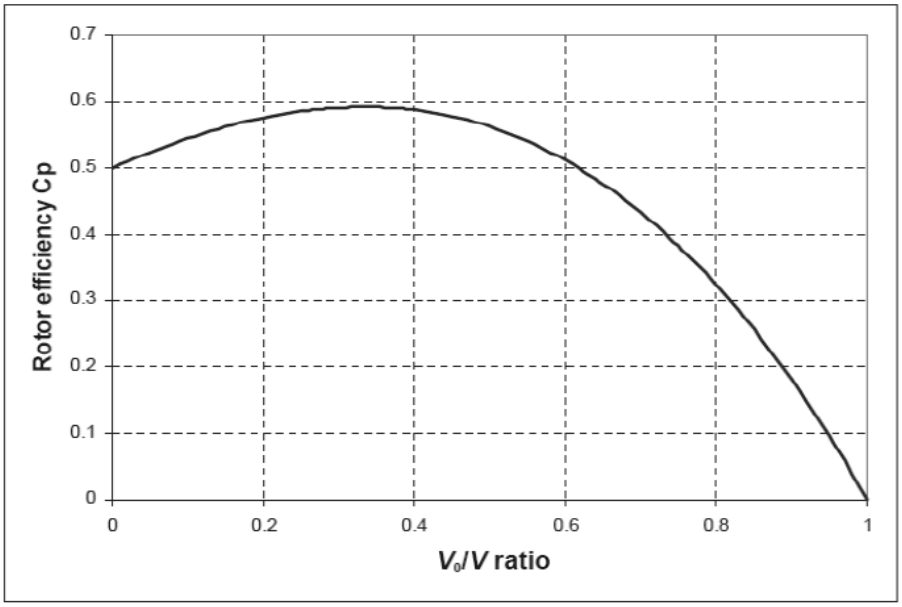

Figure 3.4.3: Rotor efficiency vs. downstream / upstream wind speed ratio [35]

As with all turbines, only a part of the energy shown in fig. 3.4.4 can be extracted. If too much kinetic energy were removed, the exiting air flow would stagnate and thus cause blockage. When the air flow approaches the inlet of the turbine, it meets a blockage imposed by the rotor-stator blades. This causes a decrease in kinetic energy, while the static pressure increases to a maximum at the turbine blade. As the air continues through the turbine, energy in the fluid is transferred to the turbine rotor blades, while the static pressure drops below the atmospheric pressure as fluid flows away from the rotor. This will eventually further reduce the kinetic energy. Then kinetic energy from the surrounding wind is entrained to bring it back to the original state.

A “disk actuator” model of a horizontal axis wind turbine gives further insight into the process.
This model can be used in explaining the Betz limit.

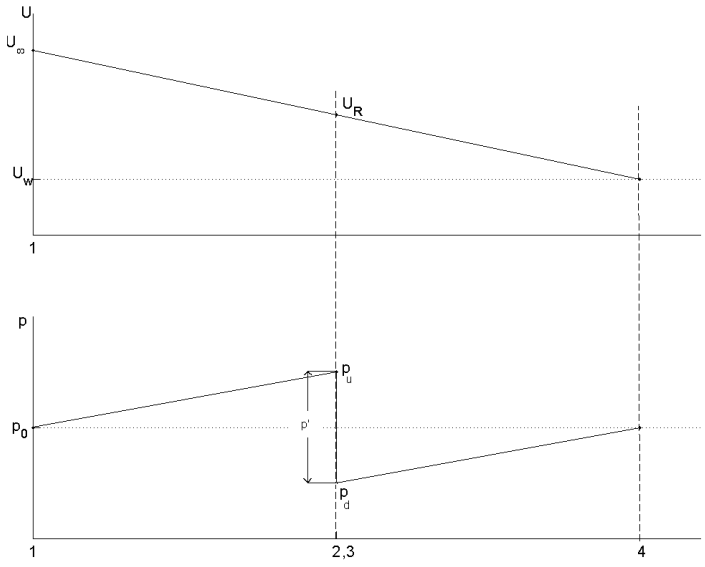

Figure 3.4.4: Velocity and pressure distribution in a stream tube

Typical velocity and pressure distributions are illustrated in Figure 3.4.4, using the disk actuator model and Betz limit theory. If the stream tube model is applied to a vertical axis wind turbine, it gives insight into the velocity and pressure distributions for a multi-bladed S-shaped vane type wind turbine. Because of the continuity principle for the stream tube, the diameter of the flow field must experience an increase as the velocity decreases giving rise to a sudden pressure drop, $\{p' = (p^u - p_d)\}$, at the rotor plane. This pressure drop contributes to the torque for rotating turbine blades.

The actuator disk theory also provides a rational basis for illustrating the flow velocity at the rotor that is different from the free-stream velocity. The Betz limit from the actuator disk theory shows the maximum theoretically possible rotor power coefficient (0.59) for a wind turbine. In reality, three major effects account for a power coefficient:

- rotation of wake behind the rotor;
- finite number of blades and associated tip losses;
- non-zero aerodynamic drag.

3.5 Rotor Performance Parameters

A wind turbine designed for a particular application should have its performance characteristics tested before proceeding to prototype fabrication. A dimensionally similar and scaled down prototype of the design model is normally tested in a wind tunnel for this purpose.

The power performance of a wind turbine is normally expressed in dimensionless form. For a given wind speed, the power coefficient, torque coefficient and the tip speed ratio are good indicators to use as a performance measure. For a particular configuration of the S-shaped multi-bladed vane type vertical axis wind turbine, these parameters are

$$C_p = \frac{P_t}{\frac{1}{2}\rho V^3 A} \tag{3.5.1}$$

where

P_t = Power developed by the turbine

A = Rotor cross-sectional area = hd ,

d = Rotor diameter,

h = Height of turbine,

ρ = Air density and

V = Free stream wind speed.

$$C_T = \frac{T_t}{\frac{1}{2}\rho V^2 AR} \tag{3.5.2}$$

where

T_t = Actual torque the shaft can develop

R = Radius of the turbine rotor

Also, λ (tip speed ratio) of equation 3.4.6 is dimensionless value that can be used in predicting the performance of the turbine. Figure 3.5.1 shows typical sample predictions for different wind turbine types.

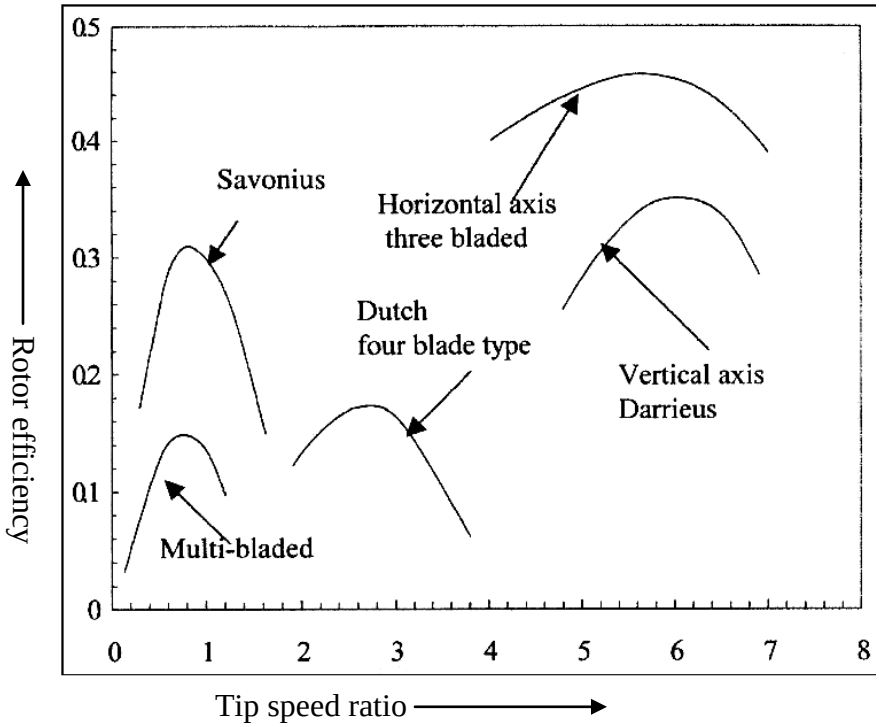

Figure 3.5.1: Rotor efficiency vs. tip speed ratio [28]

Figure 3.5.1 is a sample extract [28]. It is an illustration of modern turbine C_p –λ curves where C_p and λ are represented on the plot as y-axis and x-axis respectively.

3.6 Blade Element Momentum Theory

Blade Element Momentum (BEM) theory is a theoretical method developed for blade optimization and rotor design. The Blade Element Momentum theory, otherwise called strip theory, is a combination of basic momentum theory and blade element theory. The motion of the air flow and forces acting on the blades, determined by momentum principles are not complete without examining the shape of blades and configuration required for optimum and improved rotor power performance. The main principle of blade element theory is to consider the forces experienced by the blades of the rotor in motion through the air. This theory is therefore intimately concerned with the geometrical shape of the blade.

BEM theory becomes an essential tool that relates rotor performance to rotor geometry. A particularly important prediction of this theory is the effect of blade number. An assumption in BEM theory is that individual stream tubes (the intersection of a stream tube and the surface swept by the blades) can be analyzed independently of the remaining flow, as assumed in blade element theory.

Furthermore, an assumption associated with BEM theory is that span wise flow is negligible, meaning that airfoil data taken from two-dimensional tests are acceptable as in blade element theory. Another assumption is that flow conditions do not vary in the circumferential direction, i.e., axisymmetric flow. With this assumption, the streamtube to be analyzed is a uniform annular ring centered on the axis of revolution, as assumed in general momentum theory.

The multiple-streamtube model is a well established technique for predicting the performance of vertical axis wind turbines. It is similar in many ways to that used for horizontal axis wind turbines. The objective of the analysis is to simultaneously determine the forces acting on the blades of the turbine by a "blade element analysis" and deceleration of the wind that occurs due to the energy extracted from the air flow by the turbine, through actuator strip theory. As the rotor of the vertical axis wind turbine revolves, the blades trace the path of a vertical cylinder known as the actuator cylinder. As the wind intersects this cylinder, it must slow and any given streamtube of rectangular cross section must expand horizontally as shown schematically in Figure 3.6.1.

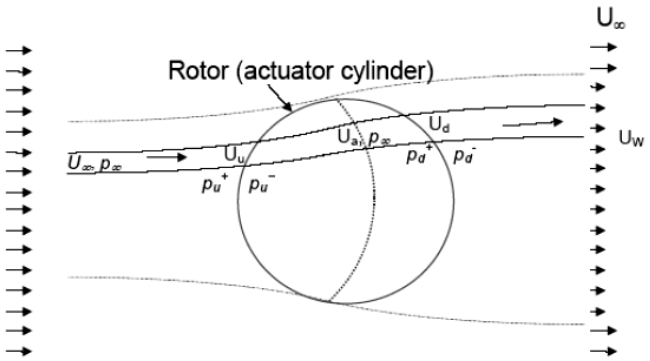

Figure 3.6.1: Plan view of actuator cylinder to analyze vertical axis wind turbines [41]

The wind turbine blade performance is determined with BEM by combining the equations of general momentum theory and blade element theory.

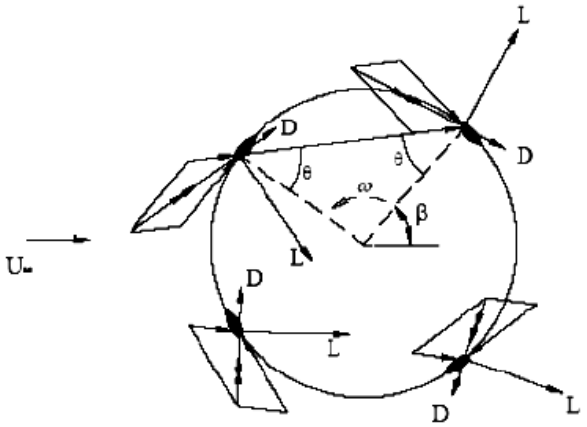

Figure 3.6.2: Lift and drag force on vertical axis wind turbine [41]

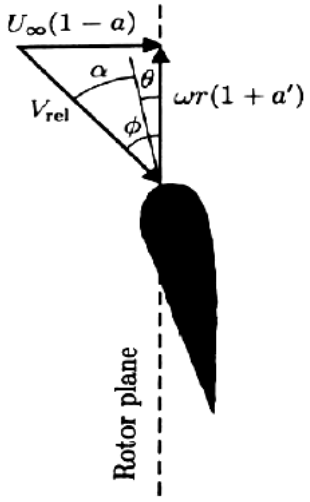

Figure 3.6.3: Velocities at the rotor plane [34]

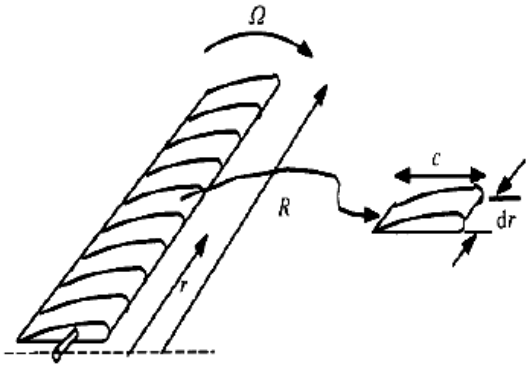

Figure 3.6.4: Schematic of blade elements

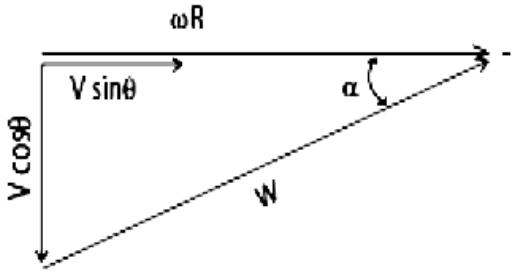

Figure 3.6.5: Component of local angle of attack

Figures 3.6.2 and 3.6.3 show that lift and drag forces, L and D, respectively, could be determined and hence the torque, power output from the blades and mechanical efficiency of the rotor could be determined. Here the symbol β represents the blade azimuth angle, φ is the angle between the resultant wind velocity, V, and the blade velocity (ωr), α is the angle of attack, γ is the blade pitch angle and θ is the angle between the streamtube and the rotor radius. The relative wind velocity V_{rel}, (W) is the vector sum of the wind velocity at the rotor U_∞ (1− a) (vector sum of the free-stream wind velocity, V_∞ and the induced axial velocity - aV_∞) and the wind velocity due to rotation of the blade. The rotational component is the sum of the velocity due to the blades motion, (ωr), and the swirl velocity of the air, a' (ωr) . The axial velocity U_∞ (1- a), is reduced by a component U_∞ a, due to the wake effect or retardation imposed by the blades, where U_∞ is the upstream undisturbed wind speed. The relative wind velocity is shown on the velocity diagram in Figure 3.6.3. The minus sign in the term U_∞ (1- a) is due to retardation of flow as the air comes into contact with the rotor. The positive sign in the term ω.r(1+ a') occurs due to the flow of air in the reverse direction of blade rotation, after air particles contact the blades and yields torque. This flow ahead and behind the rotor is not completely axial, as assumed in an ideal case. When the air exerts torque to the rotor, as a reaction, a rotational wake is generated behind the rotor. Depending on the wake length or separation, an energy loss is experienced, which resulted in a reduction of the power coefficient.

3.6.1 Torque and Power

The aerodynamic blade loads are transferred through the rotor and they are converted into torque on the low speed rotor shaft. This is the primary drive train load. The rated torque is calculated for a rated wind speed by an analysis of the forces on the surface of the rotor blades. The torque dependence on wind speed and rotor diameter follows a cubic law. It is inversely proportional to the rotor tip speed.

From the blade element analysis, the lift and drag forces acting over the blades are estimated and integrated over the total blade span, incorporating the velocity terms to obtain the shaft torque and power developed by the turbine. As shown on Figures 3.4.1, 3.6.2 and 3.6.3 for wind velocity and the force diagram, the lift and drag forces on an element of the blade will produce a differential torque about the axis of rotation as follows:

$$dQ = dQ_L + dQ_D \tag{3.6.1}$$

where dQ_L is the lift torque contribution (N-m), dQ_D is the drag torque contribution (N-m) and φ is the flow angle.

Resolving the forces acting on the blade into total normal and tangential force components yields

$$dF_N = dF_L\cos\varphi + dF_D\sin\varphi \tag{3.6.2}$$

$$dF_T = dF_L\sin\varphi - dF_D\cos\varphi \tag{3.6.3}$$

Substituting the lift and drag forces eqs. (3.4.1) and (3.4.2) into eqs (3.6.2) and (3.6.3), while considering an elemental area instead, yields

$$dF_N = 0.5\rho\, V^2_{rel}\,(C_L\cos\varphi + C_D\sin\varphi)cdr \tag{3.6.4}$$

$$dF_T = 0.5\rho\, V^2_{rel}\,(C_L\sin\varphi - C_D\cos\varphi)cdr \tag{3.6.5}$$

The elemental torque that occurs due to forces acting tangentially over the rotor blade, operating at a distance of rotor radius r from the centre, will give

$$dQ = r.dF_T \tag{3.6.6}$$

$$dQ = 0.5\rho\, V^2_{rel}\,(C_L\sin\varphi - C_D\cos\varphi)crdr \tag{3.6.7}$$

From fig. (3.6.3), the relative velocity is given as

$$V_{rel} = \frac{U_\infty(1-a)}{\sin\phi} \tag{3.6.8}$$

For a turbine rotor with a varying number of rotor blades, the solidity is defined as

$$\delta = \frac{Bc}{2\pi r} \tag{3.6.9}$$

Substituting equations (3.6.8) and (3.6.9) into (3.6.7), the elemental general equation becomes

$$dQ = \delta.\pi\rho.\frac{U_\infty^2.(1-a)^2}{\sin^2\phi}(C_L\sin\phi - C_D\cos\phi)r^2dr \tag{3.6.10}$$

The total power contribution from each blade is thus calculated from the above elemental torque contributions. By integrating along the blade length, the total power is obtained.

The elemental power from each blade element in fig. 3.6.5 is

$$dP = \frac{B}{2\pi}\Omega dQ \tag{3.6.11}$$

The total power from the turbine rotor becomes

$$P = \frac{B\Omega}{2\pi}.\int_{A_{Rotor}} dQ \tag{3.6.12}$$

Substituting this into equation (3.5.1), the power coefficient Cp is becomes

$$C_P = \frac{\sigma \int_{area} dQ}{1/2\rho_{air}V_\infty^3 A} = \frac{\sigma \int_{area} dQ}{1/2\rho_{air}V_\infty^3 hd} \tag{3.6.13}$$

3.6.2 Single Streamtube Model

This section extends a past model of Templin [1] to a vertical axis wind turbine, using actuator disk and momentum theories. The flow velocity through the turbine is assumed to be constant. The rotor aerodynamic drag is a vectorial sum of the forces on the actuator disk in the streamwise direction.

$$D = m\,(V_1 - V_2) \tag{3.6.14}$$

The power exchanged to causes the kinetic energy reduction which is given as

$$P = \dot{m}\left(V_1^2 - V_2^2\right)/2 \tag{3.6.15}$$

This power can also be written as follows (assuming a constant velocity):

$$P = D.V \tag{3.6.16}$$

An assumption is made with the following constant velocity through the streamtube:

$$V = \left(V_1 + V_2\right)/2 \tag{3.6.17}$$

From blade element theory, the aerodynamic drag force is determined by integrating the forces projected in the flow direction as follows:

$$D = \frac{B}{2\pi}\int_0^{2\pi} (F_N \cos\theta + F_T \sin\theta)d\theta \tag{3.6.18}$$

The lift and drag coefficients are two-dimensional aerofoil characteristics of the local blade element, which are functions of the angle of attack. They can also be resolved into normal force and thrust coefficients, C_N and C_T, respectively as follows:

$$C_N = C_d \cos\alpha + C_l \sin\alpha \quad (3.6.19)$$

$$C_T = C_d \sin\alpha - C_l \cos\alpha \quad (3.6.20)$$

where

$$F_N = C_N qc \quad (3.6.21)$$

$$F_T = C_T qc \quad (3.6.22)$$

The total drag force on the turbine for a given number of blades, over a complete revolution, is

$$D = \frac{Bc}{2\pi}\int_0^{2\pi} \{(C_l \cos\alpha + C_d \sin\alpha)\cos\theta + (C_l \sin\alpha - C_d \cos\alpha)\sin\theta\} q d\theta \quad (3.6.23)$$

From fig. 3.11, the local angle of attack is

$$\alpha = \arctan\left(\frac{\cos\theta}{\frac{R\omega}{V} - \sin\theta}\right) \quad (3.6.24)$$

From equation (3.6.16), the average power will then be

$$P = \frac{Bc}{2\pi} V \int_0^{2\pi} q\{(C_l \cos\alpha + C_d \sin\alpha)\cos\theta + (C_l \sin\alpha - C_d \cos\alpha)\sin\theta\} d\theta \quad (3.6.25)$$

Equation (3.6.25) can be solved numerically, given the rotor blade chord dimension and number of blades. It must be ensured that the blade solidity is kept constant. The power obtained is the shaft power, when no load is placed on the turbine. At this stage the mechanical efficiency of the turbine is determined. Then momentum theory can be used to find the dimensionless power coefficient.

Chapter-4

DESIGN AND FABRICATION

4.1 General

Wind-driven power systems that can produce large amounts of power are relatively new technologies. Many earlier models failed catastrophically because blades struck their support structure or tore off the hubs, or towers collapsed. Such failures have diminished in recent years because of improved designs, but other failures such as unacceptable material fatigue and component malfunction are common. In general, failures occur because the effects of unanticipated loads and unknown load levels and load paths are substantial. To combat such effects, wind turbine designers rely heavily on time-tested safety factors that account for this lack of knowledge. Such a design methodology greatly limits the cost effectiveness of new wind turbine designs, which is critical if wind-generated electricity is to be economically competitive with traditional energy sources.

In many respects, design codes (also labeled as modeling tools) bridge the gap between theorized predictions and experimental or observable measurements. Design codes essentially perform virtual experiments that can yield load analysis results quickly and cheaply. In many situations, virtual experimentation offers the only practical method of research and testing.

Most wind turbines have three blades. Very small turbines may use two blades for ease of construction and installation. Vibration intensity decreases with larger numbers of blades. Noise and wear are generally lower, and efficiency higher, with three instead of two blades. Turbines with larger numbers of smaller blades operate at a lower Reynolds number and so are less efficient. Small turbines with 4 or more blades suffer further losses as each blade operates partly in the wake of the other blades. Also, the cost of the turbine usually increases with the number of blades.

4.2 Application of S-shaped vane type rotor

S-shaped vane type rotor blade can be made many different ways with buckets, paddles, sails, and oil drums. All of these designs turn relatively slowly, but yield a high torque. They can be useful for grinding grain, pumping water, and many other tasks; but are not good for generating large amounts of electricity. RPMs above 1000 are generally best for producing electricity; however, drag-based vertical axis wind turbines usually turn below

100 RPM. A gearbox can be used, but then efficiency suffers and the machine may not start at all easily.

4.3 Materials

One of the strongest construction materials available (in 2006) is graphite-fibre in epoxy, but it is very expensive and only used by some manufactures for special load-bearing parts of the rotor blades. Modern rotor blades (up to 126 m diameter) are made of lightweight pultruded glass-reinforced plastic (GRP), smaller ones also from aluminium. GRP is the most common material for modern wind turbines. Wood and canvas sails were originally used on early windmills. Unfortunately they require much maintenance over their service life. Also, they have a relatively high drag (low aerodynamic efficiency) for the force they capture. For these reasons they were superseded with solid airfoils.

4.3.1 Choice of Rotor Blade Material

The material of the turbine blade plays a vital role in the wind turbines. The material of the blade should possess the high stiffness, low density and long fatigue life. In selecting materials for an application, technological considerations of material properties and characteristics are important. The economic aspects of material selection, such as availability, cost of raw materials, and cost of manufacturing, are equally important.

The important factors affecting selection of materials for S-shaped rotor blades are mentioned below:

1) One of the most important factors affecting selection of materials for engineering design is the properties of the materials. The important properties of the materials are mechanical, thermal, chemical properties etc.
2) The material of which a part is composed must be capable of performing a part's function (always it must be possible or not) with out failure.
3) A material in a given application must also be reliable.
4) A material must safely perform its function.
5) Physical attributes such as configuration, size, weight, and appearance sometimes also serve as functional requirements.
6) The environment in which a product operates strongly influences service performance.
7) A material must be readily available, and available in large enough quantity, for the intended application.
8) The cost of the materials and the cost of processing the materials into the product or part.

And in any material selection, the following requirements are focused. They are

1) High material stiffness is needed to maintain optimal shape of performance.
2) Low density is needed to reduce gravity forces,
3) Long-fatigue life is needed to reduce material degradation.

The optimal design of the rotor blades is today a complex and multifaceted task and requires optimization of properties, performance and economy.

Wind energy is captured by the rotation of the wind turbine's rotor blades. Different blade materials can be used for rotor construction. These have historically been made of wood, but because of its sensitivity to moisture and processing costs modern materials such as glass fiber reinforced plastic (GFRP), carbon fiber reinforced plastic (CFRP), steel and aluminum are replacing the traditional wooden units.

Wood is a composite of cellulose and lignin. Wood finds many engineering applications and has long been a common construction material. Woods are potentially interesting because of their low density, but their rather low stiffness makes it difficult to limit the (elastic) deflections for very large rotor blades. Even wood materials with cellulosed fibers all aligned in the major load-bearing directions are close to the maximum performance possible for wood. Furthermore, wood is a natural material and thus environmentally attractive, but at the same time difficult to obtain in reproducible and high quality, which is a requirement for stable and economical manufacturing of rotor blades and thus economically attractive wind energy.

Steel is an alloy of iron and carbon. Older style wind turbines were designed with heavier steel blades or nickel alloy steels which have higher inertia, and rotated at speeds governed by the AC frequency of the power lines. The high inertia buffered the changes in rotation speed and thus made power output more stable. The purpose of nickel alloy is lessens distortion in quenching and lowers the critical temperatures of steel and widens the range of successful heat treatment.

Nickel alloy possesses good corrosion and oxidation resistance. Alloy steel was once thought to be an optimum choice for blade fabrication, but was soon abandoned because of its high weight and low fatigue level.

Aluminium is a silvery white metal with a density about a third that of steel. Aluminum was only implemented in testing situations because it was found to have a lower fatigue

level than steel. Aluminium is ductile and good heat conductor. Aluminium is a low price metal but it has good reliability and has a low tensile strength. Aluminum is lightweight, but weaker and less stiff than steel.

The fibers and the matrix materials like polyesters, vinyl esters, epoxies etc., are combined into the composites. These composites have good properties like mechanical, thermal and chemical properties.

Firstly, the glass fibers are amorphous with isotropic properties. Most glass-reinforced products are made with E-glass (electrical glass), which has good electrical and mechanical properties and high heat resistance. E-glass is available as chopped fiber, milled fiber, continuous roving, woven roving, woven fabric, and reinforcing mat. Glass fibers for composites have good properties like moderate stiffness, high strength, and moderate density.

Carbon fibers are composed of nearly pure carbon, which forms a crystallographic lattice with a hexagonal shape called graphite. In recent years carbon fibers have become of increasing interest because of the requirements presented by the ever-larger rotor blades and the decreasing price of carbon fibers. Carbon fibers for composites have an excellent combination of very high stiffness, high strength, light weight and low density.

Aramid fibers (aromatic polyamides) are characterized by excellent environmental and thermal stability, static and dynamic fatigue resistance, and impact resistance. These fibers have the highest specific tensile strength (strength/density ratio) of any commercially available continuous-filament yarn. Aramid reinforced thermoplastic composites have excellent wear resistance. Aramid fibers have low or very low densities.

One of the most important factors in decision making is the degree of uncertainty. Whenever the designer makes a decision, he is performing a prediction of the effect of future events in technical feasibility, economic viability and trade-off between them. To make a successful prediction, good information (previous experience, outcomes from the similar circumstance, design knowledge, expertise etc.), proper methods and sometime good intuition are needed. And all geometry information, material properties, manufacturing process parameters, market change, customers' preference, development and manufacturing cost etc. can be estimated exactly and the future events are perfectly predictable.

In this analysis the PVC type had been chosen because of its high stiffness, high strength, light weight and low density. Above all this material was economically viable and by far obtainable in market.

4.4 Selection of Blade Design Parameters:

Design parameter	Main design influence	Secondary influence
Attachment point	Fatigue (downwind vs. upwind), Dynamic stall behaviour	Optimum TSR, Performance
Section pitch	Fatigue (downwind vs. upwind)	Optimum TSR, Performance
Section thickness	Dynamic stall behaviour	Performance
Section camber	None	Performance & Fatigue (downwind vs. upwind)
Overall section profile	Dynamic stall behaviour	Performance, Fatigue (downwind vs. upwind)
Chord to radius ratio	Links to attachment point and camber	
Solidity	Optimum TSR for optimum Cp, Performance	
Blade Reynolds number	Performance	
Span plan form	Performance	
Number of blades	Vibrations, Solidity, Blade Reynolds number, Chord to radius	
Strut design	Performance, Fatigue (vibrations)	

Table 4.4.1: Simplified cross influence on VAWT aerodynamic design parameters

4.5 Effect of Number of Blades on the Performance of Vertical Axis Wind Turbine:

In considering a wind turbine design, the question arises how many blades should be used. In general, as the number of blades increases so does the cost. The advantages of increasing the number of blades are improved performance and lower torque variations due to wind shear. The number of blades also affects the maximum power co-efficient. This is caused due to tip losses that occur at the tips of the blades. These losses depend on the number of blades and tip speed ratios. For lower tip speed ratios, in general, higher number of blades is chosen. This is done because the influence of number of blades on power co-efficient is larger at lower tip speed ratios. For higher design tip speed ratios higher number of blades will lead to very small and thin blades which results in manufacturing problems and a negative influence on the lift and drag properties of the blades.

Chapter-5

EXPERIMENTAL SETUP AND PROCEDURE

5.1 Introduction

The investigation on wind loading and aerodynamic effects on the four, five and six bladed S-shaped vertical axis vane type rotor have been conducted with the help of a subsonic wind tunnel together with the experiment set-up of the vane type rotor and a spring balance. The following sections describe in detail about the experimental set-up and the techniques adopted for the investigation.

5.2 The Wind Tunnel

The schematic diagram of the wind tunnel has been shown in Figure 5.2.1. An open circuit subsonic type wind tunnel was used to develop the required flow. The tunnel was 5.93 meter long with a test section of 490 mm x 490 mm in cross-section. The successive sections of the wind tunnel comprised of a converging entry, a Perspex section, a rectangular section, a fan section (two rotary axial flow fans), a butterfly valve section, a silencer with honey comb section, a diverging section, a converging section and an exit flow straightened section. The central longitudinal axis of the wind tunnel was maintained at a constant height from the floor. The converging mouth entry was incorporated into the system for easy entry of air into the tunnel and maintains uniform flow into the duct free from outside disturbances. In order to smooth the flow, the honeycomb was fixed near the outlet of the wind tunnel. The induced flow through the wind tunnel was produced by two-stage rotating axial flow fan of capacity 18.16 m^3/s at a head of 152.4 mm of water and 1475rpm with each of the fans connected to a motor of 2.25 kW capacity and 2900 rpm. A butterfly valve as shown in Figure 5.2.1 was used to control the wind speed. It was actuated by a screw thread mechanism placed behind the fan. A silencer was connected just after the butterfly valve for reduction of noise of the system. The converging and diverging section of the wind tunnel was 1550 mm long and made of 16 SWG black sheets. The angle of them was 7^0, which had been done with a view to minimizing expansion, contraction loss and reducing the possibility of flow separation. Other three outlet square (610 mm each) sections were used to make the flow straight and uniform.

5.3 Description of the Experimental Set-up

The experiment was carried out in the open circuit subsonic wind tunnel with an outlet test section of (490 mm x 490 mm) cross-section and the rotor was positioned at the exit section of the wind tunnel. The central longitudinal axis of the wind tunnel was always kept at a constant height of 990 mm from the floor. The model turbine was placed at 0.5m – rotor diameter downstream from the wind tunnel exit end as shown in Figure 5.3.1. The axis of the model was also placed coinciding with the axis of the wind tunnel.

Each time after changing the speed of axial flow fan average wind tunnel air velocity was measured directly by an electrical anemometer. This velocity distribution was along the vertical direction passing through the axis of the wind tunnel. Similarly, velocity distribution along the horizontal direction was observed as well. The anemometer was placed in front of the wind tunnel behind the rotor at different vertical distances between 100 mm downstream and 100 mm upstream of wind tunnel and average velocity was calculated. The velocity was more or less uniform throughout that can be seen from the Figure 5.3.2. The flow velocities were varied from 5m/s to 9m/s covering the Reynolds numbers up to 1.35×10^5.

A non-contact digital tachometer was used to measure the rpm of the shaft at different loading condition.

Figure 5.3.1: Set-up of the Experiment

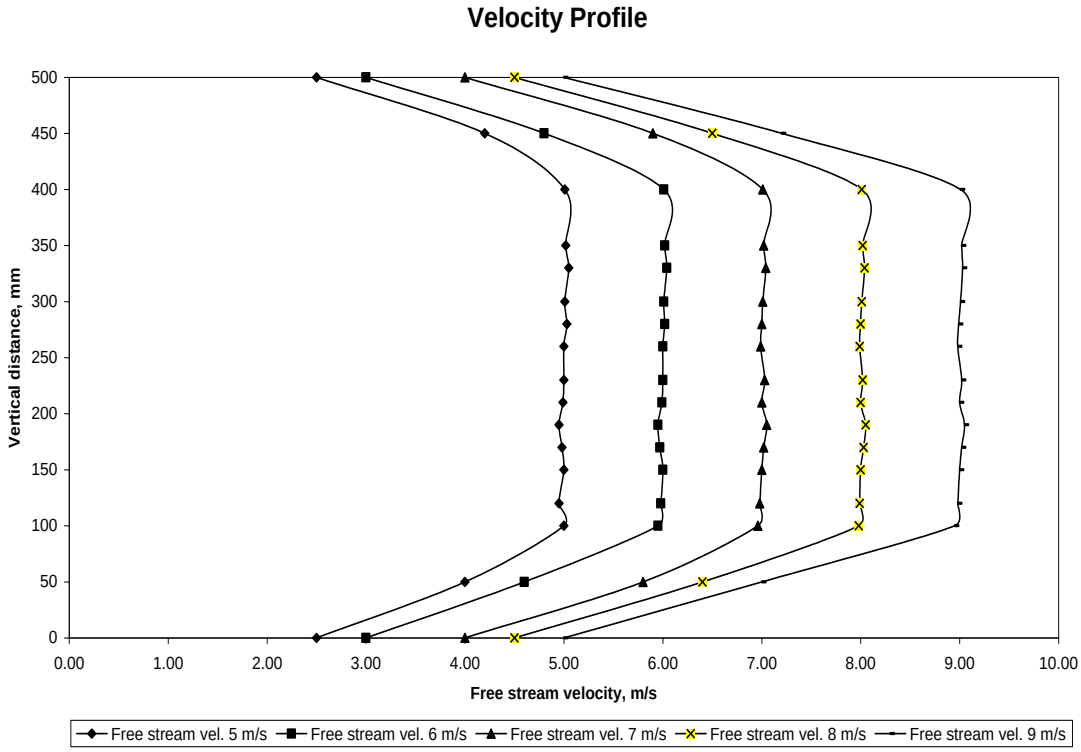

Figure 5.3.2: Velocity distribution in upstream side of test section

5.4 The Four, Five and Six Bladed Vane Type Rotor

The constructional detail of the test section is shown in Figure 5.4.1. Four, Five and Six bladed vane type rotor were made up of respectively four, five and six half cylinders (blade) of diameter, d =80 mm and height, H = 350 mm. And finally those half cylinders were given the shape of S for the purpose of making S-shaped rotor. Rotor diameter, D was 240 mm. Optimum value of d/D ratio was taken as 1/3. The cylinders were made of PVC material. Both the top and bottom ends of the rotor were fitted with end caps. The whole rotor was fixed on an iron frame by using a shaft that was inserted into it and two ball bearings. A pulley was attached at one end of shaft. A strip whose one side was tied to a spring balance and other side to a load carrying plate was prepared for passing over that pulley. A radium sticker was attached to that side of shaft. The spring balance was attached to the iron frame. The whole experimental set-up is shown in Figure 5.3.1. The cross-sectional views of four, five and six bladed S-shaped vane type rotor are shown respectively in Figure 5.4.2(a), Figure 5.4.3(a) and Figure 5.4.4(a). And their three dimensional views are shown respectively in Figure 5.4.2(b), Figure 5.4.3(b) and Figure 5.4.4(b).

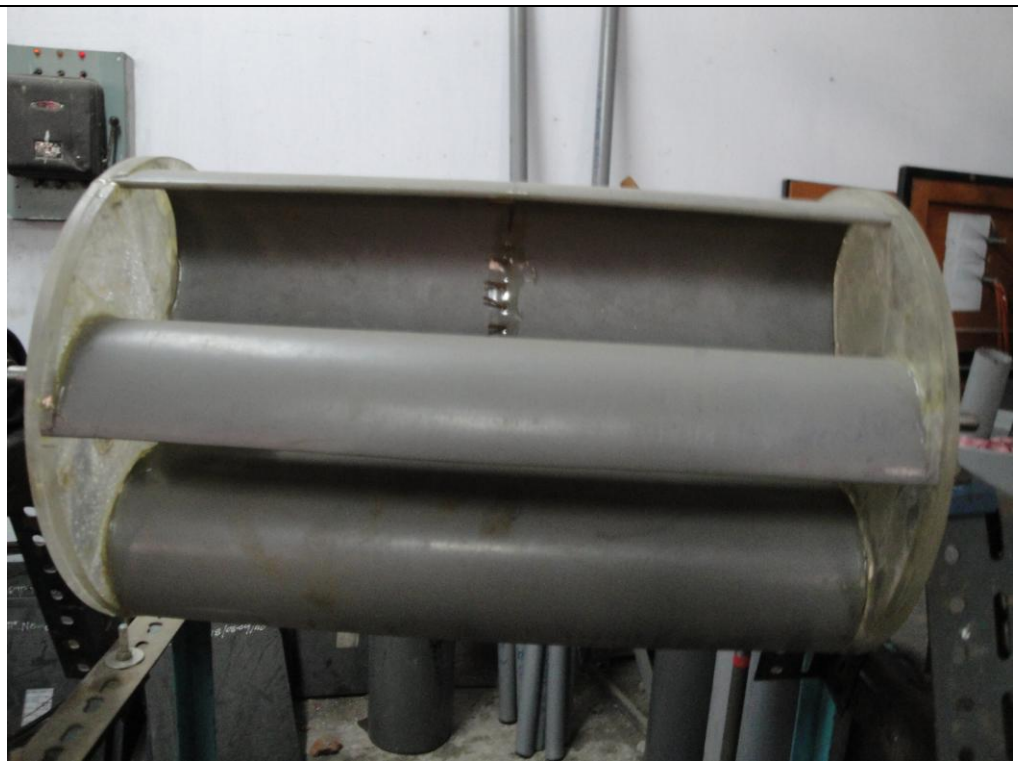

Figure 5.4.1: Constructional Details of the Test Section

5.5 Experimental Procedure

The flow velocities in the test section were varied from 5m/s to 9m/s covering the Reynolds numbers up to 1.35×10^5. The effect of temperature was considered in this experiment and the experiment was carried out at atmospheric temperature i.e. at T = 30^0C where kinematic viscosity of air was $\nu = 1.60 \times 10^{-5}$ m^2/s.

The experimental procedures are given below in brief:

a) The on button of one of the motor was pressed in order to rotate one axial flow fan for the purpose of generating free stream air of uniform velocity through the wind tunnel.

b) In front of the wind tunnel without placing the rotor model the wind velocity was measured by an anemometer at different vertical distances between 100mm upstream and 100mm downstream of wind tunnel.

c) The speed of the axial flow fan was adjusted to obtain a particular free steam velocity at the exit section of wind tunnel. The free stream velocity was first adjusted to 5 m/s.

d) The four bladed vane type rotor with structural frame was placed in front of the wind tunnel. It was placed 100 mm down stream of the tunnel exit section on a stand.

e) It was observed that the rotor with shaft was rotating because of the free stream velocity at the exit of the wind tunnel. At this condition, the light from digital non-contact tachometer was focused on the radium sticker attached to the shaft and the rpm reading at no load condition was taken.

f) At different loading condition the reading of rpm of the shaft using con-contact tachometer, the reading of weight from spring balance and the applied weight in the load carrying plate were noted down.

g) After taking all the readings up to maximum loading condition, the free stream velocity was further adjusted to 6 m/s. And the same procedures were followed.

h) Thus rapidly the free stream velocity was increased by 1 m/s and each time the same procedures were followed. The free stream velocity was raised rapidly up to 9 m/s.

i) The same procedures were followed for five and six bladed vane type rotor.

j) Output power was obtained from the above reading. Experimental values of the power coefficients were calculated from the ratio of the total output power to the theoretical available power.

k) Experimental values of the Torque coefficients were calculated from the ratio of power coefficient to the tip speed ratio.

Chapter-6

RESULTS AND DISCUSSIONS

6.1 Introduction

This chapter provides the discussions of the results of experimental investigation conducted by the wind tunnel air flow over the four, five and six bladed vane type rotor. The nature of the dynamic torque characteristics are also analyzed in this chapter. In addition, a comparative study of the existing other research works are also presented in this chapter.

6.2 Dynamic Aerodynamic Characteristics

This topic includes the analysis of power coefficient (C_P) and torque coefficient (C_Q) with respect to tip speed ratio for multi-bladed S-shaped vane type rotor at different Reynolds number. It also includes a comparative study between existing research works and present experimental results.

6.2.1 Power Coefficient

(a) Power Co-efficient for Four bladed S-shaped Vane Type Rotor:

The variation of results for four bladed S-shaped Vane Type Rotor in terms of power co-efficient versus tip speed ratio for increasing Reynolds number are shown in Figure 6.2.1.

In Figure 6.2.1 power coefficient versus tip speed ratio have been presented for 4 bladed S-shaped rotors at Reynolds numbers of 0.75×10^5, 0.90×10^5, 1.05×10^5, 1.20×10^5 and 1.35×10^5. The variations of Reynolds number were made by varying the free steam velocity. For four bladed rotor at Reynolds number of 0.75×10^5 maximum power coefficient of 0.1398 occurs at tip speed ratio of 0.6836. For further loading step by step with the decrease in rotor r.p.m., tip speed ratio also decreases from 0.6836 to 0.3644. However, the value of power co-efficient starts falling as the tip speed ratio becomes lower than 0.6836 although so far it was at increasing condition. At Reynolds number of 0.90×10^5 maximum power coefficient of 0.1411 occurs at tip speed ratio of 0.7037. From these two curves it is observed that the maximum power co-efficient is affected by changing the Reynolds number. For comparatively higher value of Reynolds number the value of maximum power co-efficient is slightly higher and it is shifted towards the higher values of tip speed ratios as the Reynolds number is increased. For Reynolds number of 1.05×10^5, 1.20×10^5 and 1.35×10^5 the repetition of same event can be observed. At Reynolds numbers of 1.05×10^5, 1.20×10^5 and 1.35×10^5 maximum

power coefficients of 0.1433, 0.1453 and 0.1483 occur at tip speed ratios of 0.7434, 0.75 and 0.77 respectively.

From this graph it is evident that with the increase of Reynolds number the maximum value of power coefficient also increases and it is shifted towards the higher values of tip speed ratios. So, it can be concluded that the increase of Reynolds number make the nature of power co-efficient versus tip speed ratio curve slightly steeper.

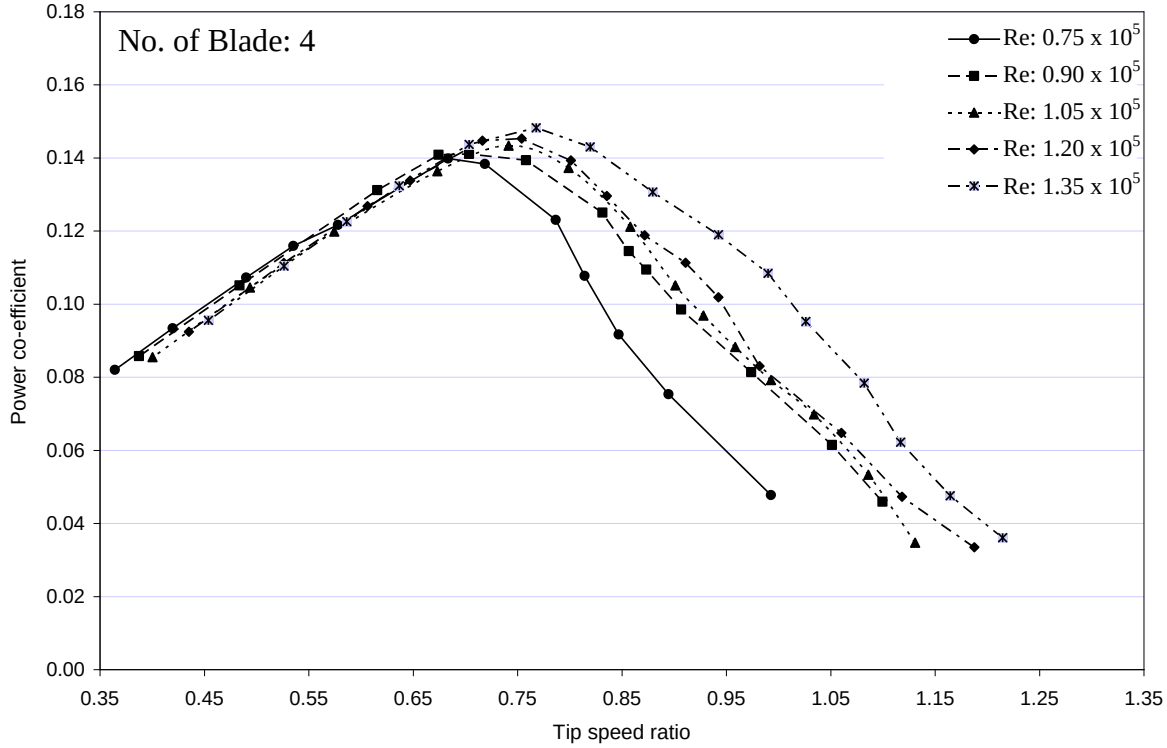

Figure 6.2.1: Comparisons of power coefficient vs. tip speed ratio for Four Bladed S-shaped Rotor at different Reynolds number

(b) Power Co-efficient for Five Bladed S-shaped Vane Type Rotor

The variation of results for five bladed S-shaped vane type rotor in terms of power co-efficient versus tip speed ratio for increasing Reynolds number are shown in Figure 6.2.2.

In Figure 6.2.2 for five bladed S-shaped rotor power co-efficient versus tip speed ratio have been presented at Reynolds numbers of 0.75×10^5, 0.90×10^5, 1.05×10^5, 1.20×10^5 and 1.35×10^5. For five bladed rotor at Reynolds number of 0.75×10^5 maximum power coefficient of 0.1421 occurs at tip speed ratio of 0.5906. For further loading step by step with the decrease in tip speed ratio from 0.5906 to 0.2262 power co-efficient also decreases from 0.1421 to 0.0618. At Reynolds number of 0.90×10^5 maximum power coefficient of 0.1464 occurs at tip speed ratio of 0.6493. For also five bladed rotor it is

observed that just like previous Figure of Four bladed vane type rotor the maximum power co-efficient is affected by changing the Reynolds number. Just as the curves of four bladed rotor the value of maximum power co-efficient increases slightly with the increase of Reynolds number and the region of this higher power co-efficient move to the region of larger values of tip speed ratios. For Reynolds number 1.05 x 10^5, 1.20 x 10^5 and 1.35 x 10^5 the repetition of same event can be observed. At Reynolds numbers of 1.05 x 10^5, 1.20 x 10^5 and 1.35 x 10^5 maximum power coefficients of 0.1516, 0.1535 and 0.1553 occur at tip speed ratios of 0.6588, 0.71 and 0.7470 respectively.

From this graph it is apparent that with the increase of Reynolds number the maximum value of power coefficient also increases and it is shifted towards the higher values of tip speed ratios. So, it can be concluded that the increase of Reynolds number make the nature of power co-efficient versus tip speed ratio curve slightly sharper.

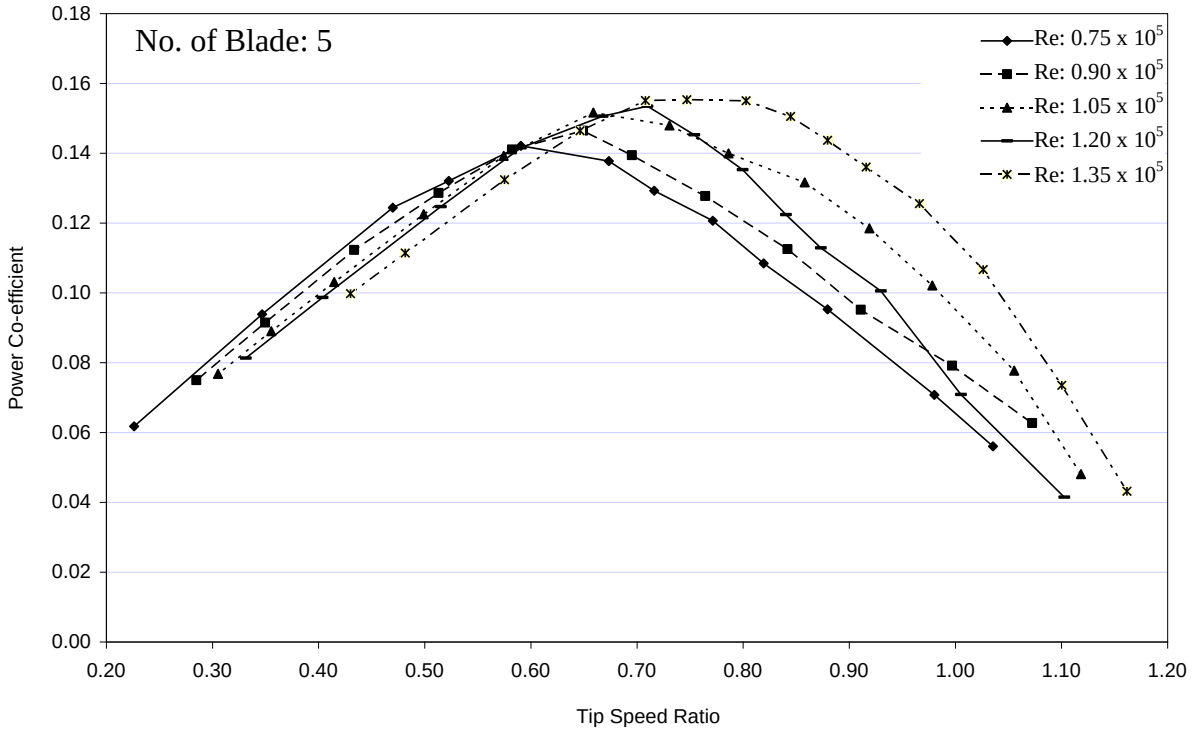

Figure 6.2.2: Comparisons of power coefficient vs. tip speed ratio for Five Bladed S-shaped Rotor at different Reynolds number

(c) Power coefficient for Six Bladed S-shaped Vane Type Rotor

The variation of results for six bladed S-shaped vane type rotor in terms of power co-efficient versus tip speed ratio for increasing Reynolds number are shown in Figure 6.2.3.

In Figure 6.2.3 for six bladed S-shaped vane type rotor power co-efficient versus tip speed ratio have been presented at Reynolds numbers of 0.75×10^5, 0.90×10^5, 1.05×10^5, 1.20×10^5 and 1.35×10^5. For six bladed rotor at Reynolds number of 0.75×10^5 maximum power coefficient of 0.1497 occurs at tip speed ratio of 0.4976. For further loading step by step as the value of tip speed ratio decreases from 0.4976 to 0.2237 power co-efficient also decreases from 0.1497 to 0.0848. For Reynolds numbers of 0.90×10^5, 1.05×10^5, 1.20×10^5 and 1.35×10^5 maximum power coefficients of 0.1519, 0.1543, 0.1574 and 0.1611 occur at tip speed ratios of 0.5864, 0.6283, 0.6566 and 0.7233 respectively. Just as previous Figures of four and five bladed vane type rotors, for also six bladed rotor it is observed that the maximum power co-efficient is affected by changing the Reynolds number. For also six bladed rotor comparatively at higher values of Reynolds number the value of maximum power co-efficient is slightly higher and the region of this higher power co-efficient move to the region of larger values of tip speed ratios.

From this graph it is apparent that with the increase of Reynolds number the maximum value of power coefficient also increases and it is shifted towards the higher values of tip speed ratios. So, it can be concluded that the increase of Reynolds number make the nature of power co-efficient versus tip speed ratio curve slightly sharper.

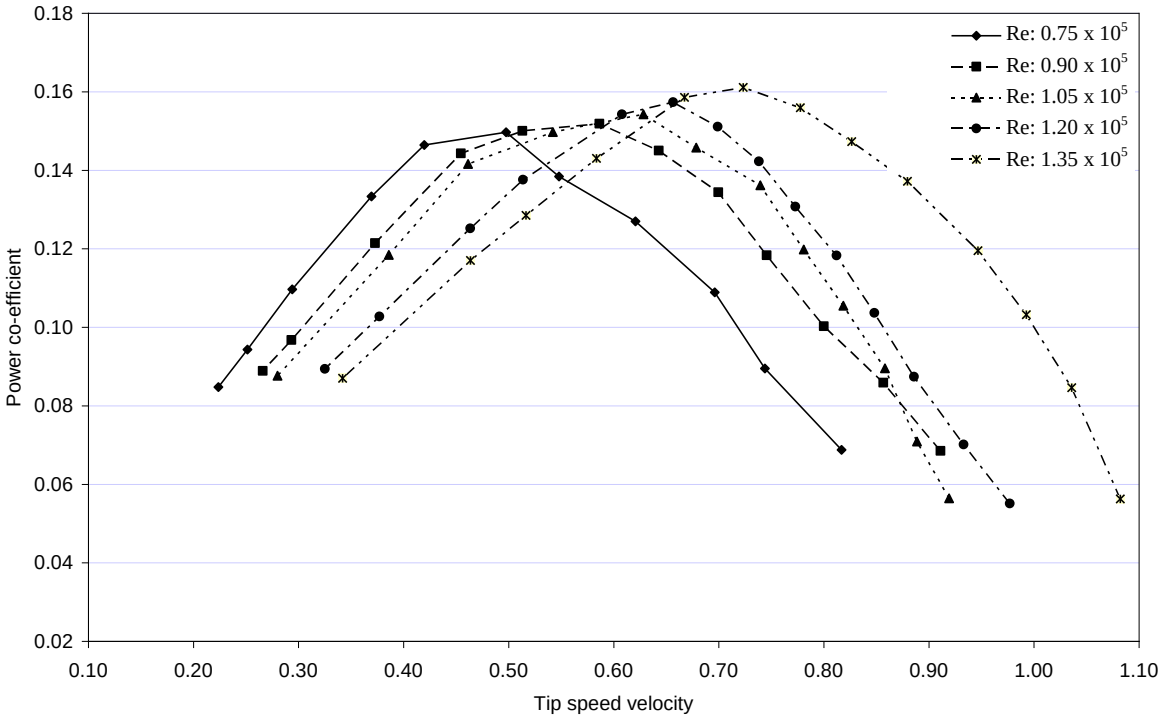

Figure 6.2.3: Comparisons of power coefficient vs. tip speed ratio for Six Bladed S-shaped Rotor at different Reynolds number

(d) Power Coefficient at Different Reynolds Number for 4, 5 and 6 Bladed S-shaped Vane Type Rotor

In Figures 6.2.4 to 6.2.8 comparisons have been made among the curves of power co-efficient versus tip speed ratio of multi-bladed rotor at different Reynolds number. In each figure a comparison has been made among different curves of power co-efficient versus tip speed ratio of four, five and six bladed rotor at a particular Reynolds number.

In Figure 6.2.4 it can be seen that for four bladed rotor at Reynolds number of 0.75×10^5 maximum power coefficient of 0.1398 occurs at tip speed ratio of 0.6836. Whereas for 5 and 6 bladed rotors at the same Reynolds number maximum power coefficients of 0.1421 and 0.1497 occur at tip speed ratios of 0.5906 and 0.4976 respectively. From this graph it is evident that with the increase in number of blades the maximum value of power coefficient also increases and it is shifted towards the lower values of tip speed ratio.

In Figures 6.2.5 to 6.2.8 the same thing can be observed. For 4, 5 and 6 bladed rotors at Reynolds number of 0.90×10^5 maximum power coefficients of 0.1411, 0.1464 and 0.1519 occur at tip speed ratios of 0.7037, 0.6493 and 0.5864 respectively. Similarly, at Reynolds number of 1.05×10^5, 1.20×10^5 and 1.35×10^5 it can be observed that the

value of maximum power co-efficient also becomes higher for higher number of bladed rotor and this maximum value of power co-efficient is shifted towards the lower values of tip speed ratio as the number of blades in the same sized rotor is increased.

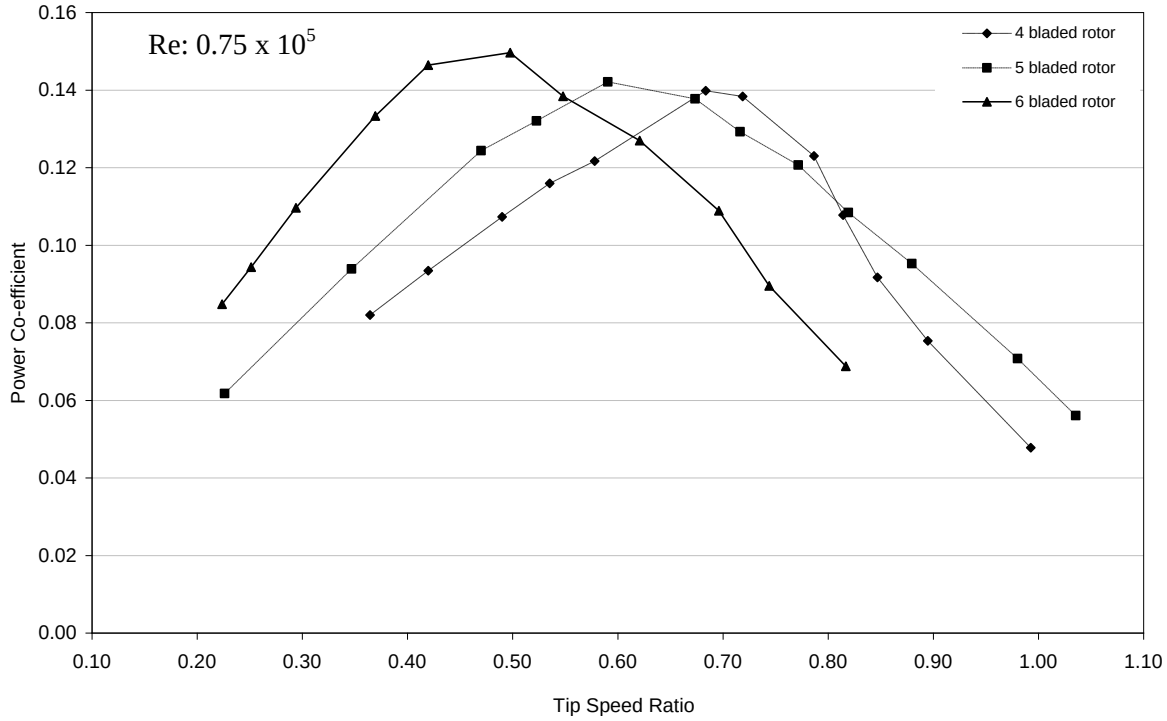

Figure 6.2.4: Comparisons of power coefficient versus tip speed ratio of 4, 5 and 6 bladed rotors at Reynolds number of 0.75×10^5

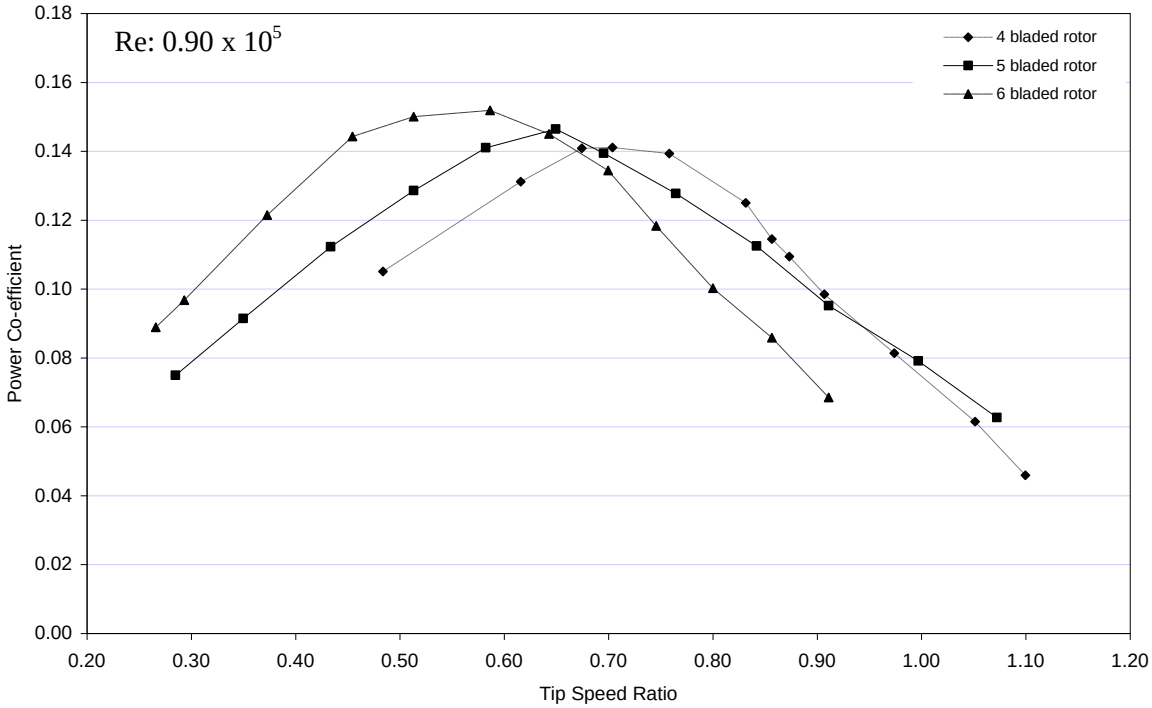

Figure 6.2.5: Comparisons of power coefficient versus tip speed ratio of 4, 5 and 6 bladed rotors at Reynolds number of 0.90 x 10^5

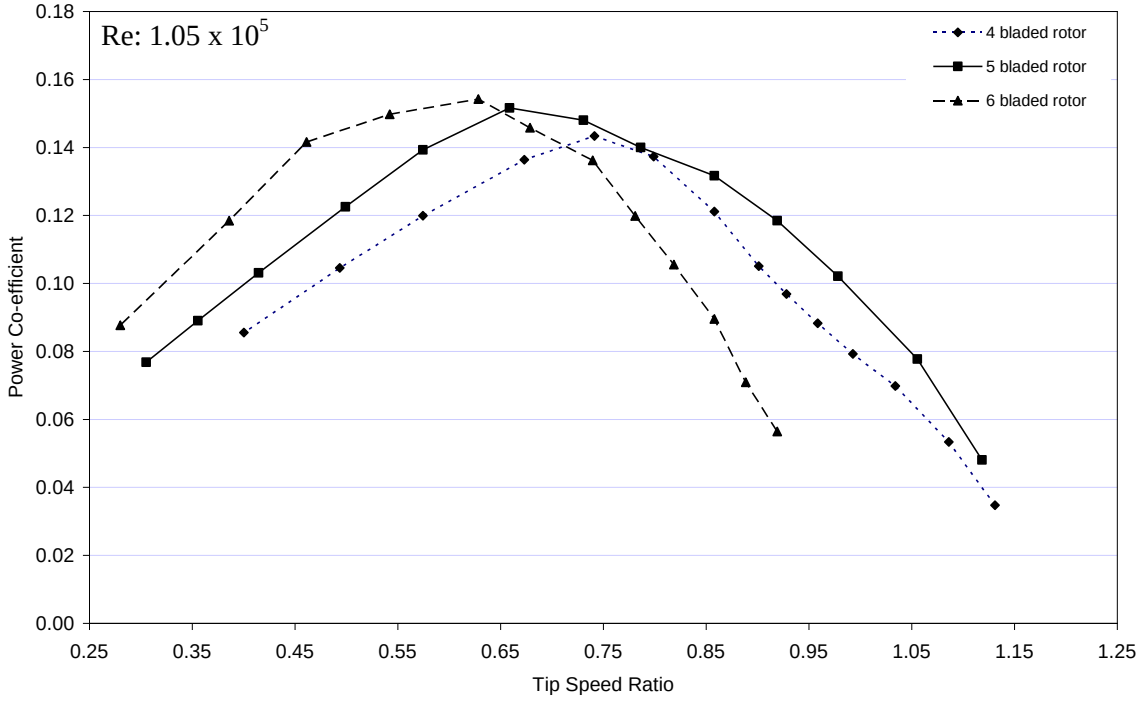

Figure 6.2.6: Comparisons of power coefficient versus tip speed ratio of 4, 5 and 6 bladed rotors at Reynolds number of 1.05 x 10^5

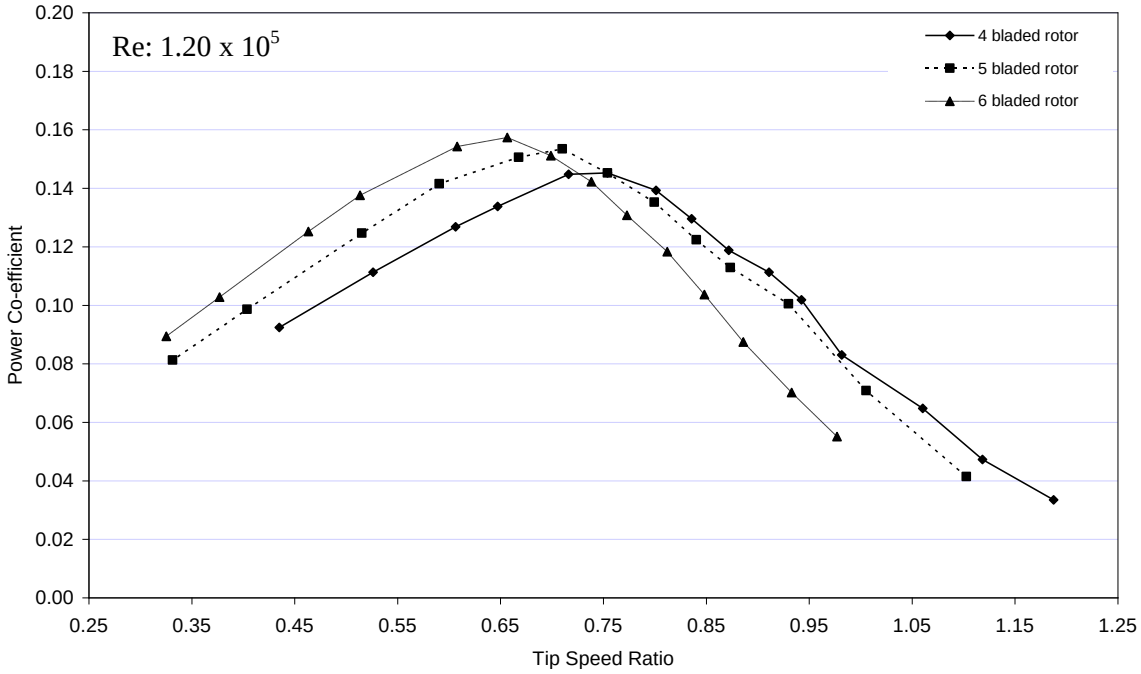

Figure 6.2.7: Comparisons of power coefficient versus tip speed ratio of 4, 5 and 6 bladed rotors at Reynolds number of 1.20 x 10^5

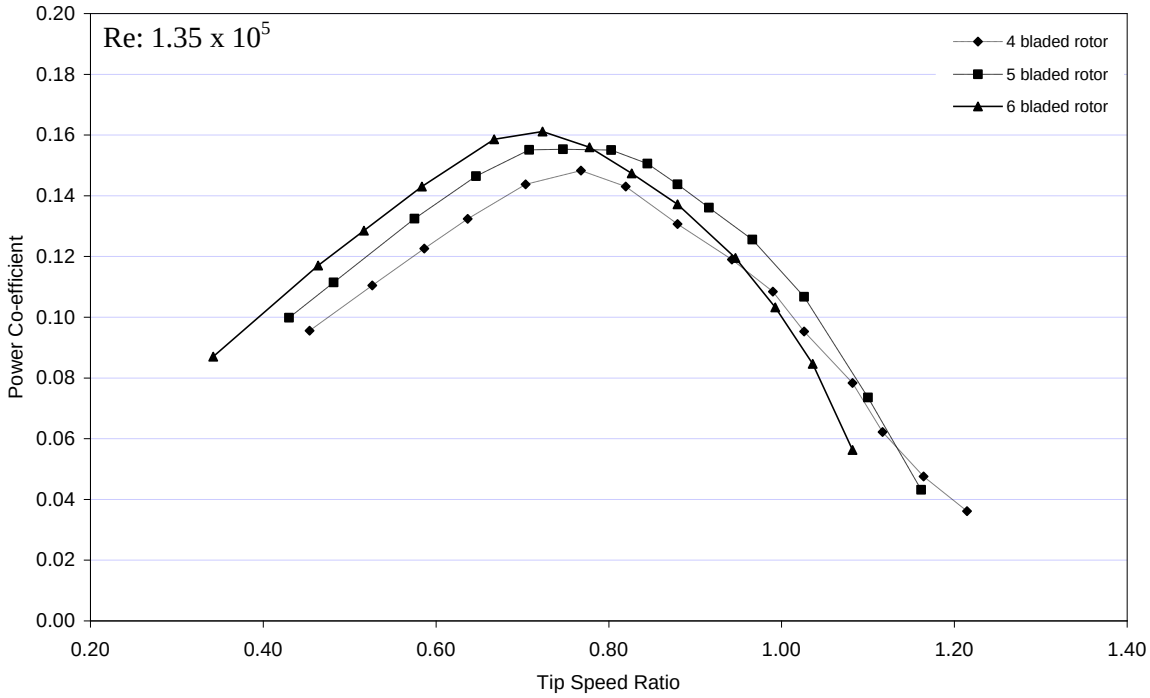

Figure 6.2.8: Comparisons of power coefficient versus tip speed ratio of 4, 5 and 6 bladed rotors at Reynolds number of 1.35 x 10^5

6.2.2 Torque Coefficient

(a) Torque Co-efficient for Four bladed S-shaped Vane Type Rotor:

The variation of results for four bladed S-shaped Vane Type Rotor in terms of torque co-efficient versus tip speed ratio for increasing Reynolds number are shown in Figure 6.2.9.

In Figure 6.2.9 torque coefficient versus tip speed ratio have been presented for 4 bladed S-shaped rotor at Reynolds numbers of 0.75×10^5, 0.90×10^5, 1.05×10^5, 1.20×10^5 and 1.35×10^5. The variations of Reynolds number were made by varying the free steam velocity of wind. For four bladed rotor at Reynolds number of 0.75×10^5 maximum torque coefficient of 0.2250 occurs at tip speed ratio of 0.3644. In this case, as the load is increased step by step rotor r.p.m. and tip speed ratio decreases accordingly. However, the value of torque co-efficient increases accordingly. This is why, for any particular Reynolds number at the lowest value of tip speed ratio highest value of torque co-efficient can be found. At Reynolds number of 0.90×10^5 maximum torque coefficient of 0.2214 occurs at tip speed ratio of 0.3875. From these two curves it is observed that the maximum torque co-efficient is affected by changing the Reynolds number. Increase of Reynolds number shows that the value of maximum torque co-efficient decreases slightly. So, it can be said that the increases in Reynolds number make the nature of the torque co-efficient versus tip speed ratio curve slightly blunt. For Reynolds number 1.05×10^5, 1.20×10^5 and 1.35×10^5 the repetition of same event can be observed. At Reynolds numbers of 1.05×10^5, 1.20×10^5 and 1.35×10^5 maximum torque coefficients of 0.2136, 0.2124 and 0.2105 occur at tip speed ratios of 0.4003, 0.44 and 0.45 respectively.

From this graph it is evident that for higher values of Reynolds number the maximum value of torque coefficient is lower and it is shifted towards the higher values of tip speed ratio.

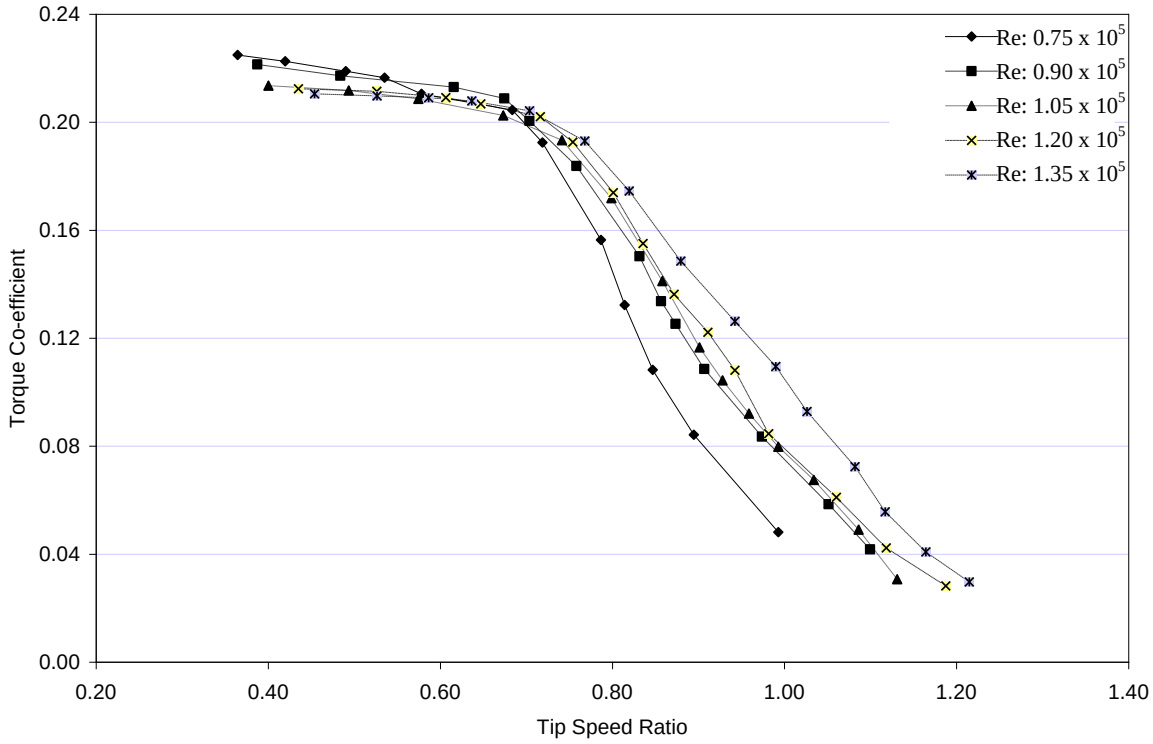

Figure 6.2.9: Comparisons of torque coefficient versus tip speed ratio for Four Bladed S-shaped Rotor at different Reynolds number

(b) Torque coefficient for Five Bladed S-shaped Vane Type Rotor

The variation of results for increasing Reynolds number for five bladed S-shaped Vane Type Rotor in terms of torque co-efficient versus tip speed ratio are shown in Figure 6.2.10.

In Figure 6.2.10 torque coefficient versus tip speed ratio have been presented for five bladed S-shaped rotor at Reynolds numbers of 0.75×10^5, 0.90×10^5, 1.05×10^5, 1.20×10^5 and 1.35×10^5. For five bladed rotor at Reynolds number of 0.75×10^5 maximum torque coefficient of 0.2731 occurs at tip speed ratio of 0.2262. For also five bladed rotor it can be observed that with the decrease in tip speed ratio the value of torque co-efficient increases. As a result, for any particular Reynolds number at the lowest value of tip speed ratio highest value of torque co-efficient can be found. At Reynolds number of 0.90×10^5 maximum torque coefficient of 0.2631 occurs at tip speed ratio of 0.2848. Just as four bladed rotor in also five bladed rotor it is observed that the maximum torque co-efficient is affected by changing the Reynolds number. From these two curves it can be said that for comparatively higher Reynolds number the value of maximum torque co-efficient is comparatively lower. So, for also five bladed rotor it can be said that the increases in

Reynolds number make the nature of the torque co-efficient versus tip speed ratio curve slightly blunt. For Reynolds numbers of 1.05 x 10^5, 1.20 x 10^5 and 1.35 x 10^5 the repetition of same event can be observed. At Reynolds numbers of 1.05 x 10^5, 1.20 x 10^5 and 1.35 x 10^5 maximum torque coefficients of 0.2516, 0.2453 and 0.2320 occur at tip speed ratios of 0.3052, 0.3314 and 0.4301 respectively.

From this graph once again it is apparent that for comparatively higher values of Reynolds number the maximum value of torque coefficient is comparatively lower and it is shifted towards the higher values of tip speed ratios.

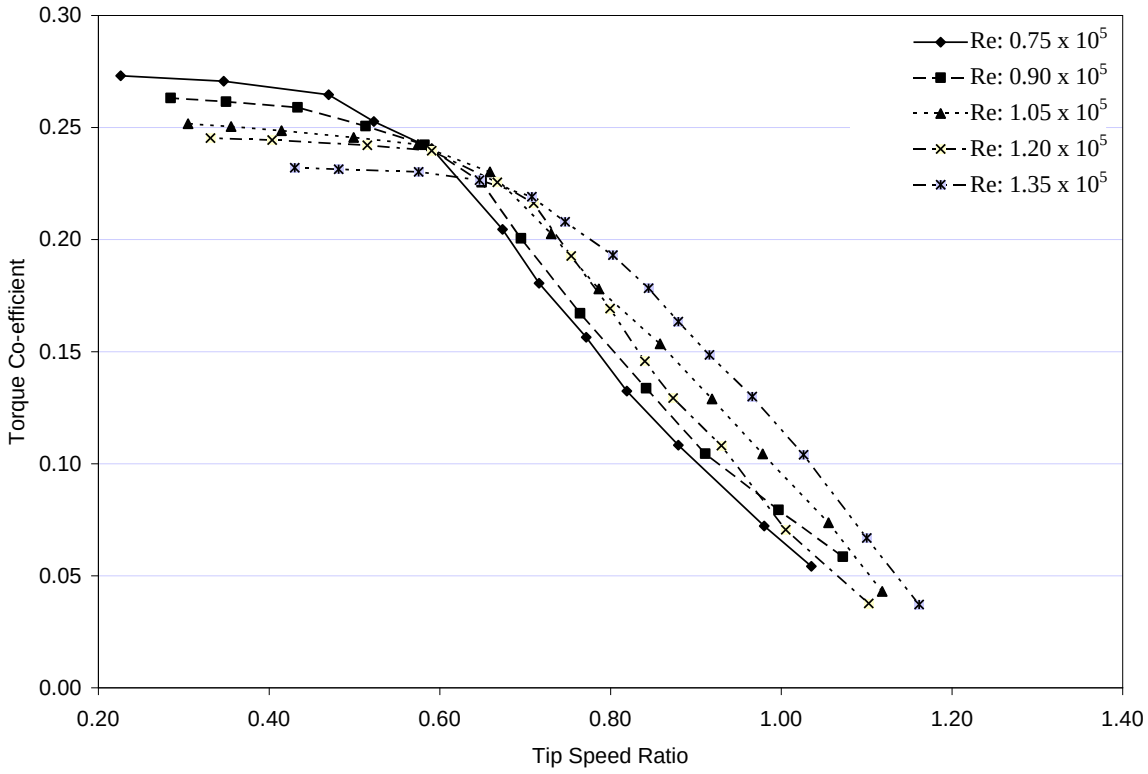

Figure 6.2.10: Comparisons of torque coefficient versus tip speed ratio for Five Bladed S-shaped Rotor at different Reynolds number

(c) Torque coefficient for Six Bladed S-shaped Vane Type Rotor

The variation of results for increasing Reynolds number for six bladed S-shaped Vane Type Rotor in terms of torque co-efficient versus tip speed ratio are shown in Figure 6.2.11.

In Figure 6.2.11 torque coefficient versus tip speed ratio have been presented for six bladed S-shaped vane type rotor at Reynolds numbers of 0.75×10^5, 0.90×10^5, 1.05×10^5, 1.20×10^5 and 1.35×10^5. For six bladed rotor at Reynolds number of 0.75×10^5 maximum torque coefficient of 0.3789 occurs at tip speed ratio of 0.2237. Just as four and five bladed rotor in six bladed rotor it can be observed that with the decrease in tip speed ratio the value of torque co-efficient increases. As a result, for any particular Reynolds number at the lowest value of tip speed ratio highest value of torque co-efficient can be found. At Reynolds number of 0.90×10^5 maximum torque coefficient of 0.3342 occurs at tip speed ratio of 0.2660. For also six bladed rotor it is seen that the values of torque co-efficient with respect to different tip speed ratios are different for different Reynolds numbers. From these two curves it can be said that for comparatively higher Reynolds number the value of maximum torque co-efficient is comparatively lower. That means the increases in Reynolds number make the nature of the torque co-efficient versus tip speed ratio curve slightly blunt. For Reynolds numbers 1.05×10^5, 1.20×10^5 and 1.35×10^5 the repetition of same event can be observed. At Reynolds numbers of 1.05×10^5, 1.20×10^5 and 1.35×10^5 maximum torque coefficients of 0.3130, 0.2749 and 0.2543 occur at tip speed ratios of 0.2801, 0.3252 and 0.3421 respectively.

From this graph again it is apparent that for comparatively higher values of Reynolds number the maximum value of torque coefficient is comparatively lower and it is shifted towards the higher values of tip speed ratio.

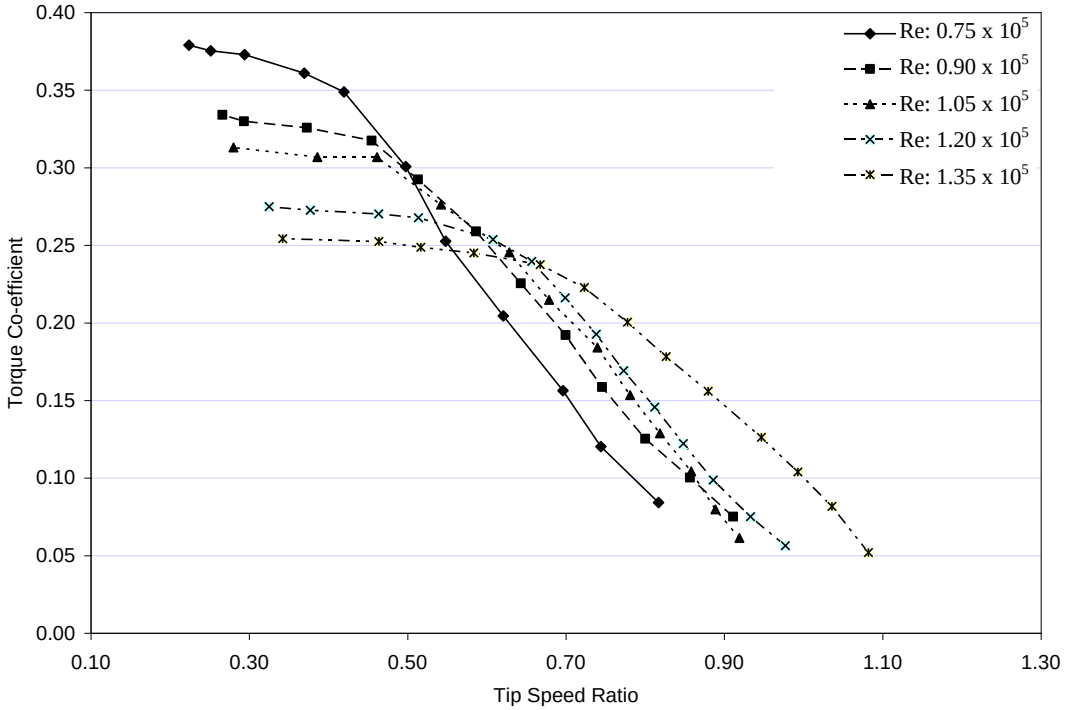

Figure 6.2.11: Comparisons of torque coefficient versus tip speed ratio for Six Bladed S-shaped Rotor at different Reynolds number

(d) Torque Coefficient at Different Reynolds number for 4, 5 and 6 Bladed S-shaped Vane Type Rotor

In Figures 6.2.12 to 5.2.16 comparisons have been made among the curves of torque co-efficient versus tip speed ratio of multi-bladed S-shaped rotor at different Reynolds number. In each figure a comparison has been made among different curves of torque co-efficient versus tip speed ratio of four, five and six bladed rotor at a particular Reynolds number.

In Figure 6.2.12 it can be observed that for four bladed rotor at Reynolds number of 0.75 x 10^5 maximum torque coefficient of 0.2250 occurs at tip speed ratio of 0.3644. Whereas for 5 and 6 bladed rotors at the same Reynolds number maximum torque coefficients of 0.2731 and 0.3789 occur at tip speed ratios of 0.2262 and 0.2237 respectively. This point is important for driving the irrigation pump especially positive displacement pump which needs higher starting torque. From this graph it is evident that for rotor having higher number of blades the maximum value of torque coefficient is also higher and it is shifted towards the lower values of tip speed ratio. That means, the increases in number of blades make the nature of torque co-efficient versus tip speed ratio curve sharper.

In Figures 6.2.13 to 6.2.16 the same thing can be observed. For 4, 5 and 6 bladed rotors at Reynolds number of 0.90 x 10^5 maximum torque coefficients of 0.2214, 0.2631 and 0.3342 occur at tip speed ratios of 0.3875, 0.2848 and 0.2660 respectively. Similarly, at Reynolds number of 1.05 x 10^5, 1.20 x 10^5 and 1.35 x 10^5 it can be observed that the value of maximum torque co-efficient becomes higher for higher number of bladed rotor and this maximum value of torque co-efficient is shifted towards the lower value of tip speed ratio as the number of blades in the same sized rotor is increased.

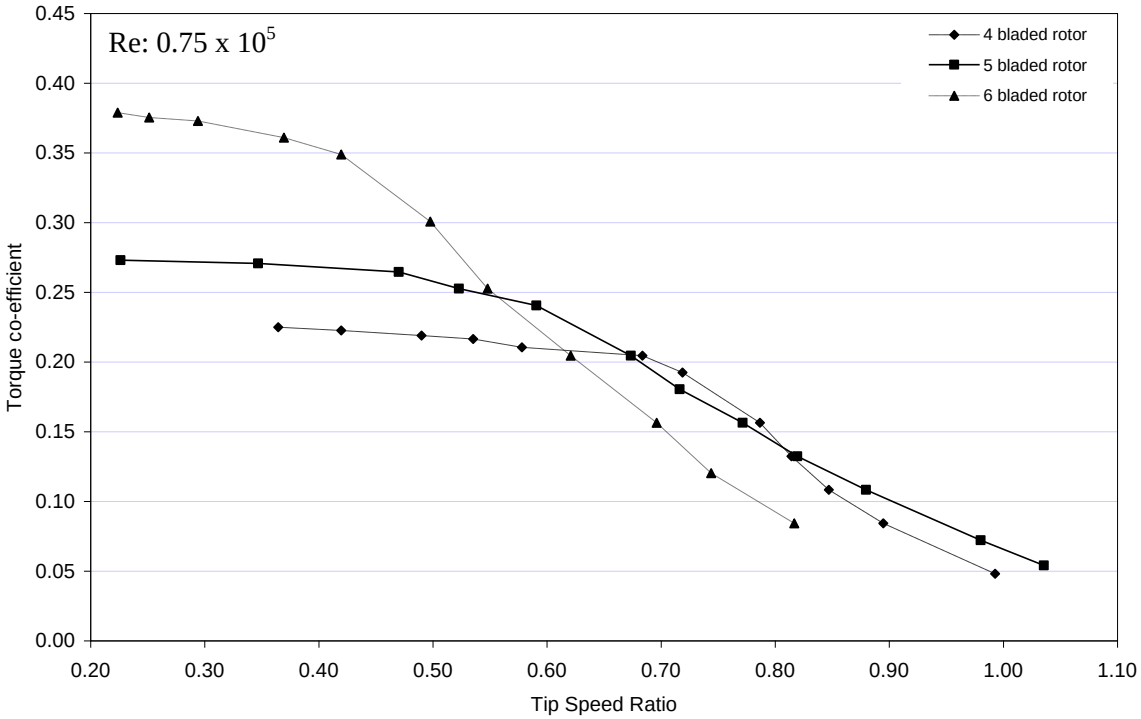

Figure 6.2.12: Comparisons of torque coefficient versus tip speed ratio of 4, 5 and 6 bladed rotors at Reynolds number of 0.75 x 10^5

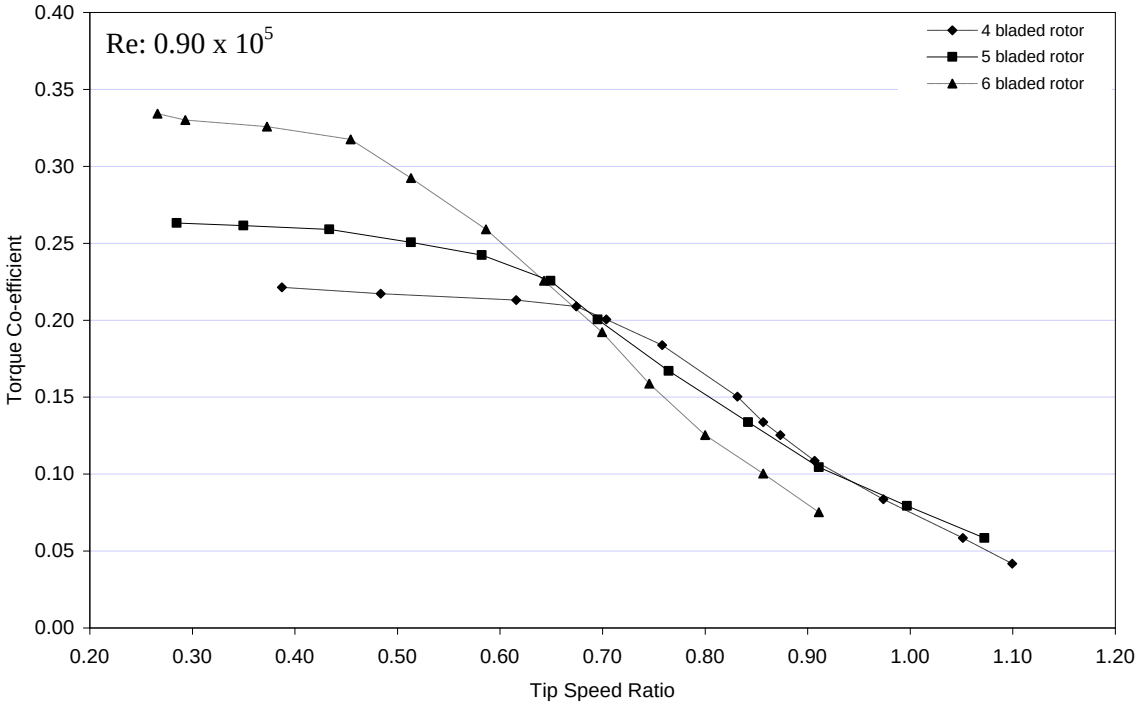

Figure 6.2.13: Comparisons of torque coefficient versus tip speed ratio of 4, 5 and 6 bladed rotors at Reynolds number of 0.90 x 10^5

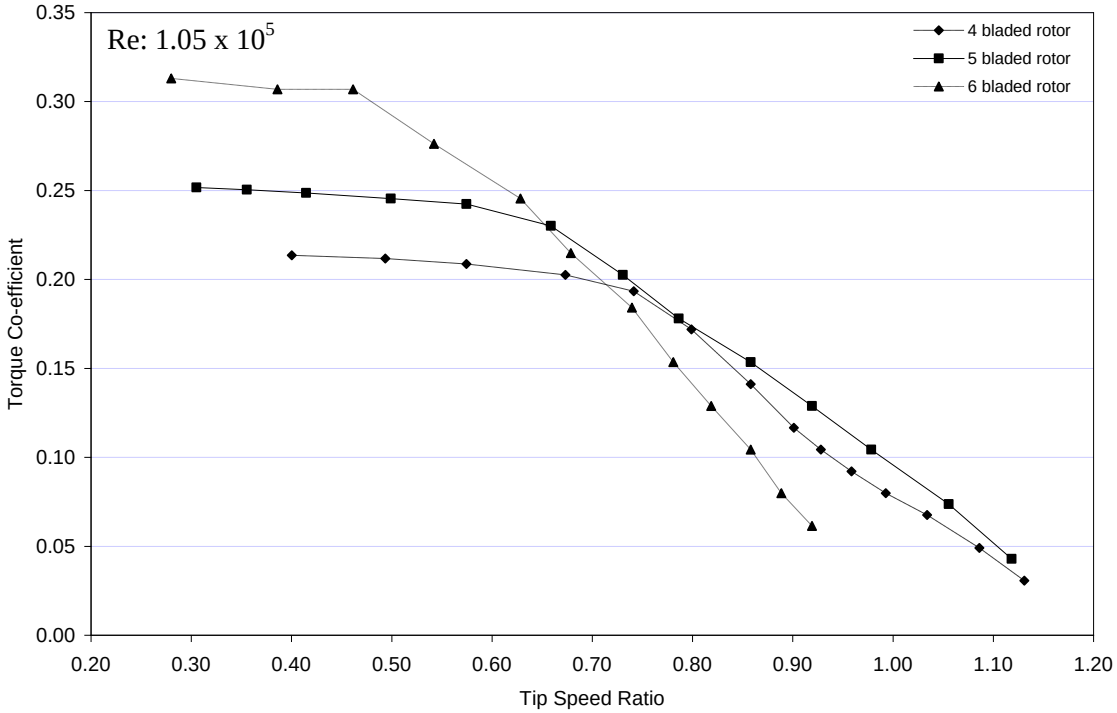

Figure 6.2.14: Comparisons of torque coefficient versus tip speed ratio of 4, 5 and 6 bladed rotors at Reynolds number of 1.05 x 10^5

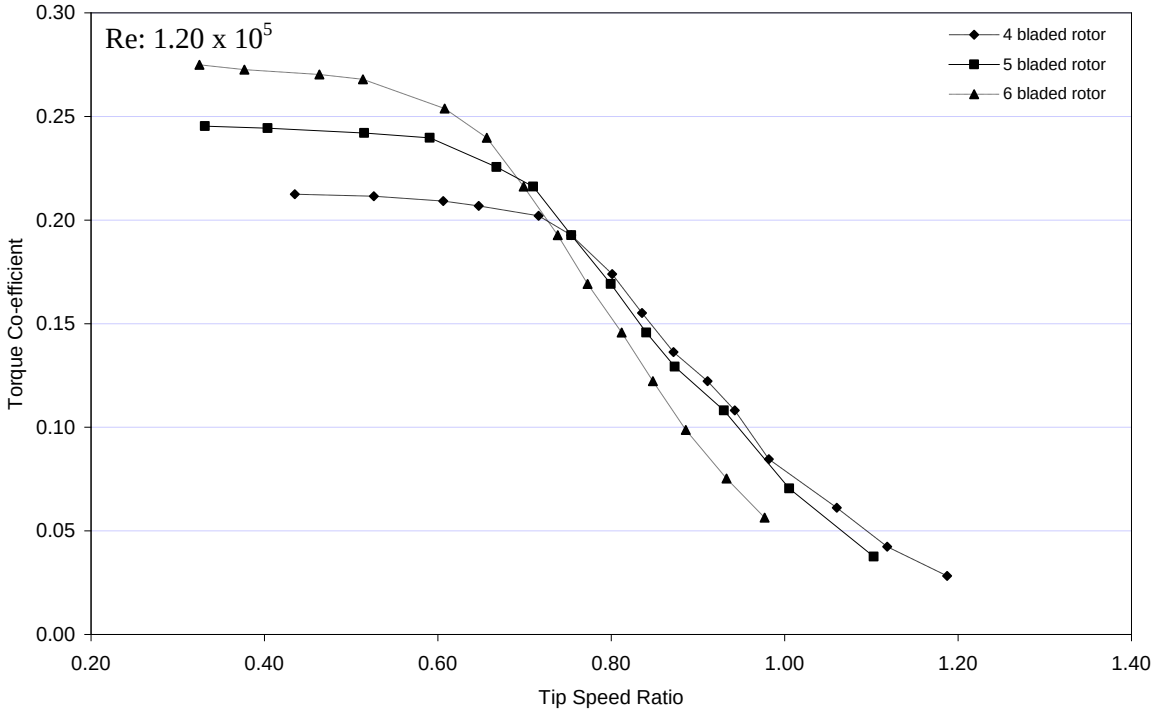

Figure 6.2.15: Comparisons of torque coefficient versus tip speed ratio of 4, 5 and 6 bladed rotors at Reynolds number of 1.20 x 10^5

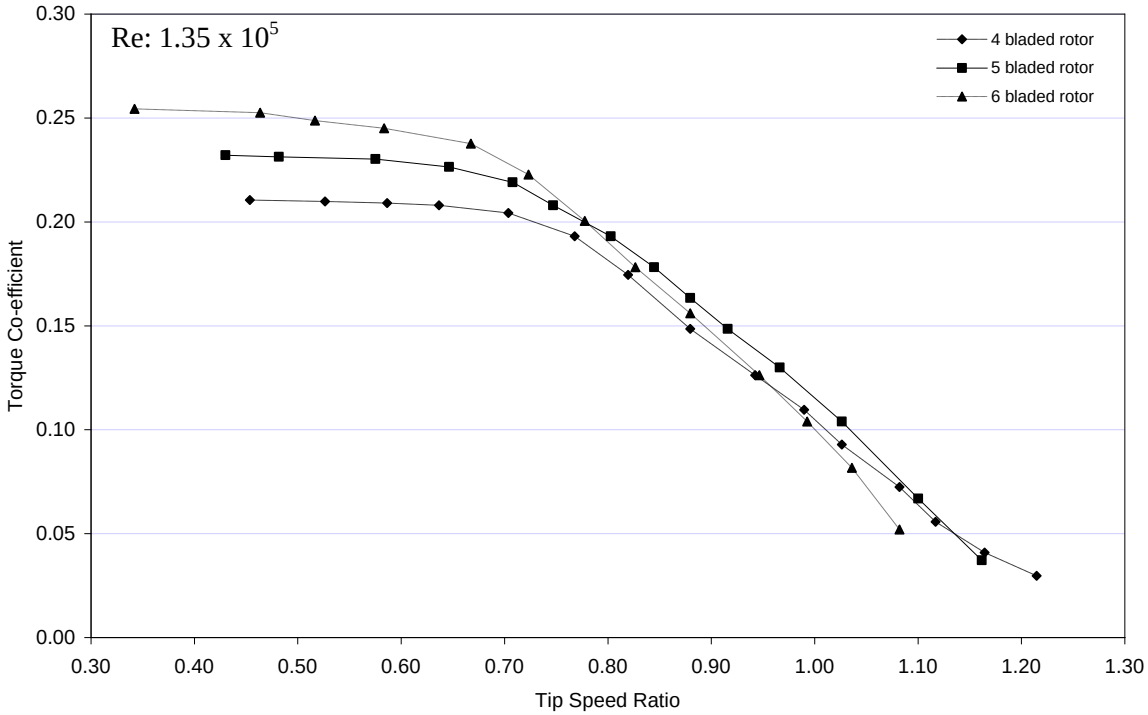

Figure 6.2.16: Comparisons of torque coefficient versus tip speed ratio of 4, 5 and 6 bladed rotors at Reynolds number of 1.35 x 10^5

6.2.3 A Comparative Study between Existing Research Works and Present Experimental Results

In Figures 6.2.17 to 6.2.32 the nature of predicted dynamic aerodynamic characteristics have been analyzed by comparing them with existing research works of Huda et al. [28], Littler [5], Bergeles et al. [17], Bowden et al. [21], Kamal et al. [49] and Ogawa et al. [25].

In Figure 6.2.17 the nature of predicted power co-efficient versus tip speed ratio curves for free stream velocities of 6 and 7 m/s has been compared with the same curve of Huda et al. [28] (without attaching deflecting plate in the experimental setup) for free stream velocity of 6.5 m/s. Here the comparison has been made on the basis of free stream velocity. However, in the case of comparing among predicted power co-efficient versus tip speed ratio curves for the different number of bladed rotors, the comparison was made based upon Reynolds number. This is because the value of Reynolds number depends not only on free stream velocity but also on diameter of the rotor. So, for the same sized rotor, the comparison can be made based upon Reynolds number but for the rotors of different size the comparison should be made based on free stream velocity. From this figure it is seen that there is a close correlation between the values predicted by the present method and those predicted by Huda et al. [28]. In Figure 6.2.17 the nature of all curves are same although because of rotor swept area, blade number, its thickness and shape the curve predicted by Huda et al. is slightly oversize. For the same reason the values of torque co-efficient with respect to tip speed ratio in the curve of Huda et al. of Figure 6.2.18 are slightly higher. However the nature of all curves is almost same. Similarly, in Figures 6.2.19 and 6.2.20 the nature of the curves of power co-efficient versus tip speed ratio and torque co-efficient versus tip speed ratio for the present thesis and for the research works of Huda et al. is same.

Similarly in Figures 6.2.21 to 6.2.32 the variation of results predicted from present thesis for four, five and six bladed S-shaped vane type rotor in terms of power co-efficient versus tip speed ratio at different free stream velocities are compared with the existing research works that coincide with this thesis work. From these figures it is seen that there is a close correlation between the values predicted by the present method and those obtained from the existing research works of Littler [5], Bergeles et al. [17], Bowden et al. [21], Kamal et al. [49] and Ogawa et al. [25]. However, because of the variation in number of blades, free stream velocities, rotor swept area, shape of the blade, its thickness and material the values of torque and power co-efficient with respect to tip speed ratio deviate in magnitude. Yet the nature of all curves in each figure is almost same.

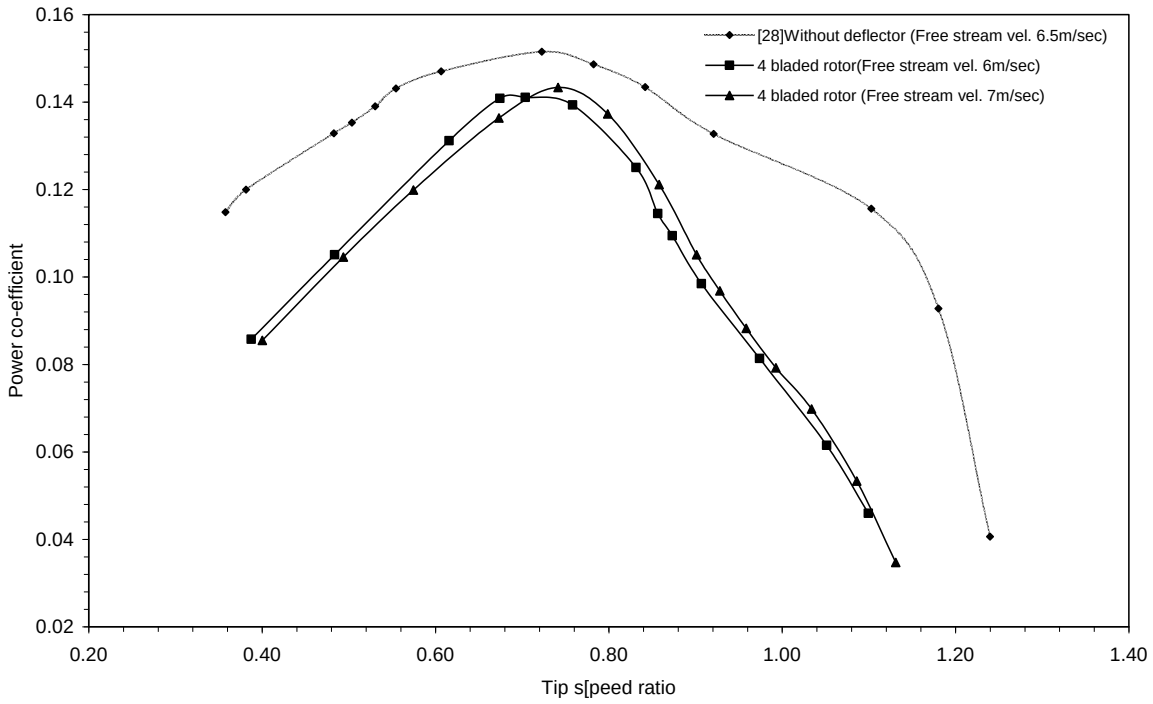

Figure 6.2.17: Comparisons of power coefficient versus tip speed ratio of present and existing experimental results [28]

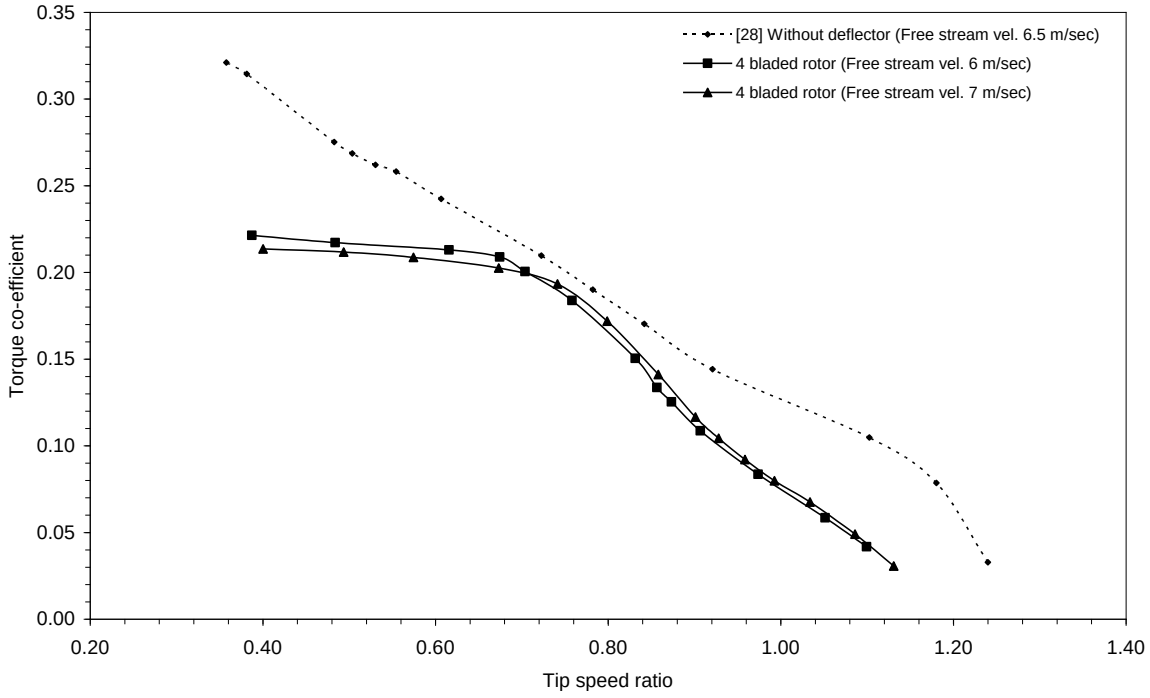

Figure 6.2.18: Comparisons of torque coefficient versus tip speed ratio of present and existing experimental results [28]

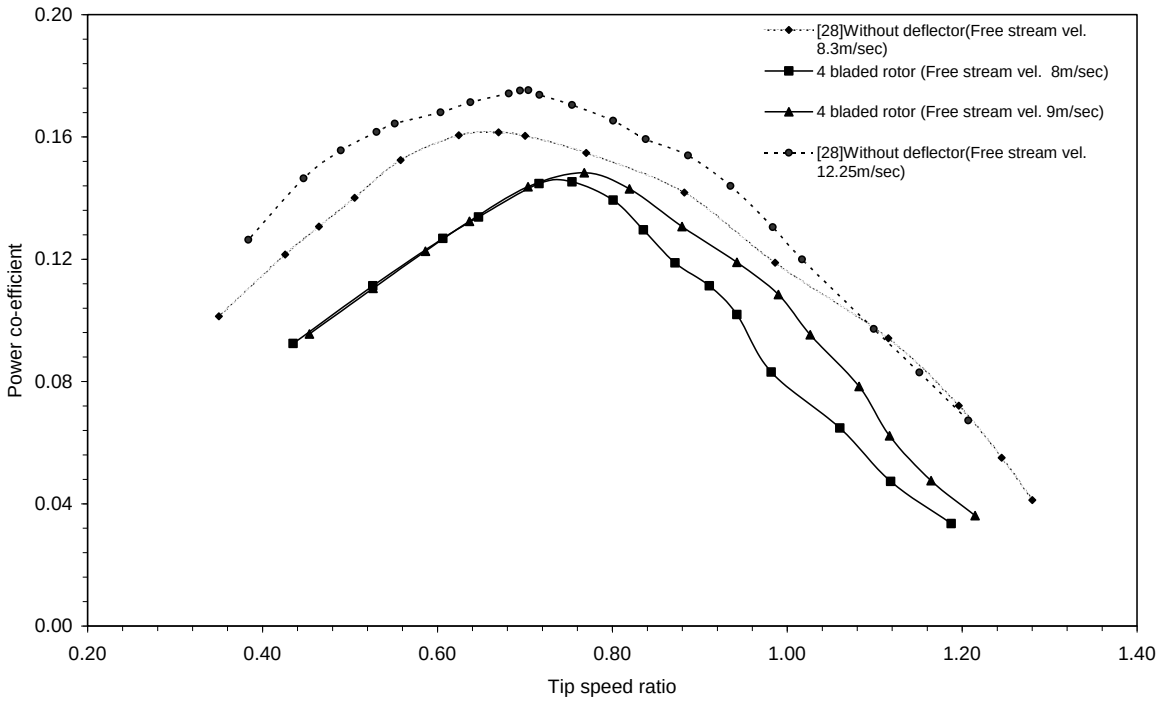

Figure 6.2.19: Comparisons of power coefficient versus tip speed ratio of present and existing experimental results [28]

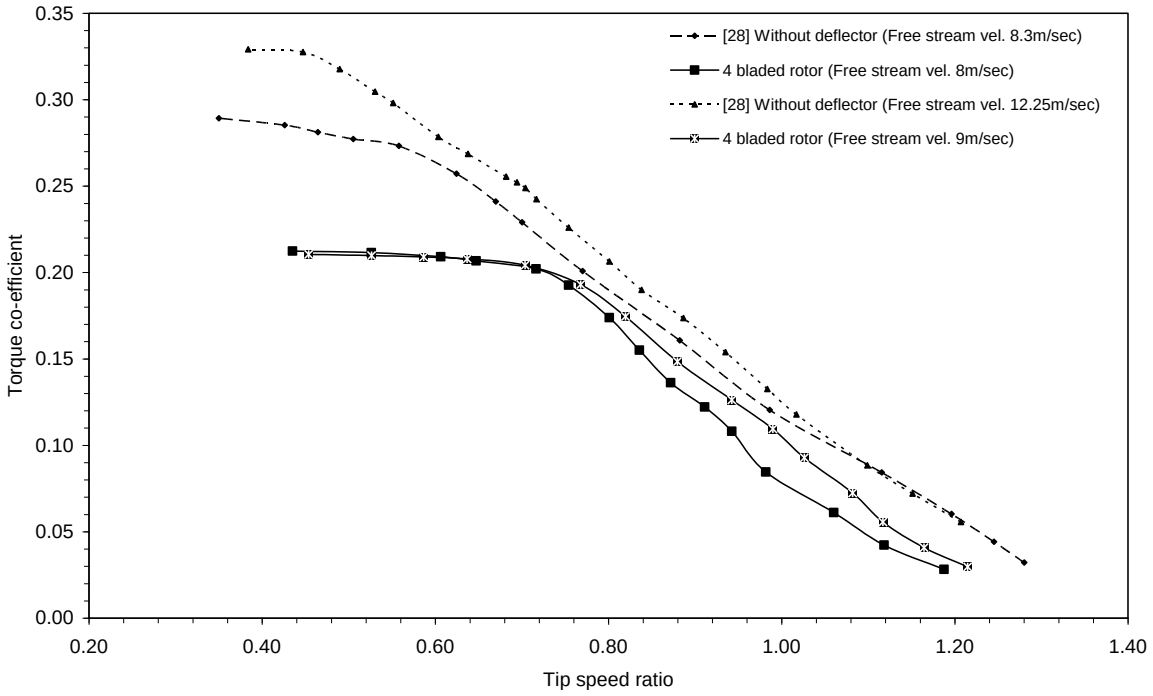

Figure 6.2.20: Comparisons of torque coefficient versus tip speed ratio of present and existing experimental results [28]

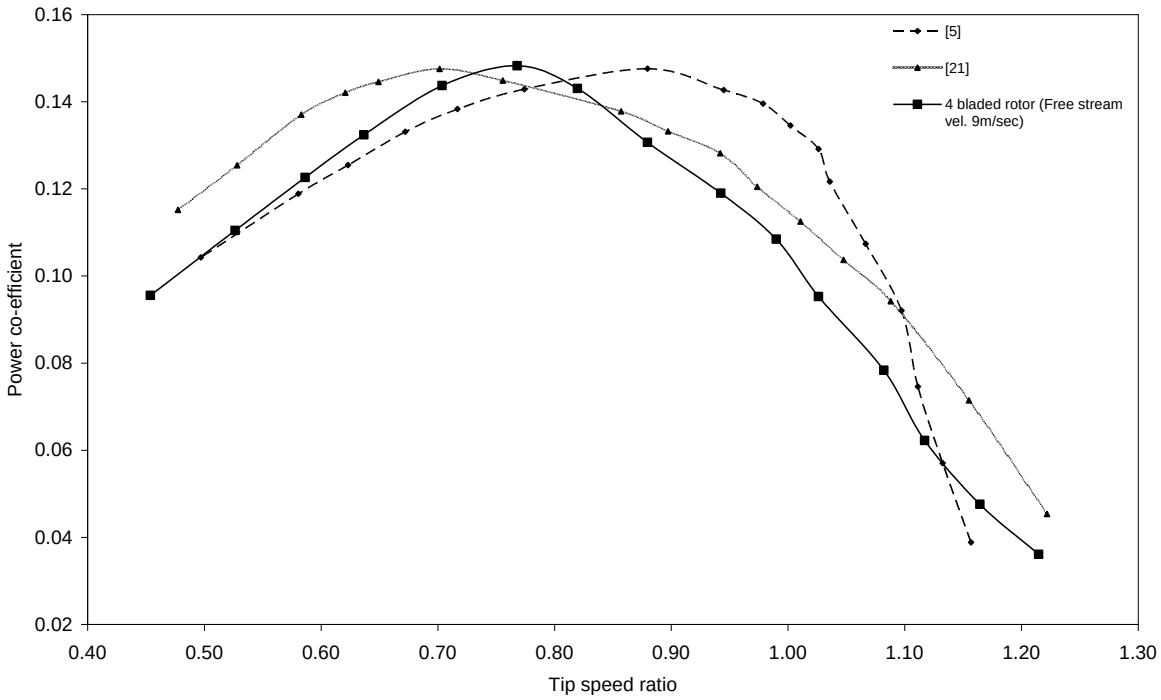

Figure 6.2.21: Comparisons of power coefficient versus tip speed ratio of present and existing experimental results [5, 21]

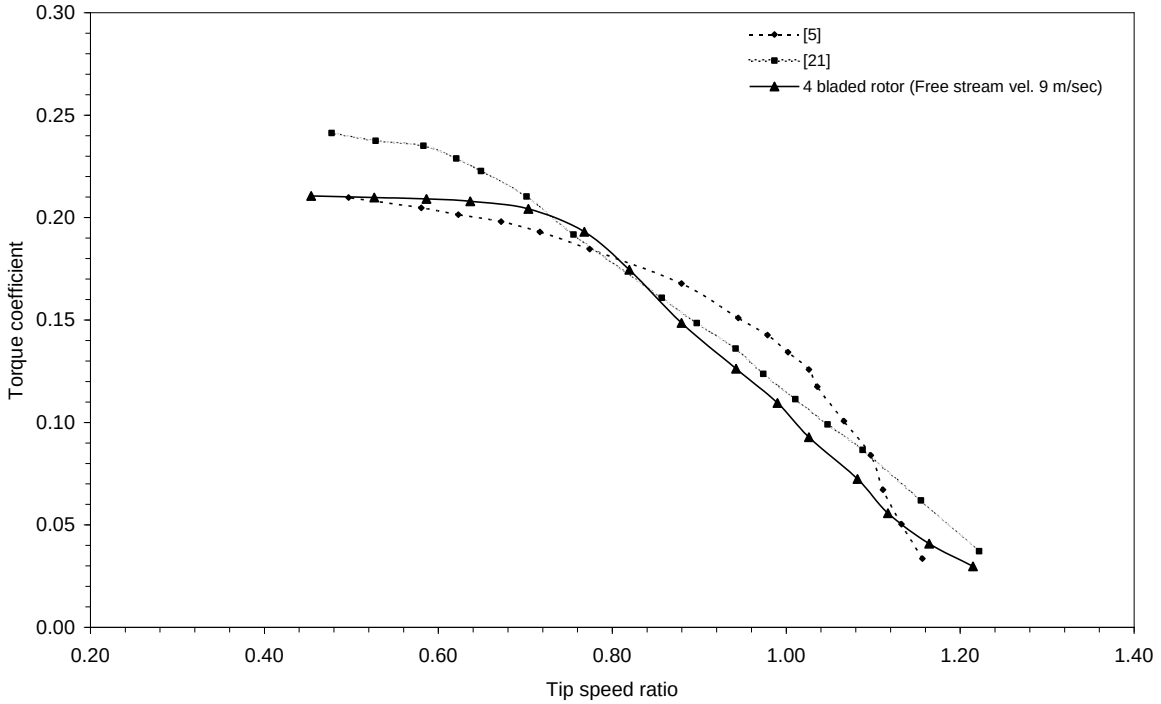

Figure 6.2.22: Comparisons of torque coefficient versus tip speed ratio of present and existing experimental results [5, 21]

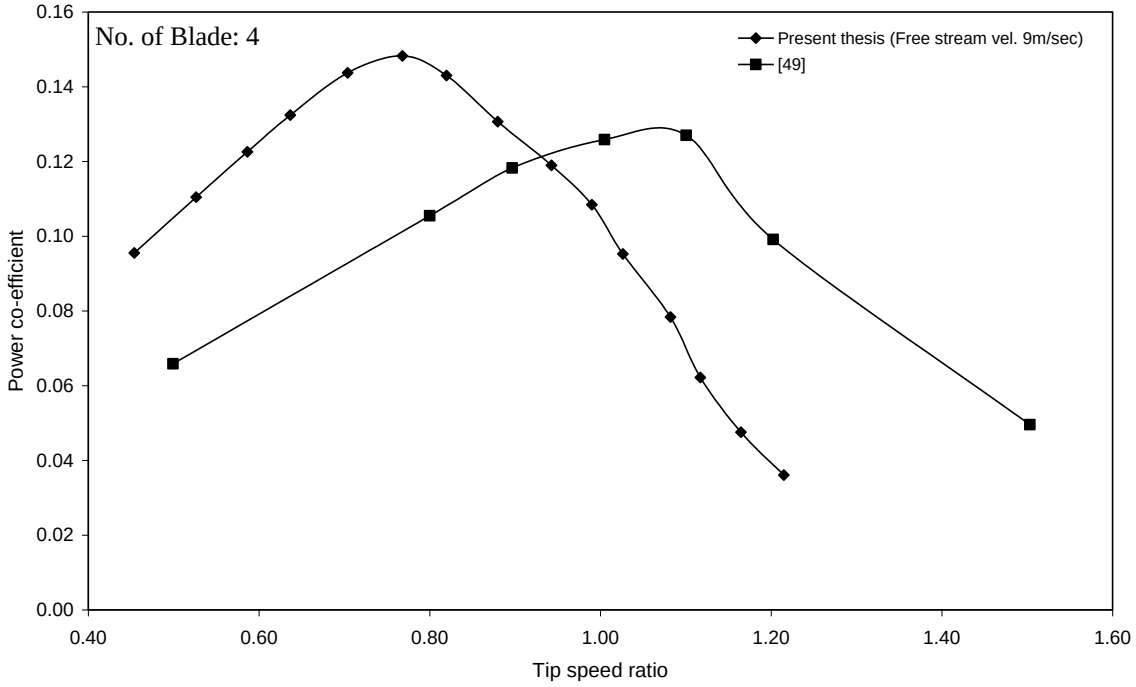

Figure 6.2.23: Comparisons of power coefficient versus tip speed ratio of present and existing experimental results [49] for four bladed rotor

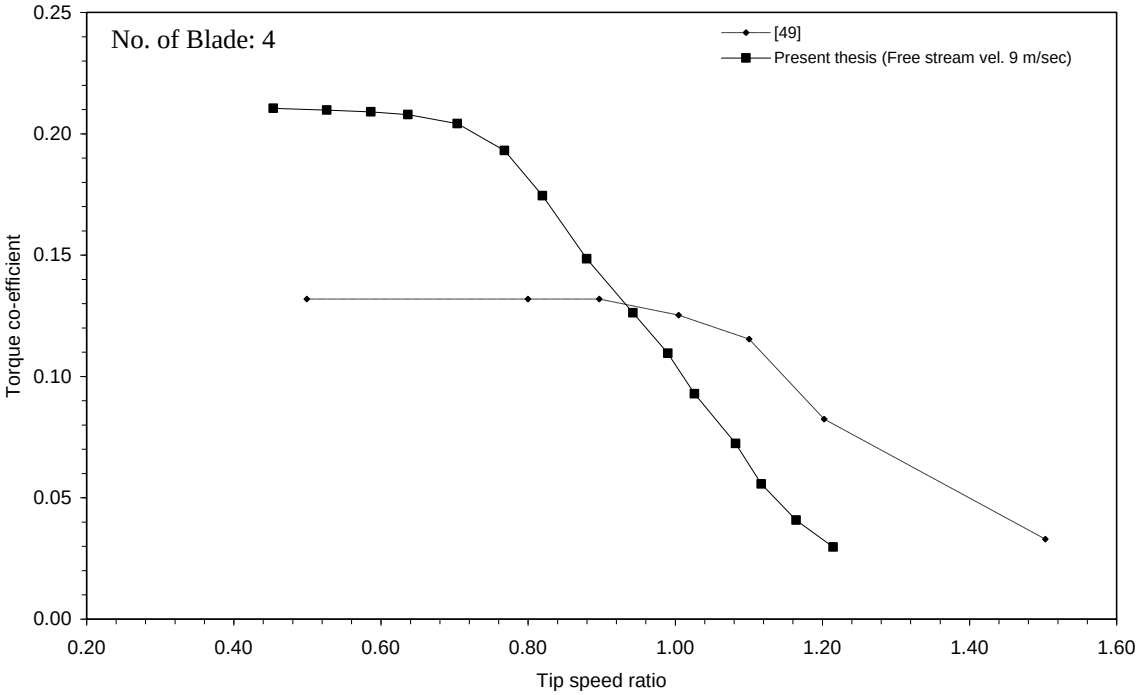

Figure 6.2.24: Comparisons of torque coefficient versus tip speed ratio of present and existing experimental results [49] for four bladed rotor

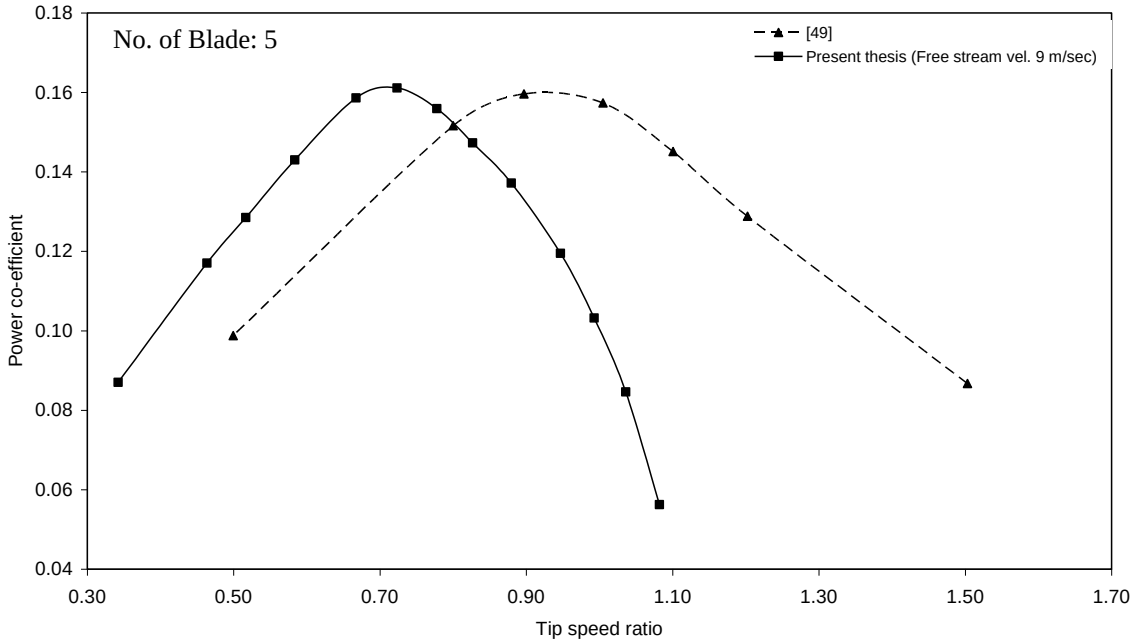

Figure 6.2.25: Comparisons of power coefficient versus tip speed ratio of present and existing experimental results [49] for five bladed rotor

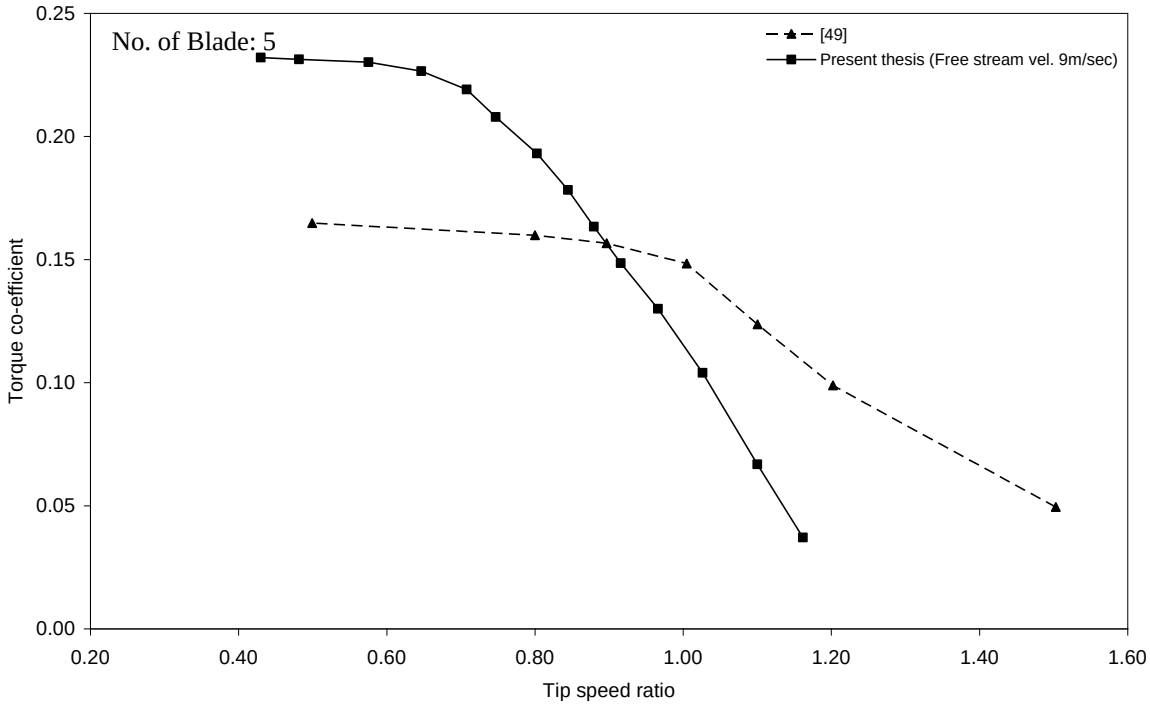

Figure 6.2.26: Comparisons of torque coefficient versus tip speed ratio of present and existing experimental results [49] for five bladed rotor

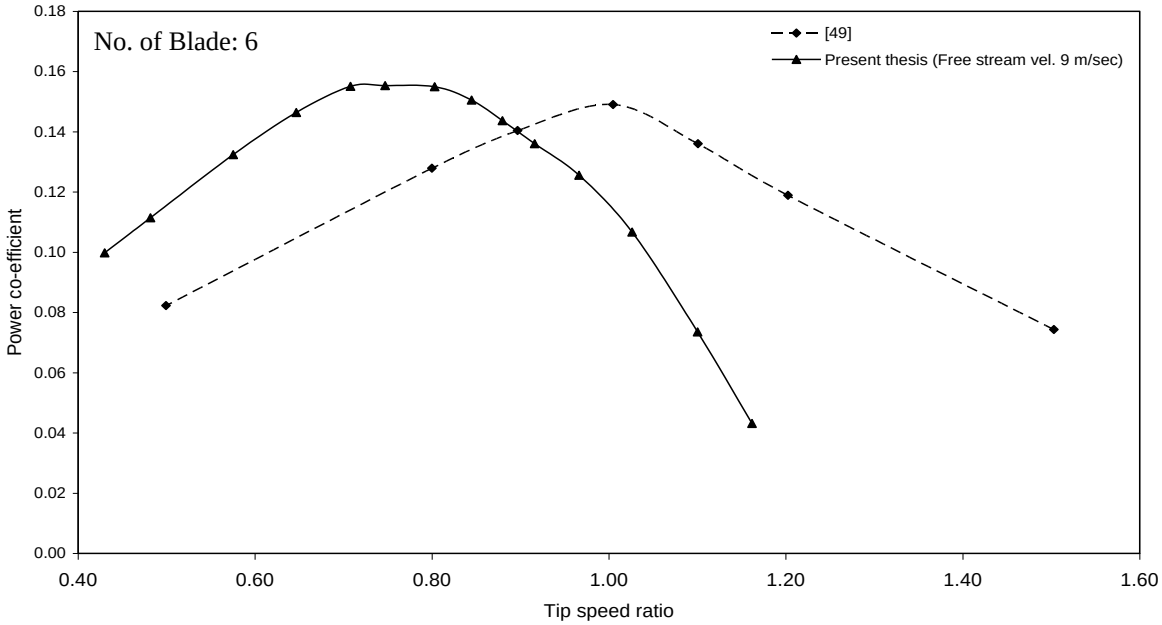

Figure 6.2.27: Comparisons of power coefficient versus tip speed ratio of present and existing experimental results [49] for six bladed rotor

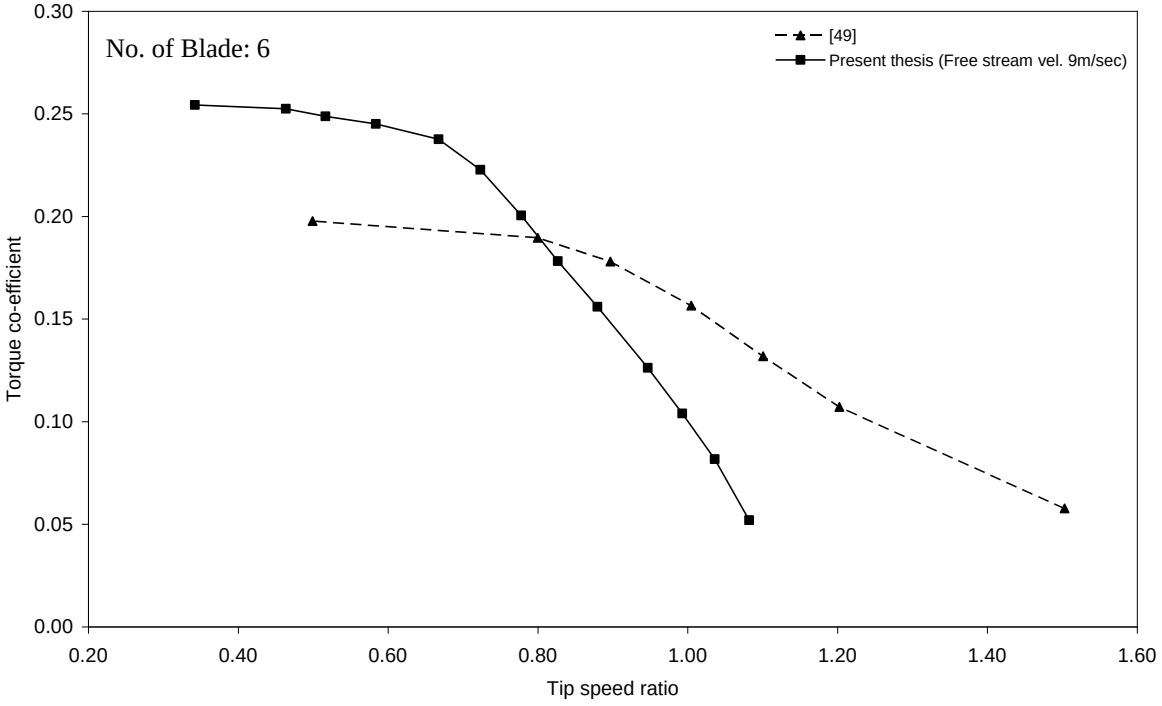

Figure 6.2.28: Comparisons of torque coefficient versus tip speed ratio of present and existing experimental results [49] for six bladed rotor

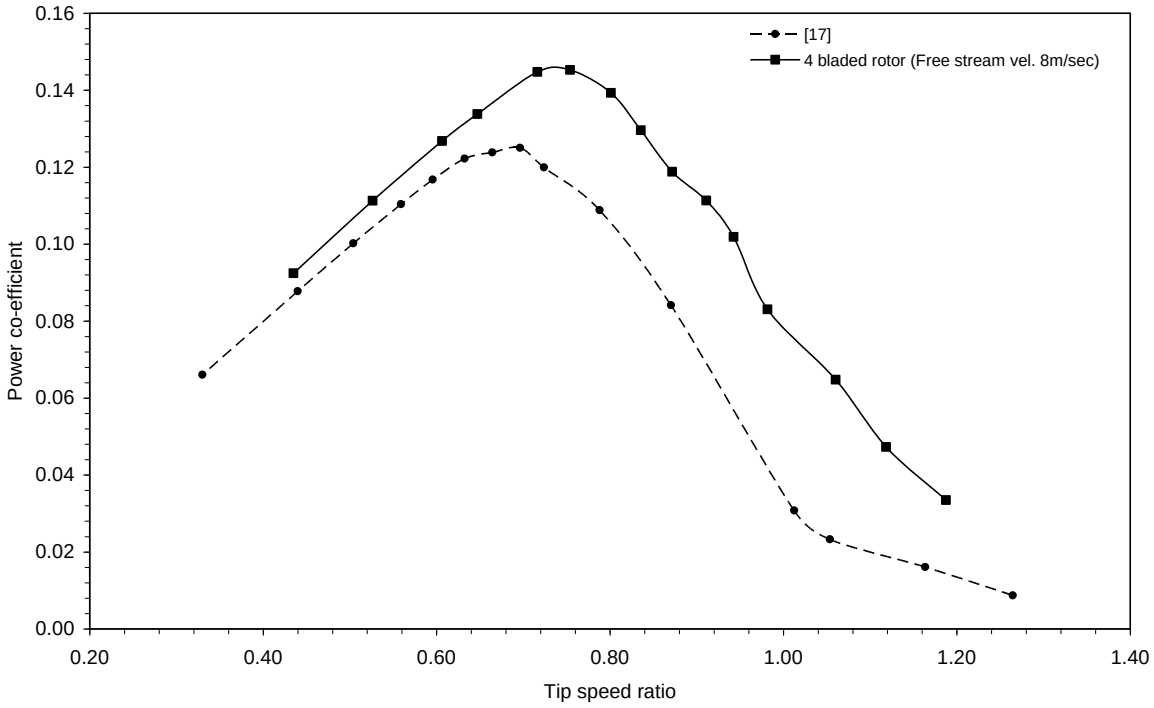

Figure 6.2.29: Comparisons of power coefficient versus tip speed ratio of present and existing experimental results [17]

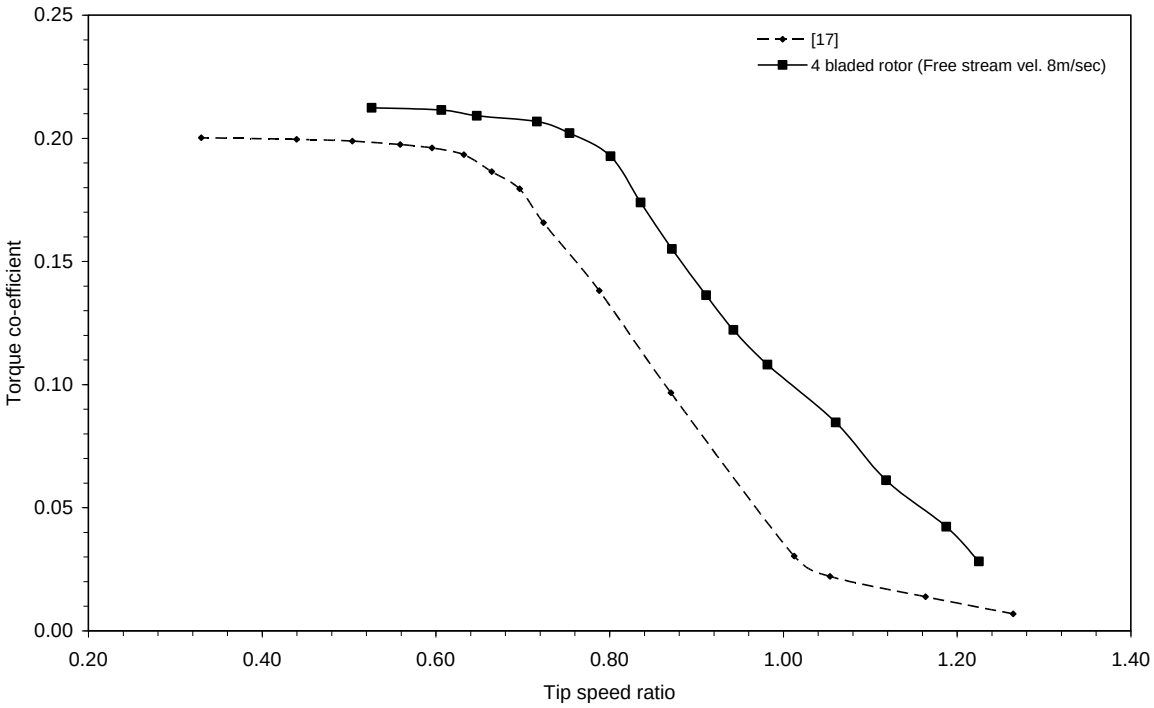

Figure 6.2.30: Comparisons of torque coefficient versus tip speed ratio of present and existing experimental results [17]

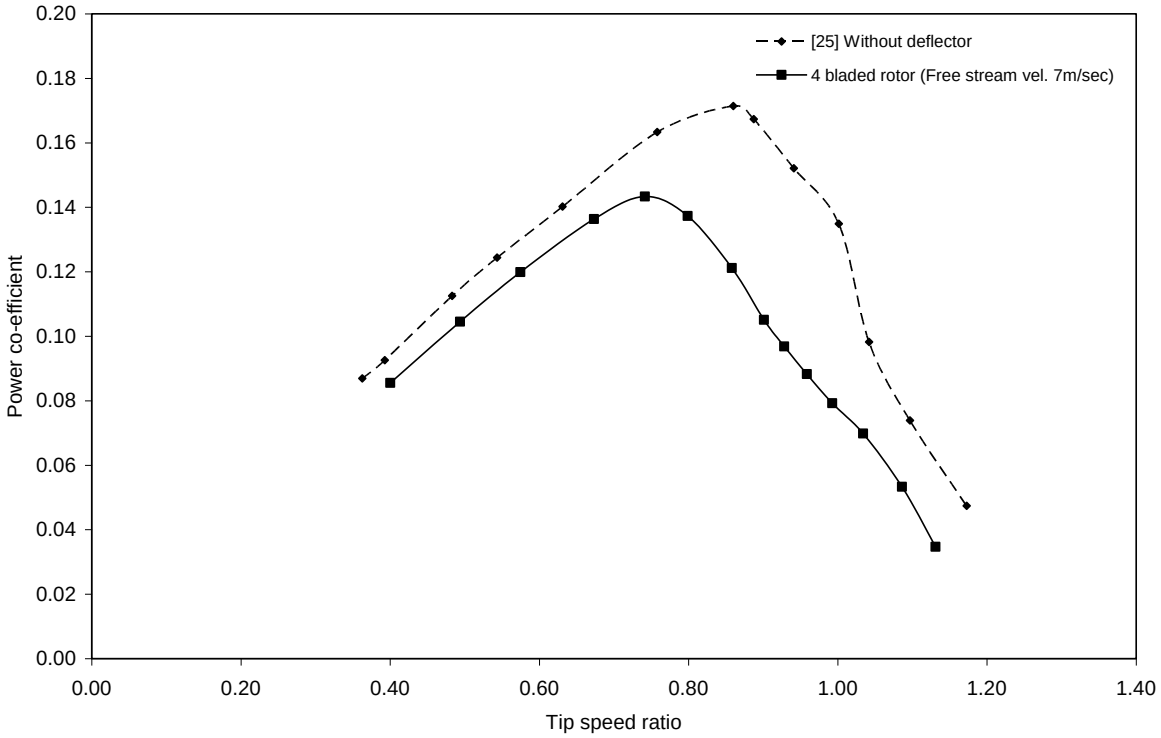

Figure 6.2.31: Comparisons of power coefficient versus tip speed ratio of present and existing experimental results [25]

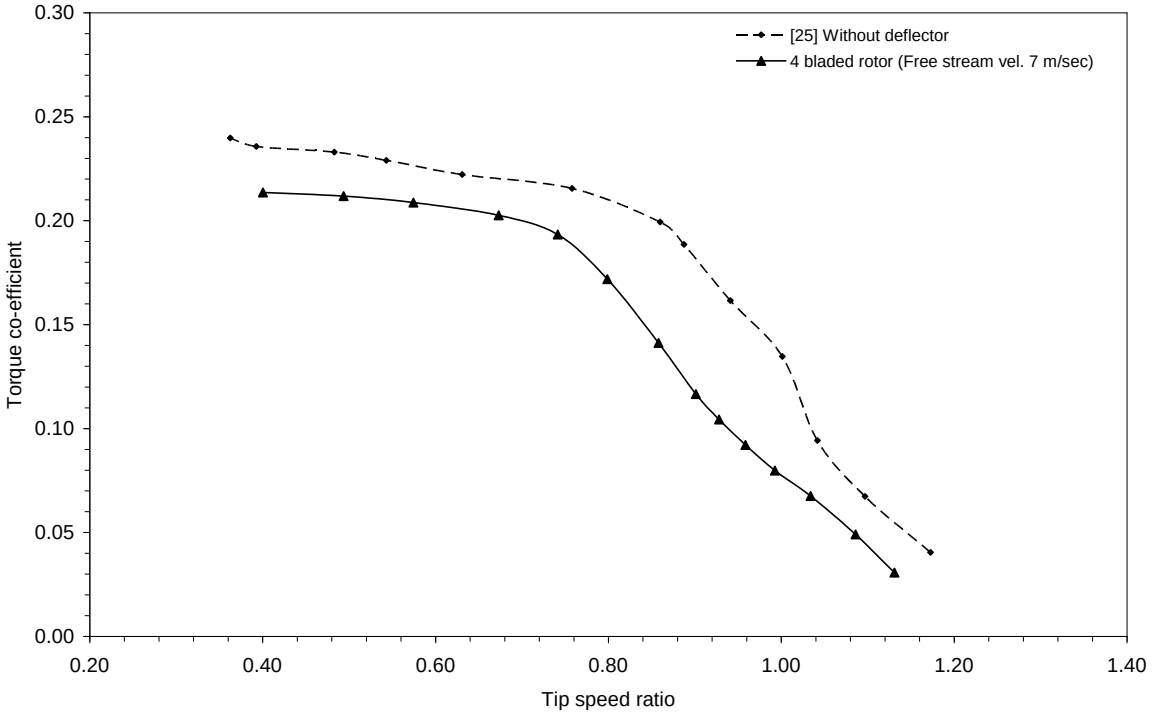

Figure 6.2.32: Comparisons of torque coefficient versus tip speed ratio of present and existing experimental results [25]

Authors	Type of Rotor	Rotor Dia. m	Rotor Height m	Rotor Area m^2	Wind Tunnel Dimensions m x m	Free Stream Velocity m/sec	Reynolds Number x 10^5	Tip Speed Ratio	Corrected Max. Cp%
Littler, R.D. (1975) [5]	S-Shaped	0.14	0.127	0.01778	0.46 x 0.46 Closed section	10	0.93	0.88	14.8
Sheldahl, Blackwell & Feltz (1977) [13]	Savonius	1.0	1.0	1.44	4.9 x 6.1 Closed section	14	9.3	0.85	19.5
Alexander & Holownia (1978) [10]	Savonius	0.383	0.46	0.176	Closed section	6-9	1.53-2.32	0.49	12.5
Baird & Pender (1980) [16]	Savonius	0.076	0.060	0.00456	0.305 x 0.305 Closed section	29.2-24.6	1.04-1.25	0.78	18.1-18.5
Bergeles & Athanassiadis (1982) [17]	Savonius	0.7	1.4	0.98	3.5 x 2.5 Closed section	8	2.8-3.7	0.70	12.5-12.8
Sivasegaram & Sivapalan (1983) [20]	S-Shaped	0.12	0.15	0.018	0.46 x 0.46 Open jet	18	1.44	0.75	20
Bowden & McAleese (1984) [21]	S-Shaped	0.164	0.162	0.0265	Circular 0.76 Open jet	10	0.87-1.09	0.68-0.72	14-15
Ogawa & Yoshida (1986) without deflector [25]	Savonius	0.175	0.3	0.0525	0.8 x 0.6 Open jet	7	0.81	0.86	17
Ogawa & Yoshida (1986) with deflector [25]	Savonius	0.175	0.3	0.0525	0.8 x 0.6 Open jet	7	0.81	0.86	21.2
Huda, Selim, Islam A.K.M.S. and Islam M.Q. (1992) without deflector [28]	S-Shaped	0.185	0.32	0.0555	Circular 0.50 Open jet	6.5-12.25	0.8-1.5	0.68-0.71	15.2-17.5
Huda, Selim, Islam A.K.M.S. and Islam M.Q. (1992) with deflector [28]	S-Shaped	0.185	0.32	0.0555	Circular 0.50 Open jet	6.5-12.25	0.8-1.5	0.68-0.71	17-21
Kamal F.M. (2008) [49]	Vane type	0.20	0.34	0.068	0.46 x 0.48 Open jet	13	1.65	0.9-1.1	12.70-15.96
Present Thesis (4 bladed vane type rotor)	Vane type	0.24	0.35	0.084	0.49 x 0.49 Open jet	5-9	0.75-1.35	0.68-0.77	13.98-14.83
Present Thesis (5 bladed vane type rotor)	Vane type	0.24	0.35	0.084	0.46 x 0.48 Open jet	5-9	0.75-1.35	0.59-0.75	14.21-15.53
Present Thesis (6 bladed vane type rotor)	Vane type	0.24	0.35	0.084	0.46 x 0.48 Open jet	5-9	0.75-1.35	0.50-0.72	14.97-16.11

Table 5.2.1: Performance of Savonius/ S-shaped rotor

Chapter-7

CONCLUSIONS AND RECOMMENDATIONS

7.1 Conclusions

The present study concerns with the dynamic conditions of Multi-bladed S-shaped Vane Type rotor at different Reynolds number. For the purpose of analyzing the dynamic conditions of rotor, the rpm of multi-bladed rotor at different loading conditions and the difference in tensions between two ends of the friction belt for different Reynolds number were measured. Finally from these data, the changes in tip Speed Ratio, power co-efficient and torque coefficient with the increase in load in the load carrying plate were determined at different Reynolds number of multi-bladed rotor. From the study, analysis and results of this research work, the following conclusions can be made:

1. For any particular bladed rotor, it is observed that the maximum power co-efficient is affected by changing the Reynolds number. For comparatively higher value of Reynolds number the value of maximum power coefficient is comparatively higher and it is shifted towards the higher value of tip speed ratio as the Reynolds number is increased. So, it can be concluded that the increase of Reynolds number make the nature of power co-efficient versus tip speed ratio curve slightly sharper.

2. For the same Reynolds number, it is observed that the maximum power co-efficient is affected by increasing no of blades. It is seen that with the increase in number of blades the maximum value of power coefficient also increases and it is shifted towards the lower value of tip speed ratio.

3. It can be concluded from the present study that by increasing the number of blades of rotor, the power output can be increased. However, there is an optimum limit that depends on the size and shape of the blades. Simultaneously, it can be said that by increasing Reynolds number, the power output can be increased. Thus it can be concluded that by increasing the number of blades of rotor to the optimum limit considering all significant factors and at the same time by increasing its Reynolds number, the power output can be increased to its maximum level.

4. For any particular bladed rotor the maximum torque co-efficient is affected by changing the Reynolds number. At higher Reynolds number the value of maximum torque co-efficient is slightly lower. So, it can be said that the increases in Reynolds

number make the nature of the torque co-efficient versus tip speed ratio curve slightly blunt.

5. At the same Reynolds number for rotor having higher number of blades the maximum value of torque coefficient is also higher and it is shifted towards the lower value of tip speed ratio. That means, the increases in number of blades make the nature of torque co-efficient versus tip speed ratio curve sharper. This point is very important for driving the irrigation pump especially positive displacement pump which needs higher starting torque.

6. It is seen that there is a close correlation between the values predicted by the present method and those obtained from the existing research works of Huda et al. [28], Littler [5], Bergeles et al. [17], Bowden et al. [21], Kamal et al. [49] and Ogawa et al. [25]. However, because of the variation in no. of blades, free stream velocities, rotor swept area, shape of the blade, its thickness and material the values of torque and power co-efficient with respect to tip speed ratio deviates in magnitude. Yet the nature of all curves in each figure (showing comparison among the nature of predicted dynamic aerodynamic characteristics and similar research works) is same.

7.2 Recommendations

1. The same experiment may be done with rotors having different shapes of blade.

2. Flow visualization technique can be applied to observe the separation.

3. Further detailed research could be conducted in this field at other Reynolds numbers.

REFERENCES

[1] Templin, R.J., "Aerodynamic Performance Theory for the NRC Vertical-Axis Wind Turbine", National Research Council of Canada, Report LTR-LA-160, June 1974.

[2] Wilson, R.E. and Lissaman, P.B.S., "Applied Aerodynamics of Wind Power Machines", Oregon State University, 1974.

[3] Park, J. "Simplified Wind Power System for Experimenters" , Helion Inc., California, USA, 1975.

[4] Strickland, J.H., "The Darrieus Turbine: A Performance Prediction Model using Multiple Streamtubes, Sandia Laboratories Report", SAND75-0431, 1975.

[5] Littler, R.D., "Further Theoretical and Experimental Investigation of the Savonius Rotor", B.E. Thesis, University of Queensland, 1975.

[6] Swamy, N.V.C. and Fritzsche, A.A., "Aerodynamic Studies on Vertical Axis Wind Turbine", International Symposium on Wind Energy Systems, Cambridge, England, September 7-9, 1976.

[7] Fanucci, J.B. and Watters, R.E., "Innovative Wind Machines: The Theoretical Performance of a Vertical-Axis Wind Turbine", Proceedings of the Vertical-Axis Wind Turbine Technology Workshop, Sandia Laboratories, SAND 76-5586, P.P. III-61-95, 1976.

[8] Holme, O., "A Contribution to the Aerodynamic Theory of the Vertical Axis Wind Turbine", Proceedings of the International Symposium on Wind Energy Systems, Cambridge, p.p. C4-55-72, 1976.

[9] Jansen, W.A.M. and Smulders, P.T., "Rotor Design for Horizontal Axis Windmills", Steering Committee for Wind Energy in Developing Countries (SWD), P.O. Box 85, Amersfoort, The Netherlands, 1977.

[10] Sheldahi, R.E., Blackwell, B.F. and Feltz, L.V., "Wind Tunnel Performance Data for Two and Three Bucket Savonius Rotors", Journal of Energy, vol.2, No.3, 1977.

[11] Lysen, E.H., Bos, H.G. and Cordes, E.H., "Savonius Rotors for Water Pumping", SWD publication, P.O. Box 85, Amersfoort, The Netherlands, 1978.

[12] Beurskens, H.J.M., "Feasibility Study of Windmills for Water Supply in Mara Region, Tanzania", Steering Committee on Wind Energy for Developing Countries (SWD), P.O. Box 85, Amersfoort, The Netherlands, 1978.

[13] Alexander, A.J. and B.P. Holownia, "Wind Tunnel Tests on a Savonius Rotor", J. Industrial Aerodynamics, vol. 3, 1978.

[14] Beurskens, H.J.M., "Low Speed Water Pumping Wind Mills: Rotor Tests and Overall Performance"' Proc. of 3rd Int. Symp. On Wind Energy Systems, Copenhagen, Denmark, August 26-29, pp K2 501-520, 1980.

[15] Noll, R.B. and Ham, N.D., "Analytical Evaluation of the Aerodynamic Performance of a Hi-Reliability Vertical-Axis Wind Turbine", Proceedings of AWEA National Conference, 1980.

[16] Baird, J.P. and Pender, S.F., "Optimization of a Vertical Axis Wind Turbine for Small Scale Applications, 7th Australian Hydraulic and Fluid Mechanics Conference, Brisbane, 1980.

[17] Bergeles, G. and Athanassiadis N., "On the Flow Field of the Savonius Rotor", Journal of Wind Engineering, vol. 6, 1982.

[18] Lysen, E.H., "Introduction to Wind Energy", 2nd Edition, SWD Publication, P.O. Box 85, Amersfoort, The Netherlands, 1983.

[19] Paraschivoiu, I. and Delclaux, F., "Double Multiple Stream Tube Model with Recent Improvements", Journal of Energy, vol. 7, no. 3, p.p. 250-255, 1983.

[20] Sivasegaram, S. and Sivapalan, S., "Augmentation of Power in Slow Running Vertical Axis Wind Rotors using Multiple Vanes", Journal of Wind Engineering, vol. 7, no. 1, 1983.

[21] Bowden, G.J. and McAleese, S.A., "The Properties of Isolated and Coupled Savonius Rotors", Journal of Wind Engineering, vol. 8, no. 4, pp. 271-288, 1984.

[22] Paraschiviu, I., Fraunic, P. and Beguier, C., "Stream Tube Expansion Effects on the Darrieus Wind Turbine", Journal of Propulsion, vol. 1, no. 2, pp. 150-155, 1985.

[23] Mandal, A.C., "Aerodynamics and Design Analysis of Vertical Axis Darrieus Wind Turbine", Ph.D. Thesis Vrije University Brussel, Belgium 1986.

[24] Sawada, T., Nakamura, M. and Kamada, S., "Blade Force Measurement and Flow Visualization of Savonius Rotors", Bull. JSME. Vol.29, pp. 2095-2100, 1986.

[25] Ogawa, T. and Yoshida, H., "The Effects of a Deflecting Plate and Rotor End Plates", Bulletin of JSME, vol. 29, no. 253, pp. 2115-2121, 1986.

[26] Aldos, T.K. and Obeidat, K.M., "Performance Analysis of Two Savonius Rotors Running Side by Side Using The Discrete Vortex Method", Wind Engineering, Vol. 11, No. 5, 1987.

[27] Gavalda, J., Massons, J. and Diaz, F., "Drag and Lift Coefficients of the Savonius Wind Machine", Wind Engineering, Vol. 15, pp. 240-246, 1991.

[28] Huda, M.D., Selim, M.A., Islam, A.K.M.S. and Islam, M.Q., "The Perfomance of an S-Shaped Savonius Rotor with a Deflecting Plate" RERIC International Energy Journal: Vol. 14, No. 1, pp. 25-32, June 1992.

[29] Islam, A.K.M.S., Islam, M.Q., Mandal, A.C. and Razzaque, M.M. "Aerodynamic Characteristics of a Stationary Savonius Rotor", RERIC Int. Energy Journal, Vol. 15, No. 2, pp. 125-135, 1993.

[30] Islam, A.K.M.S., Islam, M.Q., Razzaque, M.M. and Ashraf, R., "Static Torque and Drag Characteristics of an S-Shaped Savonius Rotor and Prediction of Dynamic Characteristics", Wind Engineering, Vol. 19, No. 6, U.K., 1995.

[31] Burton, J.D., Hijazin, M. and Rizvi, S., "Wind and Solar Driven Reciprocating Lift Pumps", Journal of Wind Engineering. Vol.15, No. 2: pp 95-108, 1995.

[32] Fujisawa, N., "Velocity Measurements and Numerical Calculations of Flow Fields in and around Savonius Rotors" Journal of Wind Engineering and Industrial Aerodynamics, Vol. 59, Issue 1, Pages 39-50, January 1996.

[33] Rasmussen, F., Petersen, J.T., Volund, P., Leconte, P., Szechenyi, E., Westergaard, C., "Soft Rotor Design for Flexible Turbines" Research funded in part by THE EUROPEAN COMMISSION in the framework of the Non Nuclear Energy Programme JOULE 3.EC, 1998.

[34] Spera, D. A., "Wind Turbine Technology", ASME Press, 1998

[35] Patel, M.R., Wind and Solar Power Systems, CRC Press, NY, 1999.

[36] Rahman, M., "Aerodynamic Characteristics of a Three Bladed Savonius Rotor", M.Sc. Engg. Thesis, Dept of Mechanical Engg., BUET, 2000.

[37] Ammara, I., Leclerc, L., and Masson, C., "A Viscous Three Dimensional Differential/ Actuator-Disk Method for the Aerodynamic Analysis of Wind Farms," Journal of Solar Energy Engineering, vol. 124, pp. 345 - 356, November, 2002.

[38] Bhuiyan, H. K, "Aerodynamic Characteristics of a Four Bladed Savonius Rotor", M.Sc. Engg. Thesis, Dept of Mech. Engg., BUET, 2003.

[39] Iida, A., Mizuno, A. and Fukudome, K., "Numerical Simulation of Aerodynamic Noise Radiated form Vertical Axis Wind Turbines", Proceedings of the 18 International Congress on Acoustics, 2004.

[40] Hyosung, S. and Soogab, L. "Response Surface Approach to Aerodynamic Optimization Design of Helicopter Rotor Blade" Vol. 64, no. 1, pp. 125-142 [18 page(s) (article)] (19 ref.), 2005.

[41] Cooper P. and Kennedy O., "Development and Analysis of a Novel Vertical Axis Wind Turbine" University of Wollongong, Wollongong, 3, 2005.

[42] Song, S.H., Jeong, B.C., Lee, H.I., J.J., Oh, J.H. and Venkataramanan, G., "Emulation of Output Characteristics of Rotor Blades using a Hardware –in-loop Wind Turbine Simulator" Volume 3, Issue, Page(s): 1791-1796, 6-10 March 2005.

[43] Saha, U.K. and Rajkumar, M.J., "On the performance analysis of Savonius rotor with twisted blades" Department of Mechanical Engineering, Indian Institute of Technology Guwahati, Guwahati-781 039, August 2005.

[44] Islam, M.Q., Hasan, M.N. and Saha, S., "Experimental Investigation of Aerodynamic Characteristics of Two, Three and Four Bladed S-Shaped Stationary Savonius Rotors" Proceedings of the International Conference on Mechanical Engineering (ICME05-FL-23), Dhaka-1000, Bangladesh, 28- 30 December 2005.

[45] Maeda, T. and Kawabuchi, H., "Effect of Wind Shear on the Characteristics of a Rotating Blade of a Field Horizontal Axis Wind Turbine" Journal of Fluid Science and Technology, Vol. 2, No. 1 pp. 152-162, 2007.

[46] Gupta, R., Biswas, A. and Sharma K.K., "Comparative study of a three-bucket Savonius rotor with a combined three-bucket Savonius–three-bladed Darrieus rotor" Department of Mechanical Engineering, National Institute of Technology (NIT), Silchar 788 010, Assam, India, December 2007.

[47] Saha, U.K. and Maity, D., "Optimum Design Configuration of Savonius Rotor through Wind Tunnel Experiments", Journal of Wind Engineering and Industrial Aerodynamics, Volume 96, Issues 8-9, Pages 1359-1375, August-September 2008.

[48] Ajedegba, J.O., "Effects of Blade Configuration on Flow Distribution and Power Output of a Zephyr Vertical Axis Wind Turbine", M.Sc. Engg. Thesis, Dept of Mech. Engg., The Faculty of Engineering and Applied Science, University of Ontario Institute of Technology, July, 2008.

[49] Kamal, F.M. and Islam, M.Q., "Aerodynamic Characteristics of a Stationary Five Bladed Vertical Axis Vane Type Wind Turbine" Journal of Mechanical Engineering, Vol. ME39, No. 2, IEB, December 2008.

APPENDICES

Appendix-A

Experimental Data and Characteristic Curve

Four Bladed Vertical Axis Vane Type Rotor

Reynolds number 0.75×10^5		
Tip speed ratio, λ	Power Co-efficient	Torque Co-efficient
1.1058	0.0000	0.0000
0.9927	0.0478	0.0481
0.8947	0.0753	0.0842
0.8470	0.0917	0.1083
0.8143	0.1078	0.1323
0.7867	0.1230	0.1564
0.7188	0.1383	0.1925
0.6836	0.1398	0.2045
0.5781	0.1217	0.2105
0.5353	0.1159	0.2165
0.4901	0.1073	0.2189
0.4197	0.0934	0.2225
0.3644	0.0820	0.2250

Variation of power coefficient with tip speed ratio at Reynolds number of 0.75×10^5 for Four Bladed S-shaped Rotor

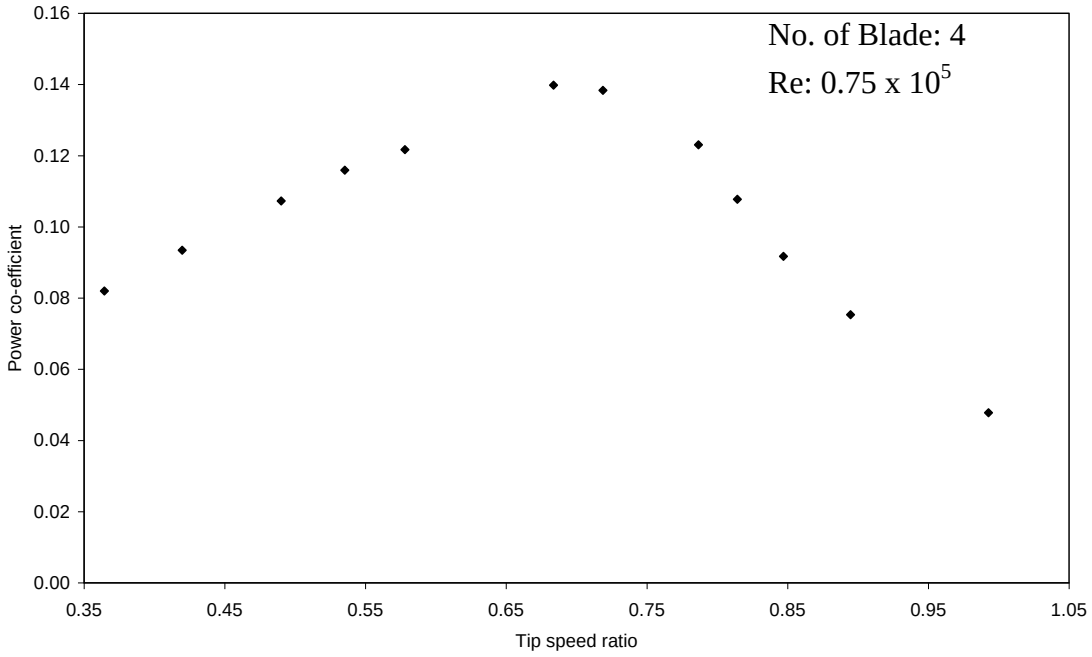

Variation of torque coefficient with tip speed ratio at Reynolds number of 0.75×10^5 for Four Bladed S-shaped Rotor

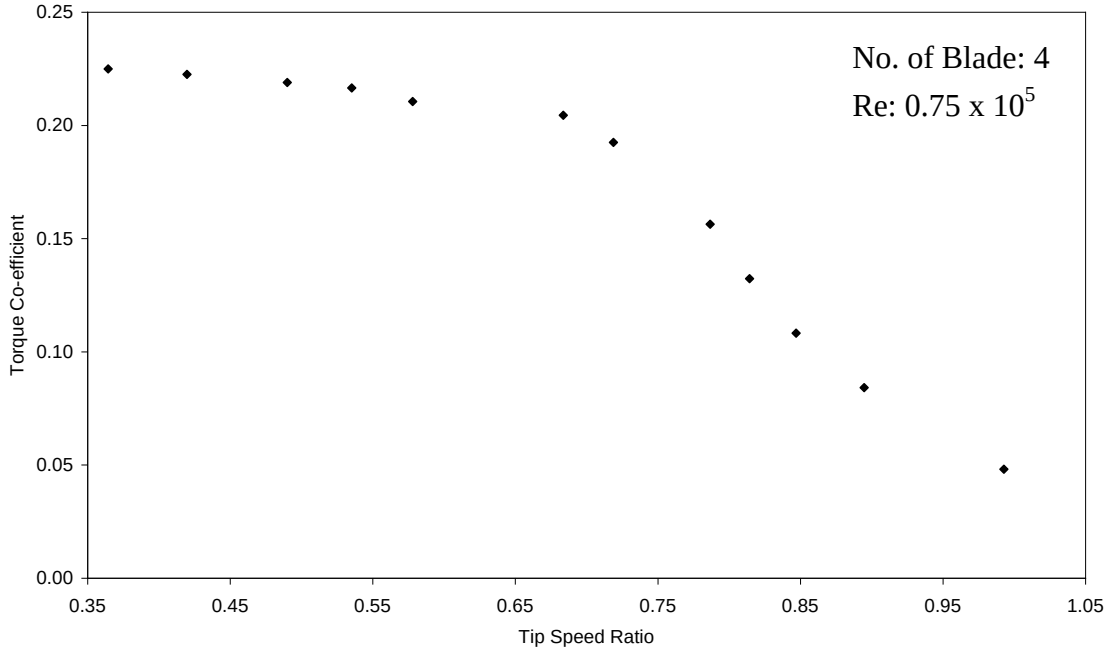

Four Bladed Vertical Axis Vane Type Rotor

Reynolds number 0.90 x 10^5		
Tip speed ratio, λ	Power Co-efficient	Torque Co-efficient
1.1519	0.0000	0.0000
1.0996	0.0459	0.0418
1.0514	0.0615	0.0585
0.9739	0.0814	0.0835
0.9069	0.0985	0.1086
0.8734	0.1094	0.1253
0.8566	0.1145	0.1337
0.8315	0.1250	0.1504
0.7582	0.1393	0.1838
0.7037	0.1411	0.2005
0.6744	0.1408	0.2088
0.6158	0.1312	0.2130
0.4838	0.1051	0.2172
0.3875	0.0858	0.2214

Variation of power coefficient with tip speed ratio at Reynolds number of 0.90×10^5 for Four Bladed S-shaped Rotor

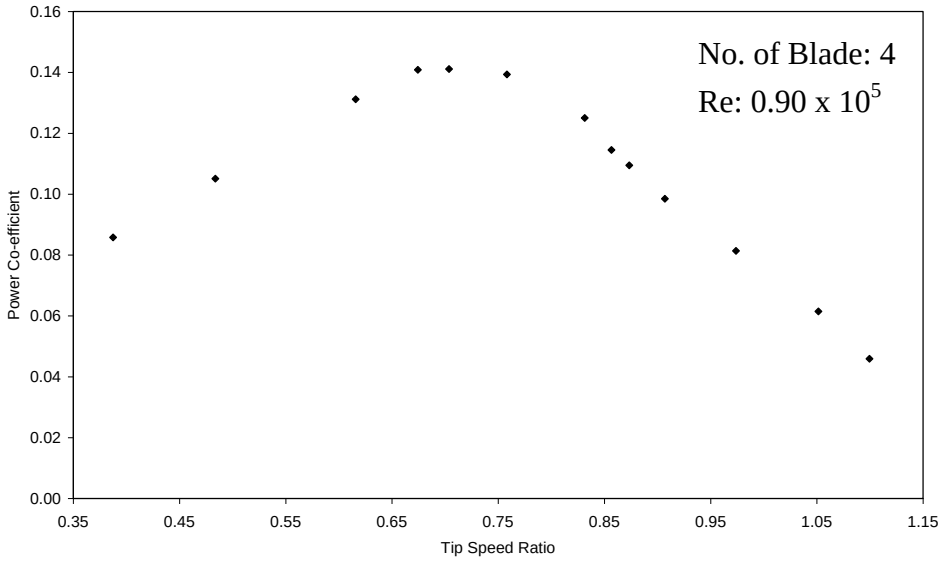

Variation of torque coefficient with tip speed ratio at Reynolds number of 0.90×10^5 for Four Bladed S-shaped Rotor

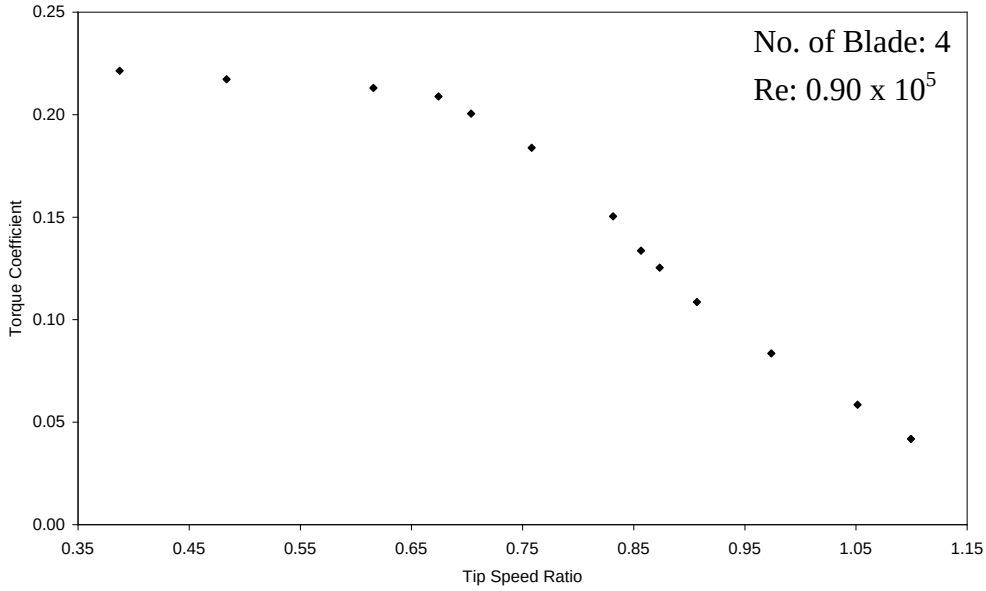

Four Bladed Vertical Axis Vane Type Rotor

Reynolds number 1.05×10^5		
Tip speed ratio, λ	Power Co-efficient	Torque Co-efficient
1.1579	0.0000	0.0000
1.1310	0.0347	0.0307
1.0861	0.0533	0.0491
1.0340	0.0698	0.0675
0.9927	0.0792	0.0798
0.9586	0.0883	0.0921
0.9281	0.0968	0.1043
0.9012	0.1051	0.1166
0.8581	0.1211	0.1412
0.7989	0.1373	0.1718
0.7414	0.1433	0.1933
0.6732	0.1363	0.2025
0.5745	0.1199	0.2087
0.4937	0.1045	0.2117
0.4003	0.0855	0.2136

Variation of power coefficient with tip speed ratio at Reynolds number of 1.05×10^5 for Four Bladed S-shaped Rotor

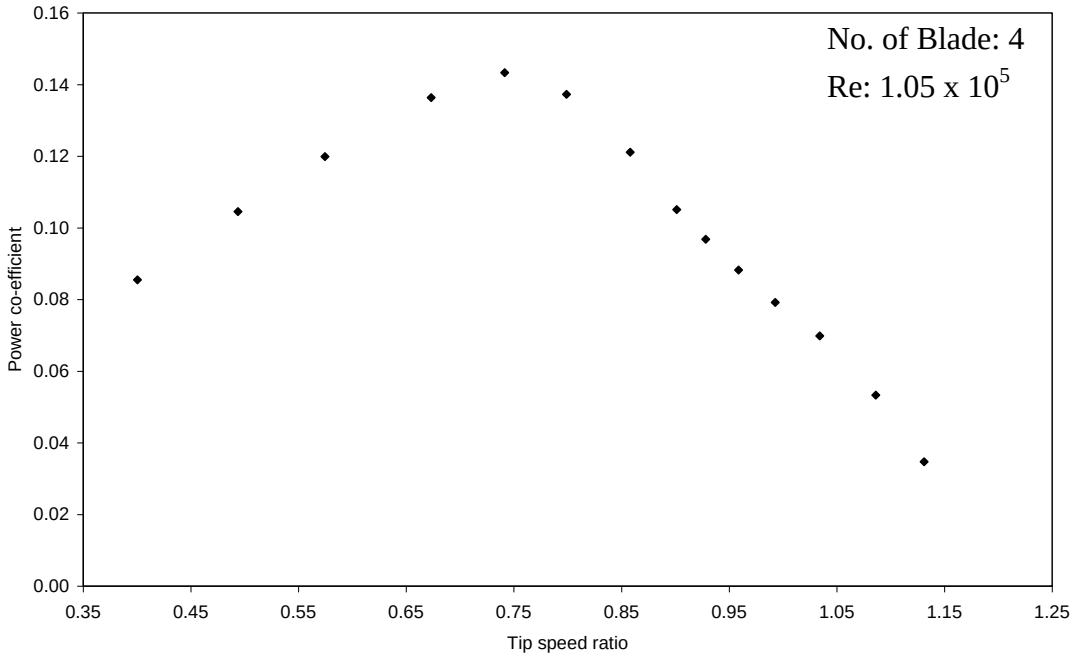

Variation of torque coefficient with tip speed ratio at Reynolds number of 1.05×10^5 for Four Bladed S-shaped Rotor

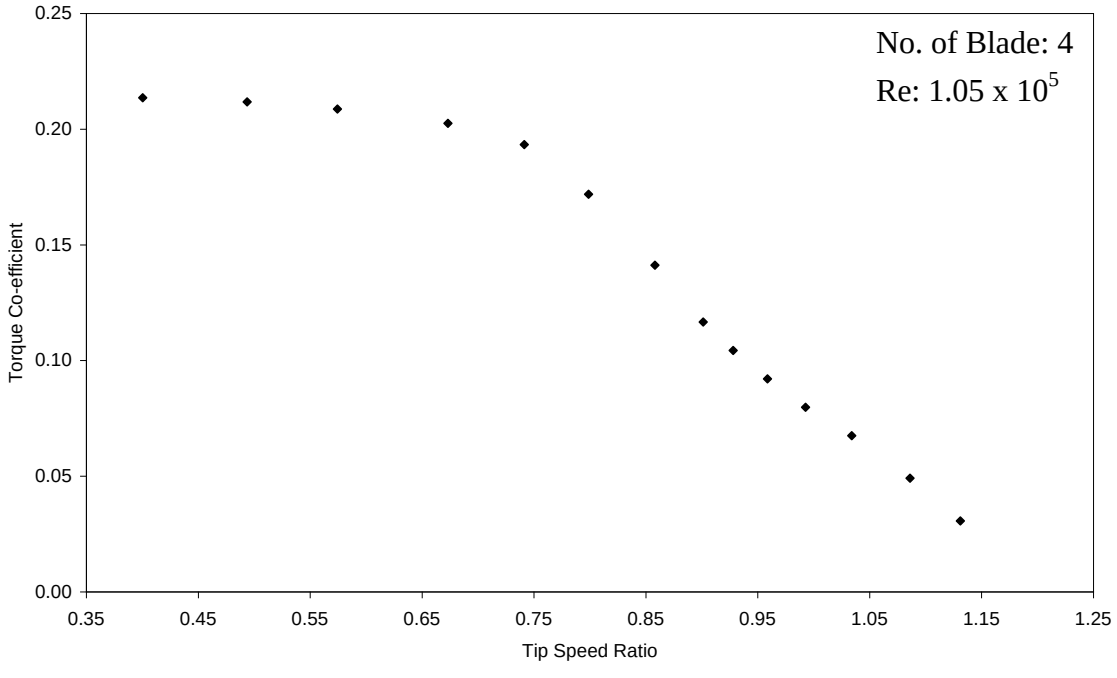

Four Bladed Vertical Axis Vane Type Rotor

Reynolds number 1.20 x 10^5		
Tip speed ratio, λ	Power Co-efficient	Torque Co-efficient
1.23	0.0000	0.0000
1.19	0.0335	0.0282
1.12	0.0473	0.0423
1.06	0.0648	0.0611
0.98	0.0830	0.0846
0.94	0.1019	0.1081
0.91	0.1113	0.1222
0.87	0.1188	0.1363
0.84	0.1296	0.1551
0.80	0.1393	0.1739
0.75	0.1453	0.1927
0.72	0.1447	0.2021
0.65	0.1338	0.2068
0.61	0.1268	0.2091
0.53	0.1113	0.2115
0.44	0.0924	0.2124

Variation of power coefficient with tip speed ratio at Reynolds number of 1.20×10^5 for Four Bladed S-shaped Rotor

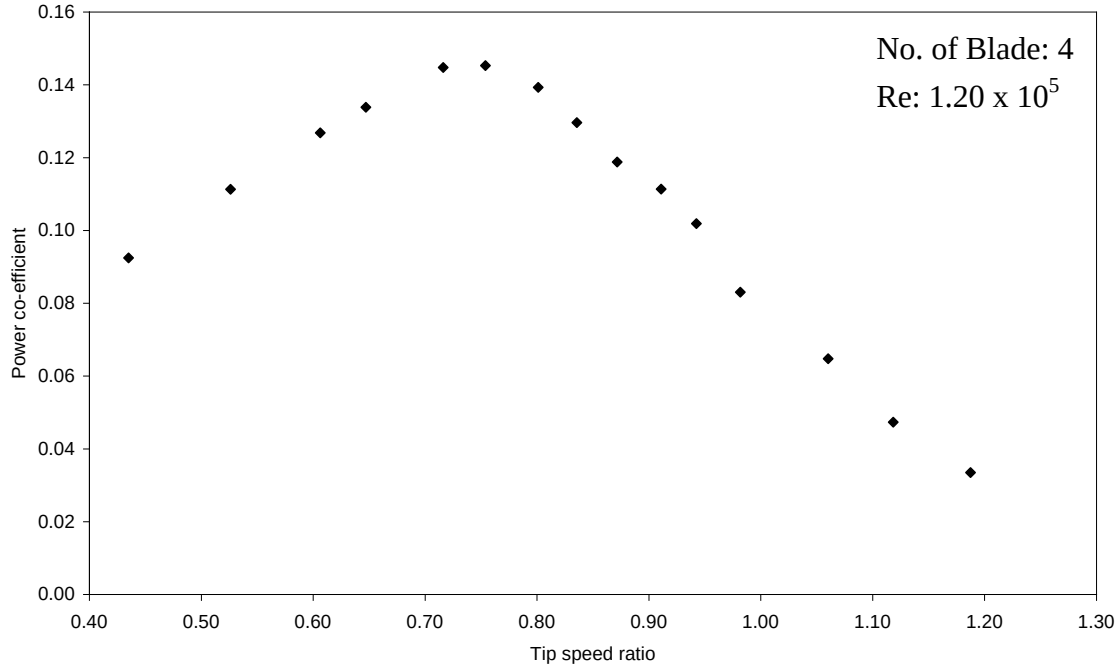

Variation of torque coefficient with tip speed ratio at Reynolds number of 1.20×10^5 for Four Bladed S-shaped Rotor

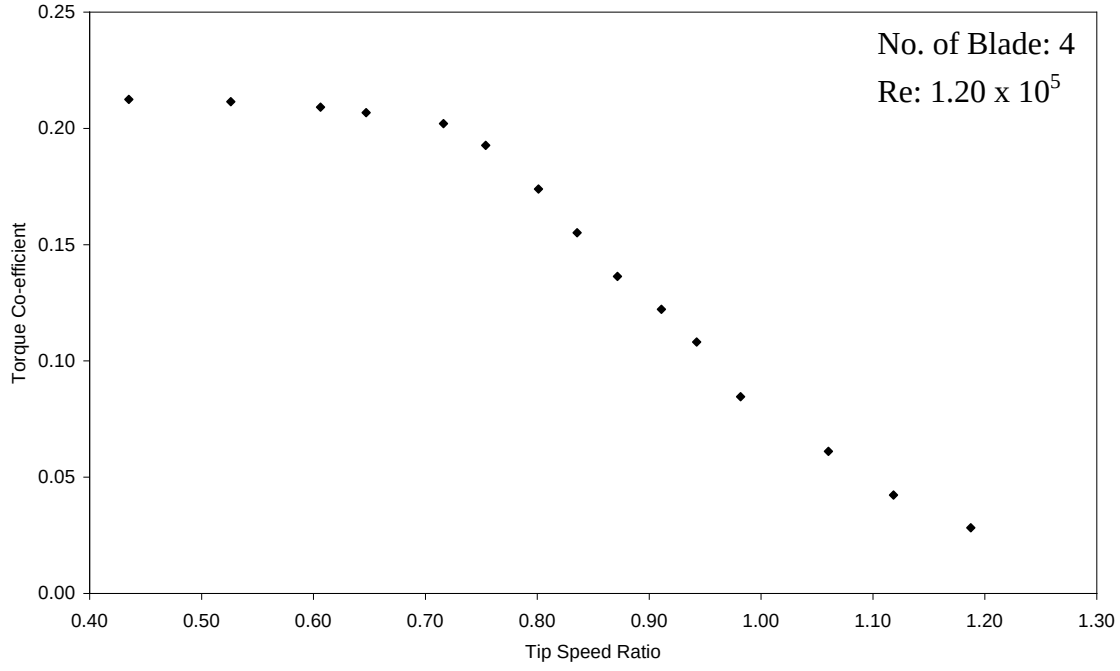

Four Bladed Vertical Axis Vane Type Rotor

Reynolds number 1.35 x 10^5		
Tip speed ratio, λ	Power Co-efficient	Torque Co-efficient
1.27	0.0000	0.0000
1.21	0.0361	0.0297
1.16	0.0476	0.0408
1.12	0.0622	0.0557
1.08	0.0783	0.0724
1.03	0.0953	0.0928
0.99	0.1084	0.1095
0.94	0.1190	0.1262
0.88	0.1306	0.1485
0.82	0.1430	0.1745
0.77	0.1483	0.1931
0.70	0.1437	0.2042
0.64	0.1324	0.2079
0.59	0.1226	0.2090
0.53	0.1104	0.2098
0.45	0.0955	0.2105

Variation of power coefficient with tip speed ratio at Reynolds number of 1.35×10^5 for Four Bladed S-shaped Rotor

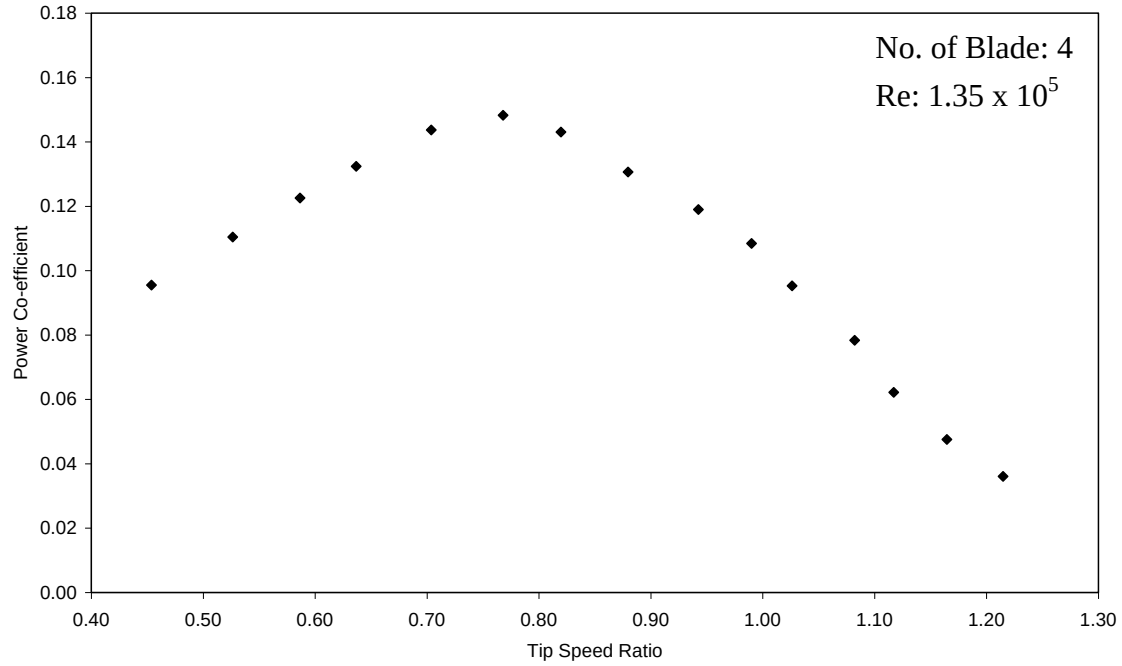

Variation of torque coefficient with tip speed ratio at Reynolds number of 1.35×10^5 for Four Bladed S-shaped Rotor

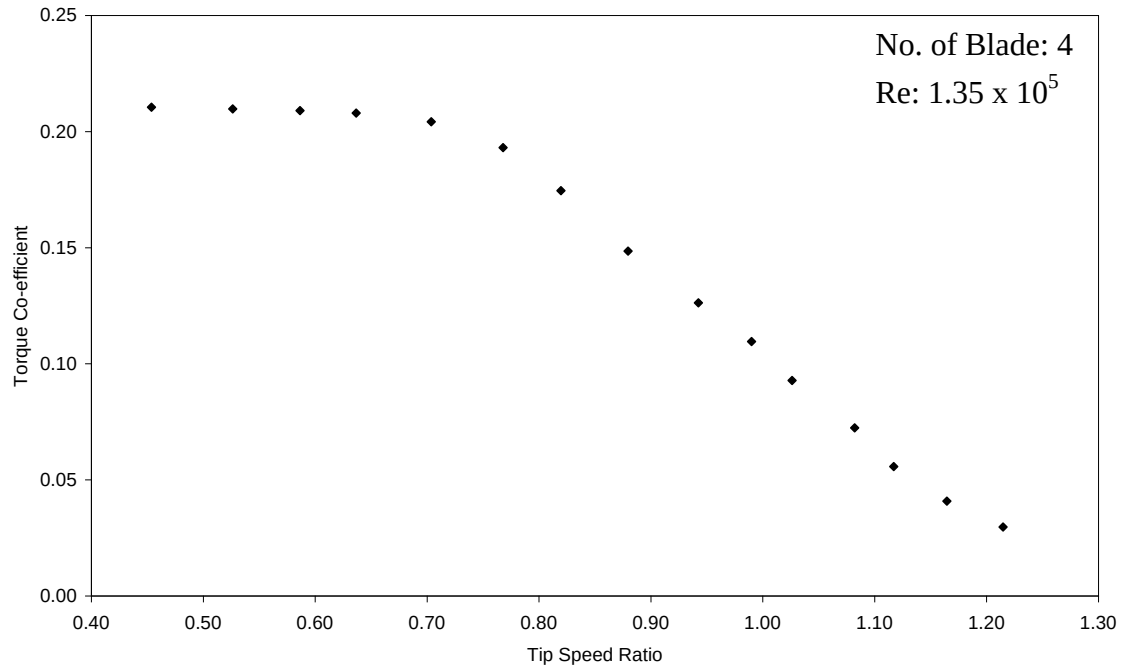

Five Bladed Vertical Axis Vane Type Rotor

Reynolds number 0.75×10^5		
Tip speed ratio, λ	Power Co-efficient	Torque Co-efficient
1.1435	0.0000	0.0000
1.0355	0.0561	0.0541
0.9802	0.0707	0.0722
0.8796	0.0952	0.1083
0.8193	0.1084	0.1323
0.7716	0.1207	0.1564
0.7163	0.1292	0.1804
0.6736	0.1377	0.2045
0.5906	0.1421	0.2406
0.5228	0.1321	0.2526
0.4700	0.1244	0.2646
0.3468	0.0939	0.2707
0.2262	0.0618	0.2731

Variation of power coefficient with tip speed ratio at Reynolds number of 0.75×10^5 for Five Bladed S-shaped Rotor

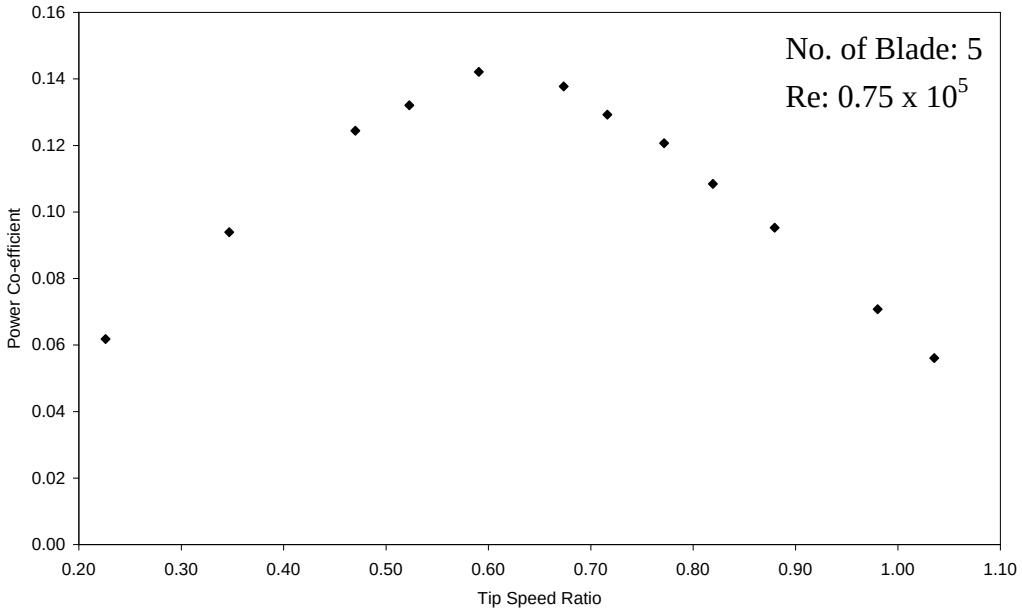

Variation of torque coefficient with tip speed ratio at Reynolds number of 0.75×10^5 for Five Bladed S-shaped Rotor

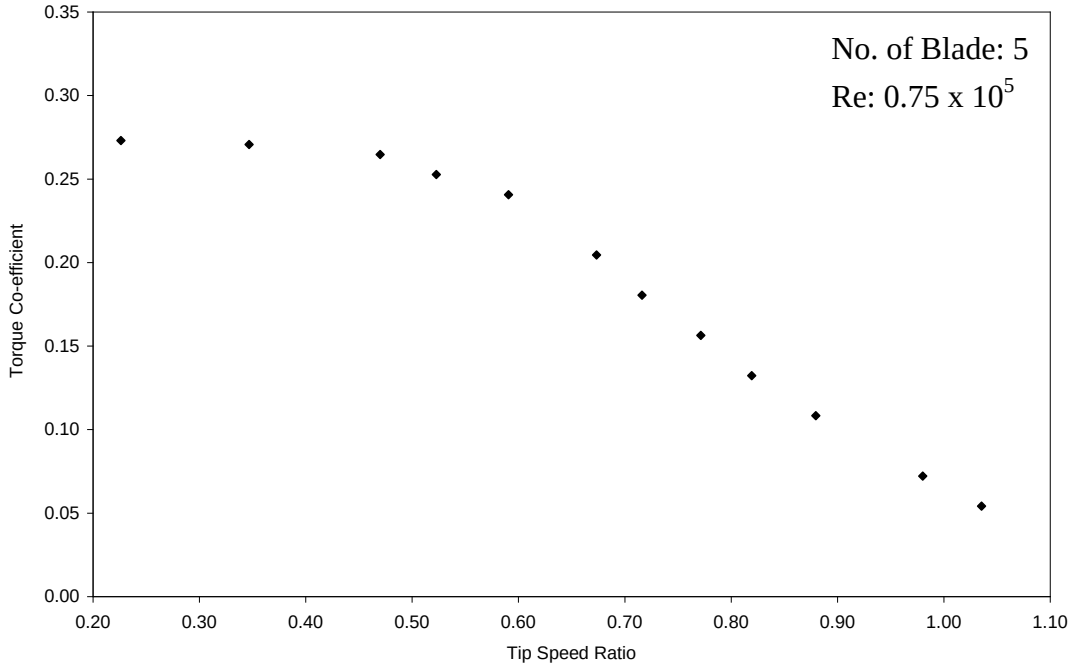

Five Bladed Vertical Axis Vane Type Rotor

Reynolds number 0.90 x 10^5		
Tip speed ratio, λ	Power Co-efficient	Torque Co-efficient
1.1519	0.0000	0.0000
1.0723	0.0627	0.0585
0.9969	0.0791	0.0794
0.9111	0.0951	0.1044
0.8419	0.1125	0.1337
0.7645	0.1277	0.1671
0.6953	0.1394	0.2005
0.6493	0.1464	0.2256
0.5822	0.1411	0.2423
0.5131	0.1286	0.2506
0.4335	0.1123	0.2590
0.3498	0.0915	0.2615
0.2848	0.0750	0.2631

Variation of power coefficient with tip speed ratio at Reynolds number of 0.90×10^5 for Five Bladed S-shaped Rotor

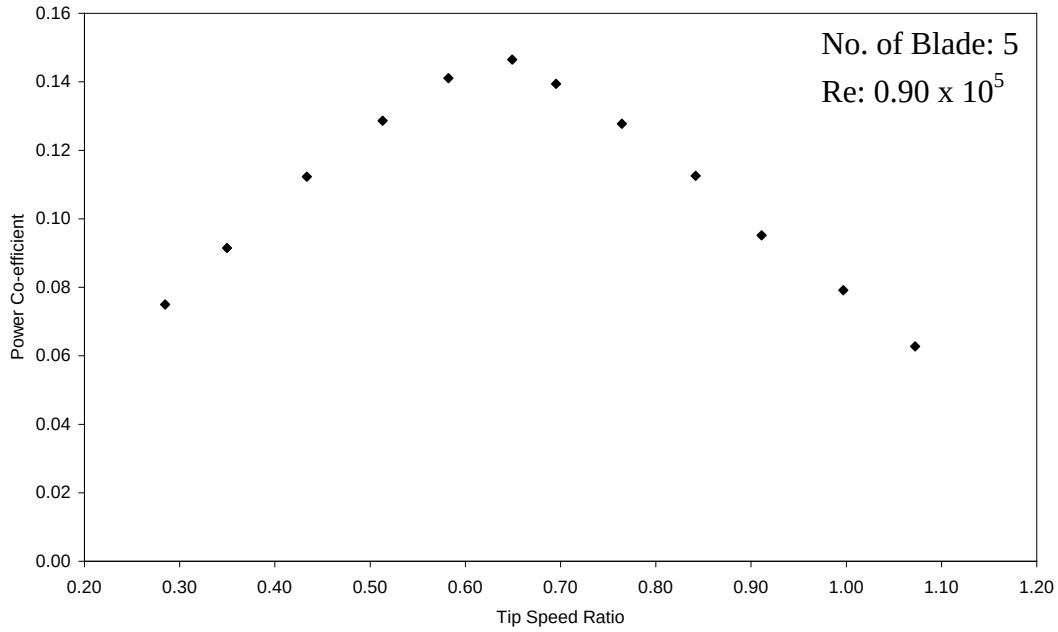

Variation of torque coefficient with tip speed ratio at Reynolds number of 0.90×10^5 for Five Bladed S-shaped Rotor

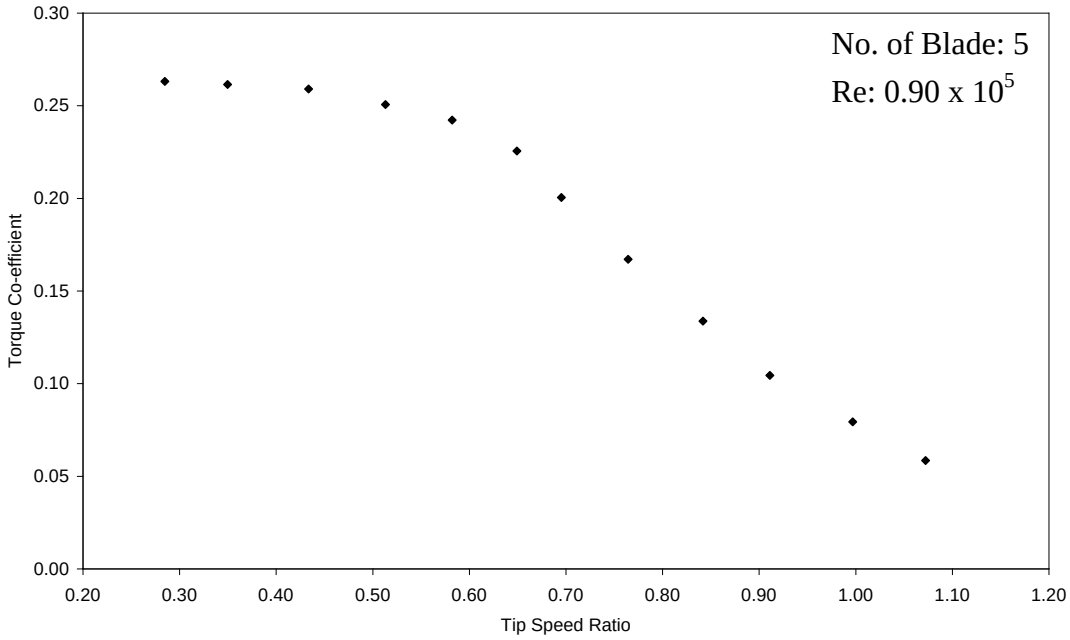

Five Bladed Vertical Axis Vane Type Rotor

Reynolds number 1.05×10^5		
Tip speed ratio, λ	Power Co-efficient	Torque Co-efficient
1.1669	0.0000	0.0000
1.1184	0.0480	0.0430
1.0556	0.0777	0.0736
0.9784	0.1021	0.1043
0.9191	0.1185	0.1289
0.8581	0.1317	0.1534
0.7863	0.1400	0.1780
0.7306	0.1480	0.2025
0.6588	0.1516	0.2302
0.5745	0.1393	0.2424
0.4991	0.1225	0.2455
0.4147	0.1031	0.2486
0.3554	0.0890	0.2504
0.3052	0.0768	0.2516

Variation of power coefficient with tip speed ratio at Reynolds number of 1.05×10^5 for Five Bladed S-shaped Rotor

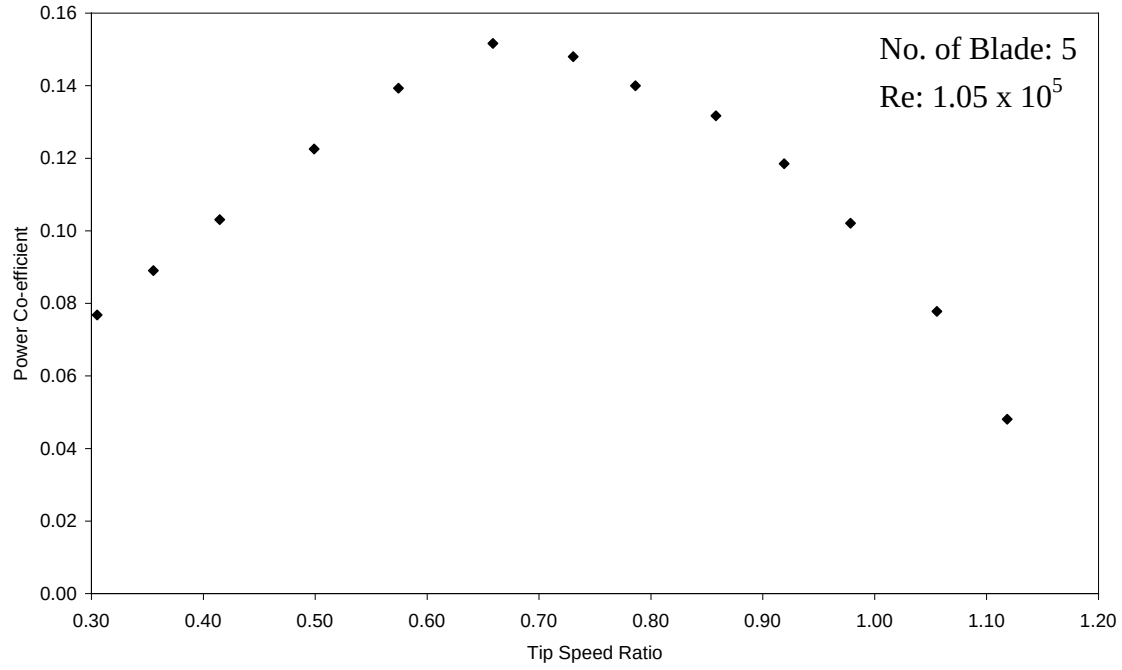

Variation of torque coefficient with tip speed ratio at Reynolds number of 1.05×10^5 for Five Bladed S-shaped Rotor

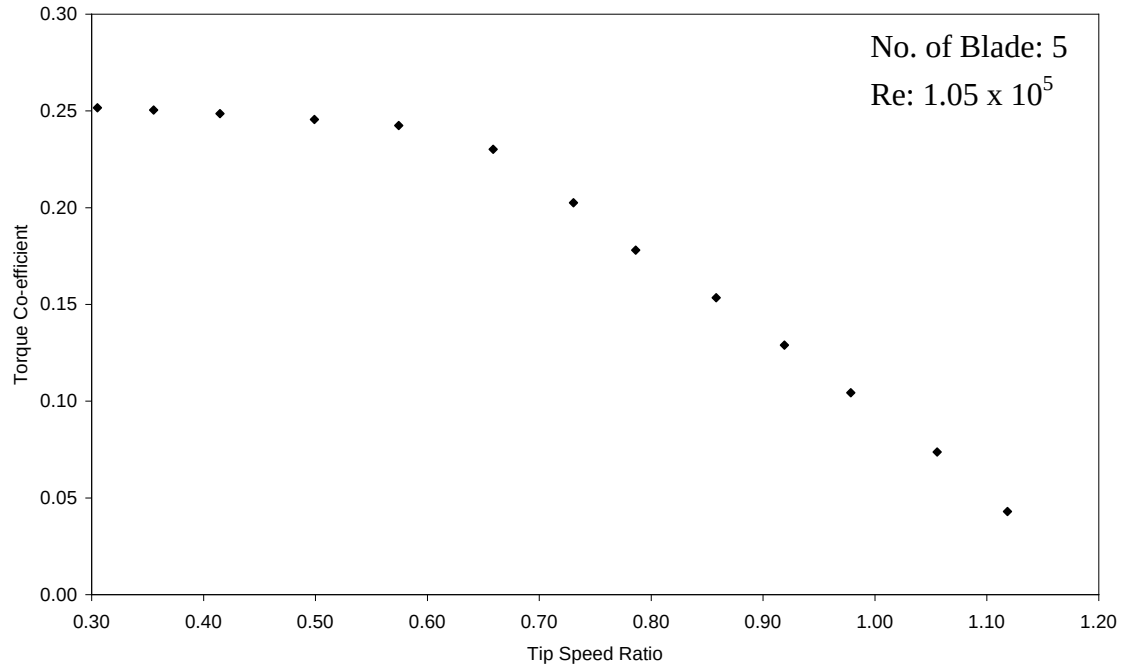

Five Bladed Vertical Axis Vane Type Rotor

Reynolds number 1.20 x 10^5		
Tip speed ratio, λ	Power Co-efficient	Torque Co-efficient
1.1702	0.0000	0.0000
1.1027	0.0415	0.0376
1.0053	0.0709	0.0705
0.9299	0.1005	0.1081
0.8734	0.1129	0.1292
0.8404	0.1224	0.1457
0.7995	0.1353	0.1692
0.7540	0.1453	0.1927
0.7100	0.1535	0.2162
0.6676	0.1506	0.2256
0.5906	0.1415	0.2396
0.5152	0.1247	0.2420
0.4037	0.0986	0.2443
0.3314	0.0813	0.2453

Variation of power coefficient with tip speed ratio at Reynolds number of 1.20×10^5 for Five Bladed S-shaped Rotor

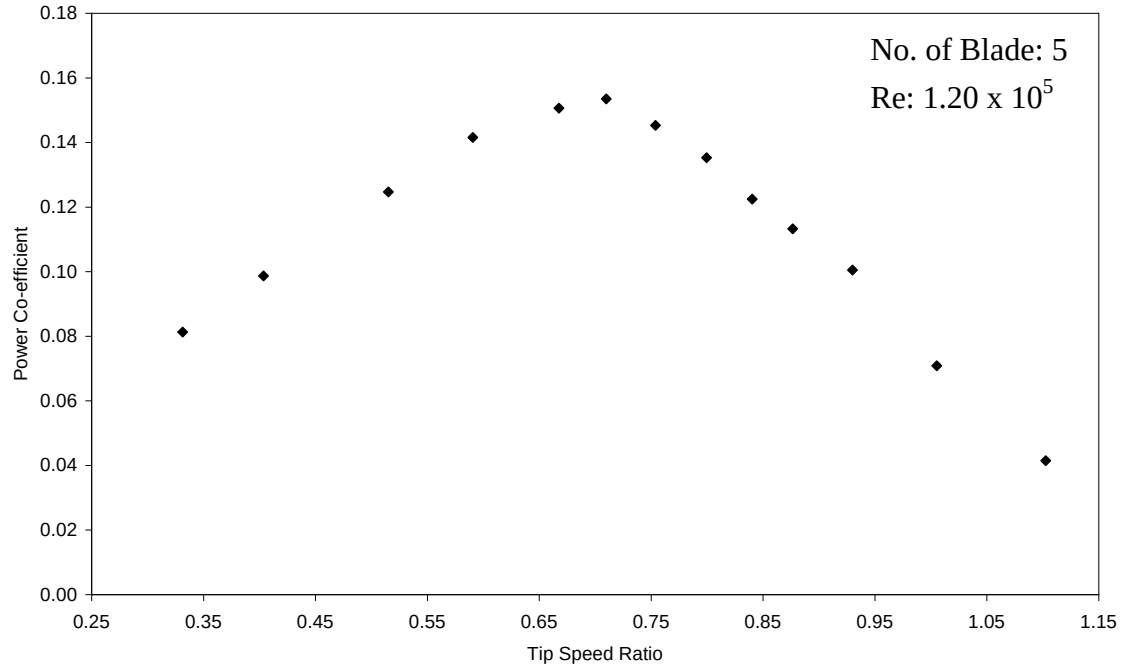

Variation of torque coefficient with tip speed ratio at Reynolds number of 1.20×10^5 for Five Bladed S-shaped Rotor

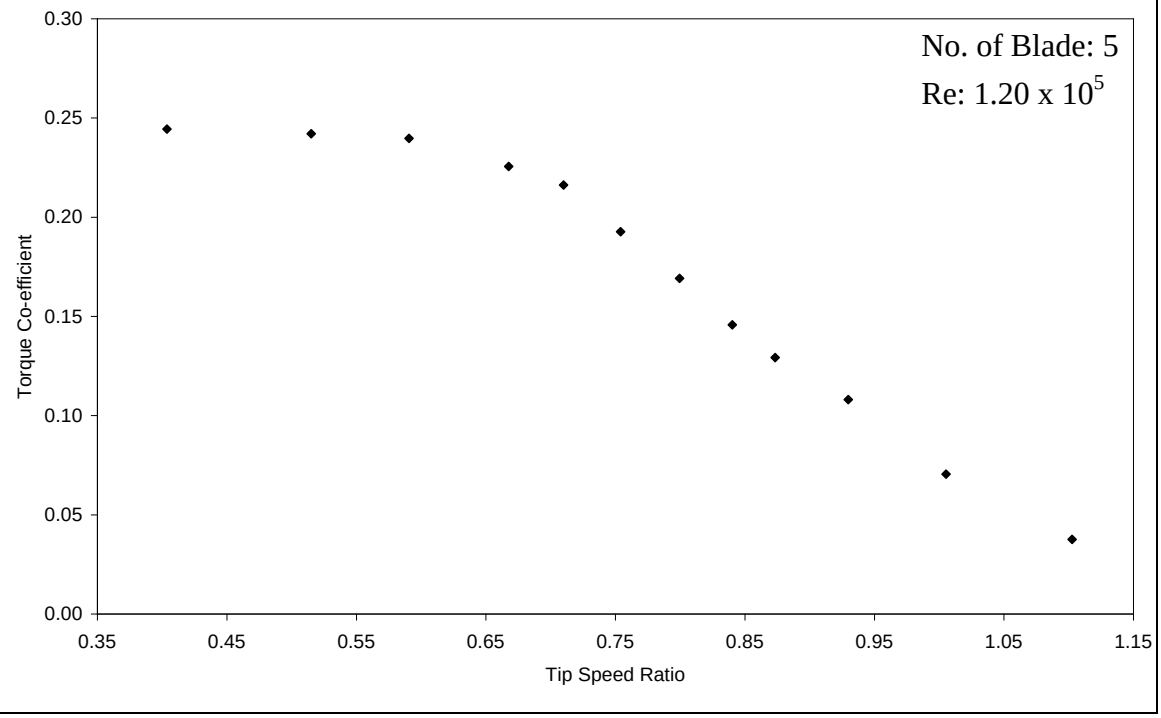

Five Bladed Vertical Axis Vane Type Rotor

Reynolds number 1.35 x 10^5		
Tip speed ratio, λ	Power Co-efficient	Torque Co-efficient
1.1868	0.0000	0.0000
1.1617	0.0431	0.0371
1.1003	0.0735	0.0668
1.0263	0.1067	0.1040
0.9662	0.1256	0.1299
0.9160	0.1360	0.1485
0.8796	0.1437	0.1634
0.8447	0.1505	0.1782
0.8029	0.1550	0.1931
0.7470	0.1553	0.2079
0.7079	0.1551	0.2191
0.6465	0.1464	0.2265
0.5753	0.1324	0.2302
0.4817	0.1114	0.2313
0.4301	0.0998	0.2320

Variation of power coefficient with tip speed ratio at Reynolds number of 1.35×10^5 for Five Bladed S-shaped Rotor

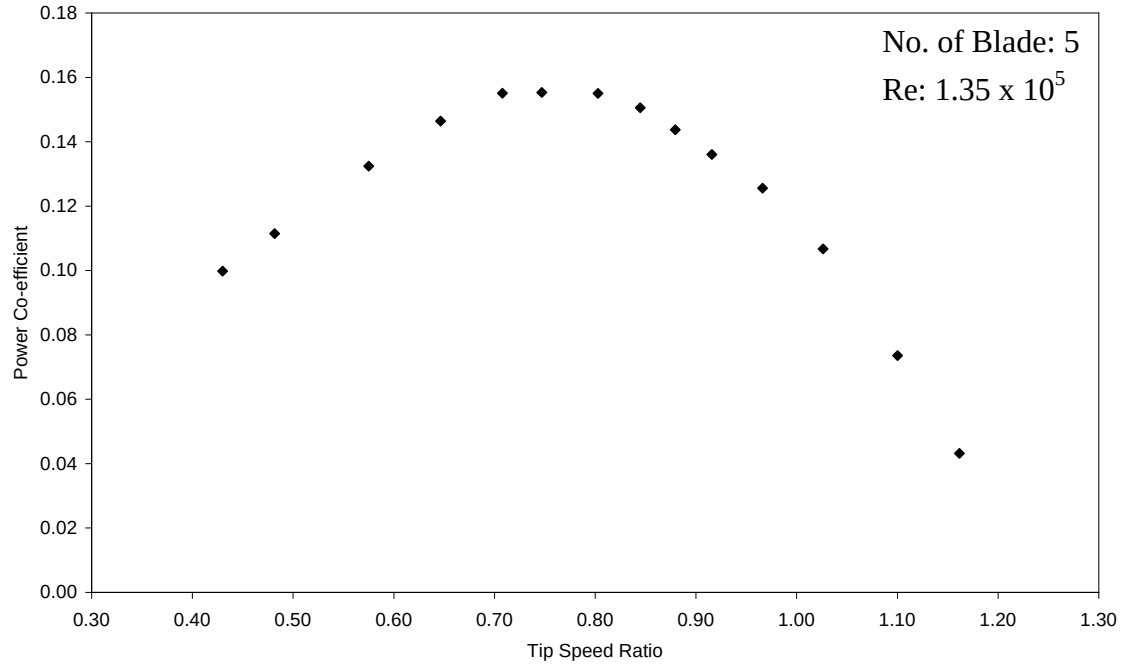

Variation of torque coefficient with tip speed ratio at Reynolds number of 1.35×10^5 for Five Bladed S-shaped Rotor

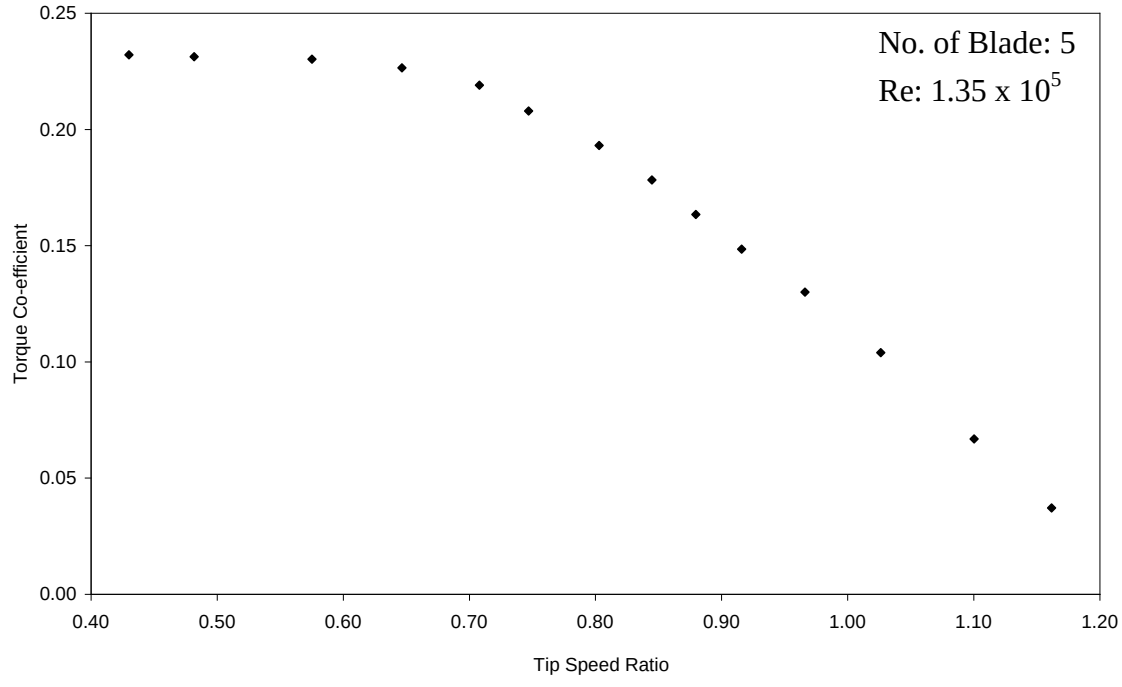

Six Bladed Vertical Axis Vane Type Rotor

Reynolds number 0.75×10^5		
Tip speed ratio, λ	Power Co-efficient	Torque Co-efficient
0.9299	0.0000	0.0000
0.8168	0.0688	0.0842
0.7439	0.0895	0.1203
0.6962	0.1089	0.1564
0.6208	0.1269	0.2045
0.5479	0.1384	0.2526
0.4976	0.1497	0.3007
0.4197	0.1464	0.3489
0.3695	0.1333	0.3609
0.2941	0.1097	0.3729
0.2513	0.0943	0.3753
0.2237	0.0848	0.3789

Variation of power coefficient with tip speed ratio at Reynolds number of 0.75×10^5 for Six Bladed S-shaped Rotor

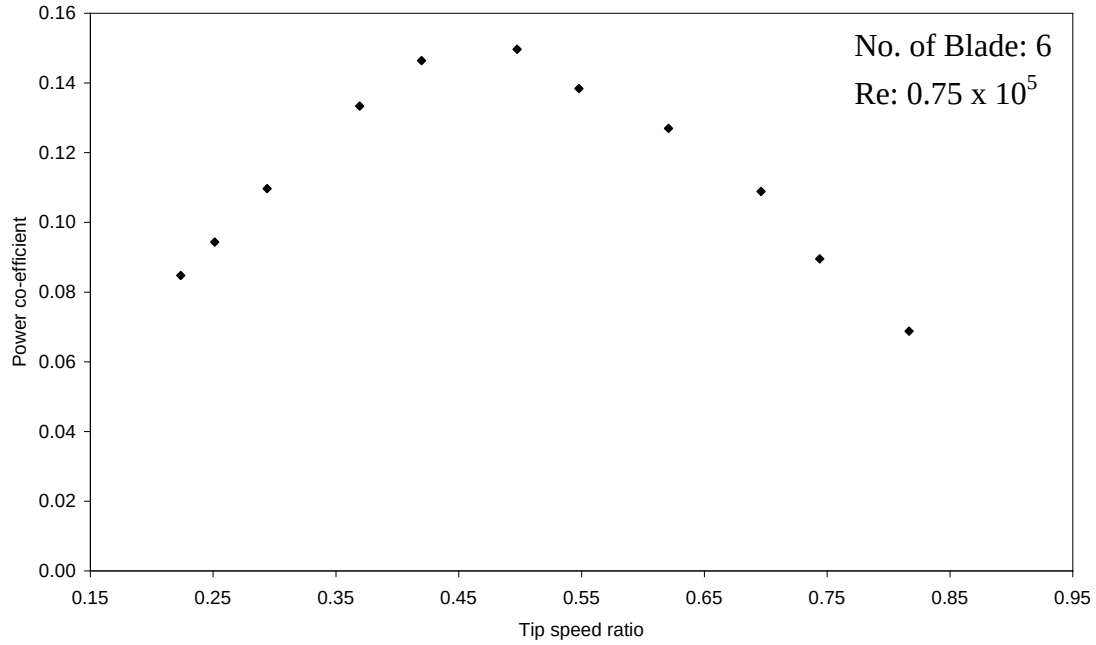

Variation of torque coefficient with tip speed ratio at Reynolds number of 0.75×10^5 for Six Bladed S-shaped Rotor

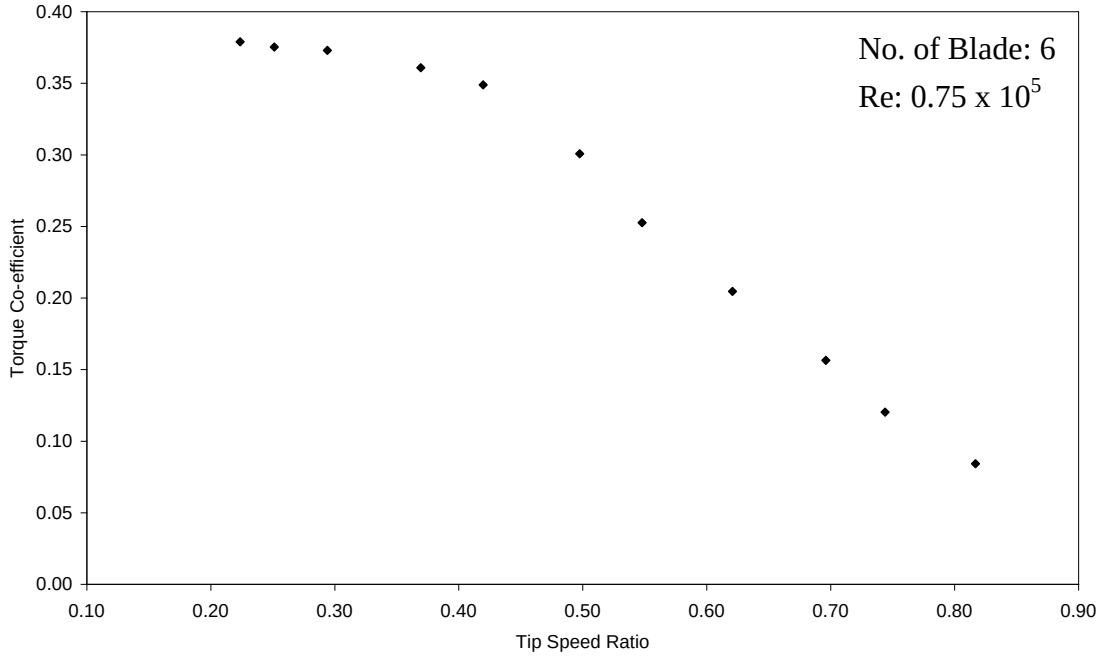

Six Bladed Vertical Axis Vane Type Rotor

Reynolds number 0.90 x 10^5		
Tip speed ratio, λ	Power Co-efficient	Torque Co-efficient
0.9739	0.0000	0.0000
0.9111	0.0685	0.0752
0.8566	0.0859	0.1002
0.8001	0.1003	0.1253
0.7456	0.1183	0.1587
0.6995	0.1344	0.1921
0.6430	0.1450	0.2256
0.5864	0.1519	0.2590
0.5131	0.1500	0.2924
0.4545	0.1443	0.3174
0.3728	0.1215	0.3258
0.2932	0.0968	0.3300
0.2660	0.0889	0.3342

Variation of power coefficient with tip speed ratio at Reynolds number of 0.90×10^5 for Six Bladed S-shaped Rotor

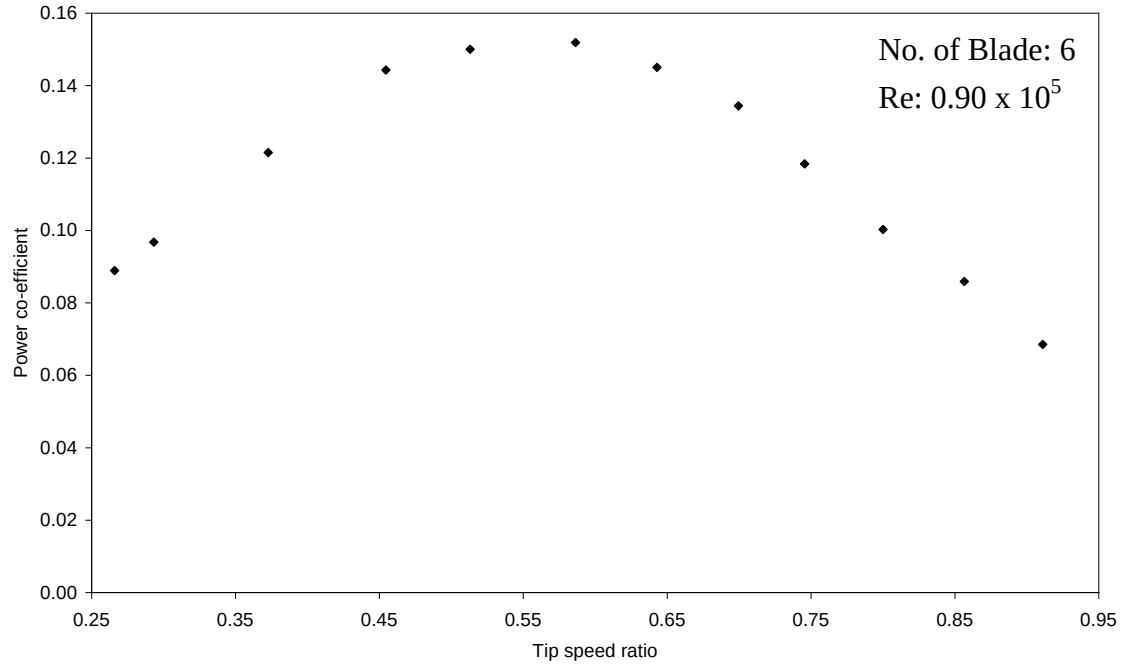

Variation of torque coefficient with tip speed ratio at Reynolds number of 0.90×10^5 for Six Bladed S-shaped Rotor

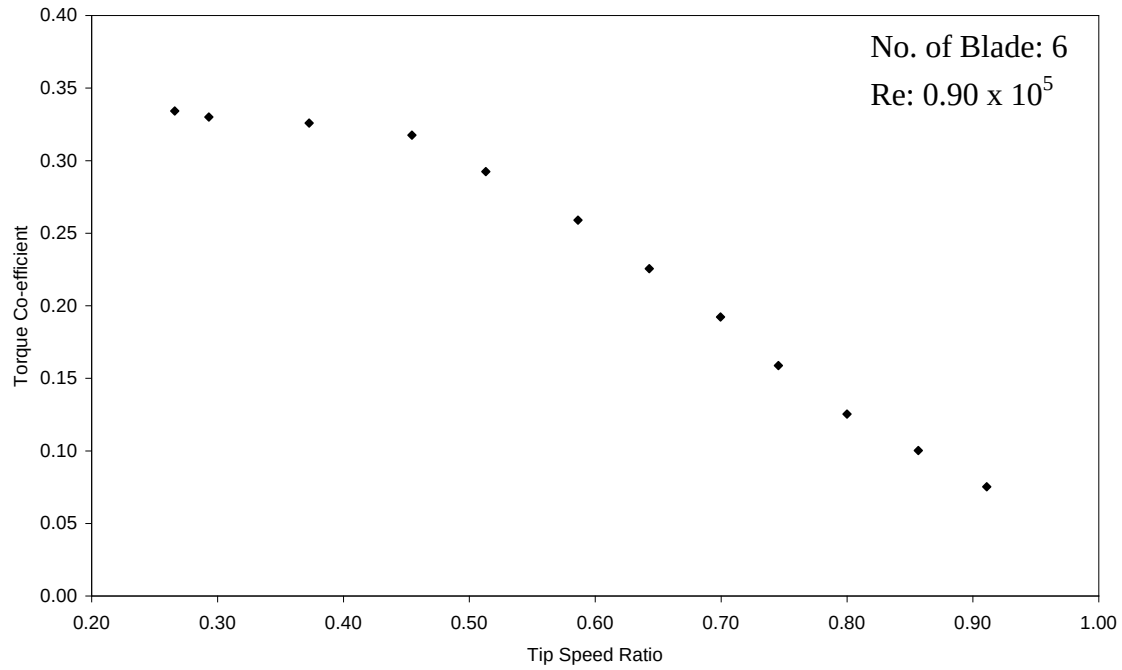

Six Bladed Vertical Axis Vane Type Rotor

Reynolds number 1.05×10^5		
Tip speed ratio, λ	Power Co-efficient	Torque Co-efficient
1.0053	0.0000	0.0000
0.9191	0.0564	0.0614
0.8886	0.0709	0.0798
0.8581	0.0895	0.1043
0.8186	0.1055	0.1289
0.7809	0.1198	0.1534
0.7396	0.1362	0.1841
0.6786	0.1458	0.2148
0.6283	0.1543	0.2455
0.5422	0.1497	0.2762
0.4614	0.1416	0.3069
0.3860	0.1184	0.3069
0.2801	0.0877	0.3130

Variation of power coefficient with tip speed ratio at Reynolds number of 1.05×10^5 for Six Bladed S-shaped Rotor

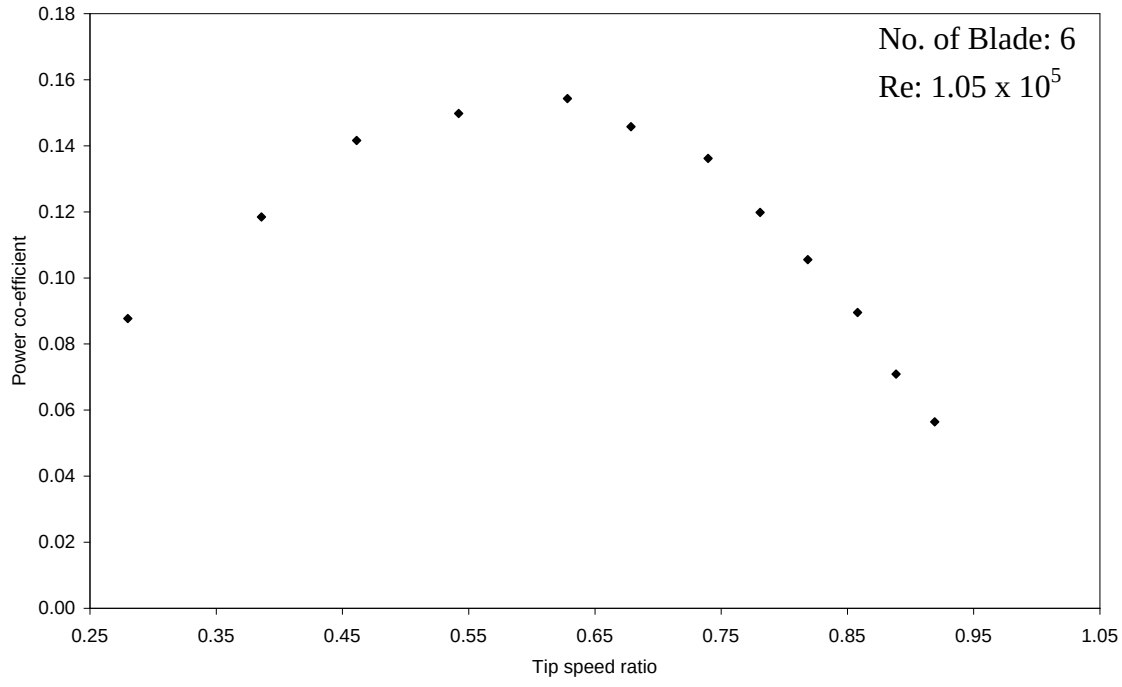

Variation of torque coefficient with tip speed ratio at Reynolds number of 1.05×10^5 for Six Bladed S-shaped Rotor

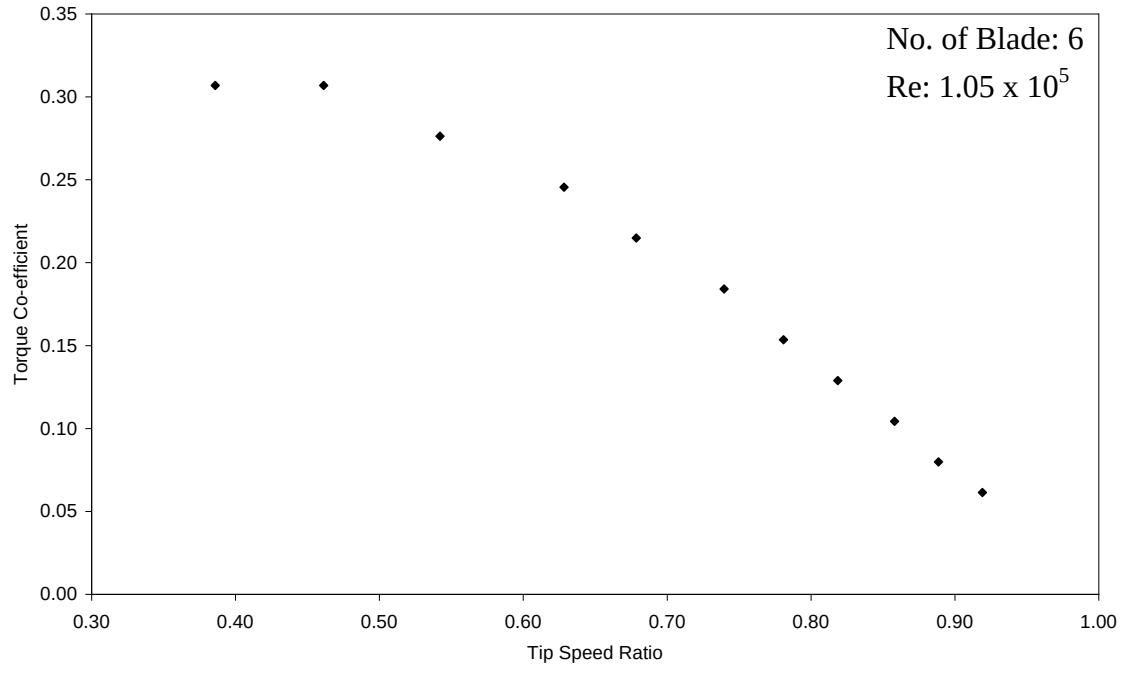

Six Bladed Vertical Axis Vane Type Rotor

Reynolds number 1.20 x 10^5		
Tip speed ratio, λ	Power Co-efficient	Torque Co-efficient
1.0446	0.0000	0.0000
0.9770	0.0551	0.0564
0.9331	0.0702	0.0752
0.8859	0.0874	0.0987
0.8482	0.1036	0.1222
0.8121	0.1183	0.1457
0.7728	0.1307	0.1692
0.7383	0.1422	0.1927
0.6990	0.1511	0.2162
0.6566	0.1574	0.2396
0.6079	0.1543	0.2537
0.5137	0.1376	0.2678
0.4634	0.1252	0.2702
0.3770	0.1027	0.2725
0.3252	0.0894	0.2749

Variation of power coefficient with tip speed ratio at Reynolds number of 1.20×10^5 for Six Bladed S-shaped Rotor

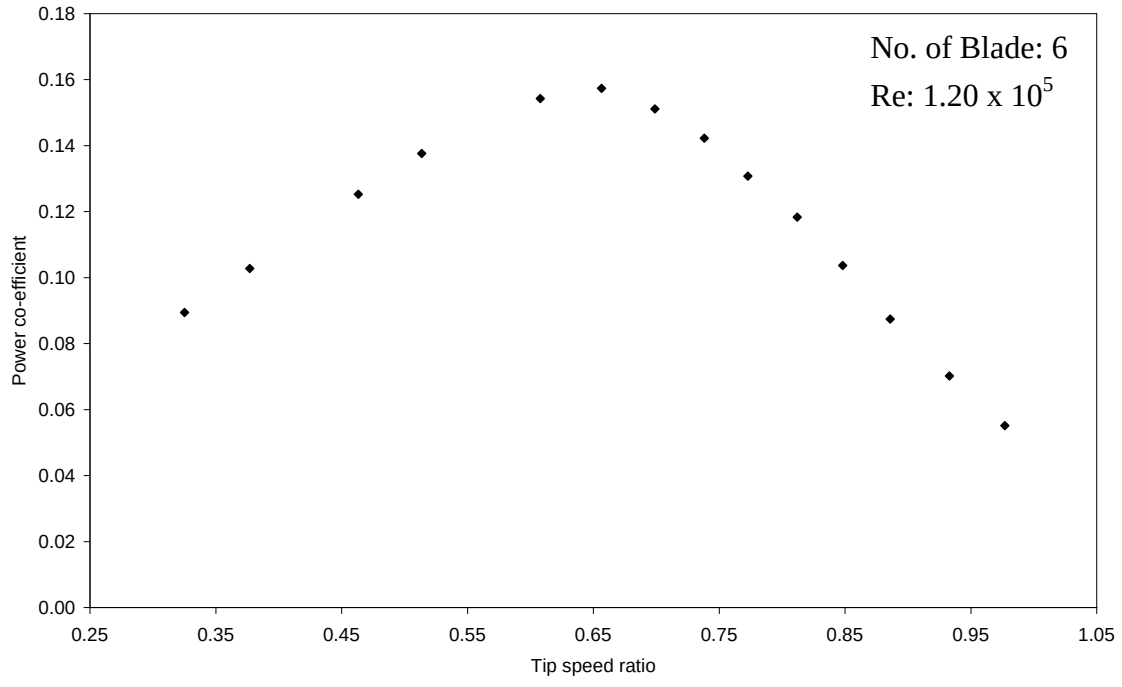

Variation of torque coefficient with tip speed ratio at Reynolds number of 1.20×10^5 for Six Bladed S-shaped Rotor

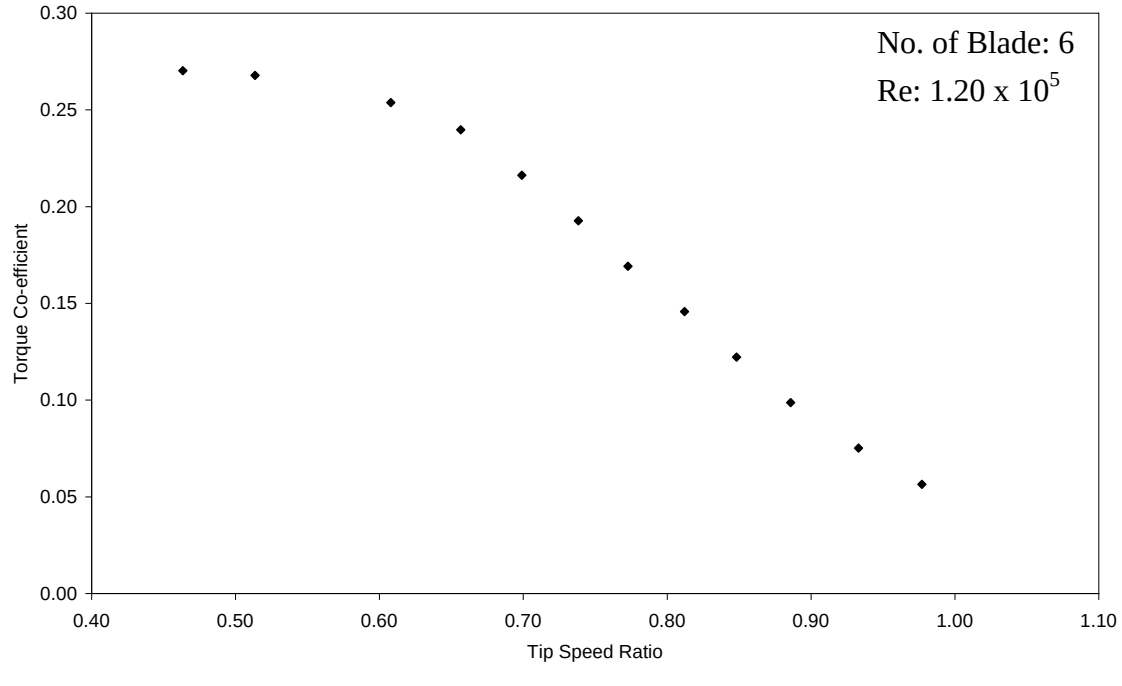

Six Bladed Vertical Axis Vane Type Rotor

Reynolds number 1.35 x 10^5		
Tip speed ratio, λ	Power Co-efficient	Torque Co-efficient
1.1031	0.0000	0.0000
1.0821	0.0562	0.0520
1.0360	0.0846	0.0817
0.9927	0.1032	0.1040
0.9467	0.1195	0.1262
0.8796	0.1372	0.1559
0.8266	0.1473	0.1782
0.7777	0.1559	0.2005
0.7233	0.1611	0.2228
0.6674	0.1586	0.2376
0.5836	0.1430	0.2450
0.5166	0.1285	0.2488
0.4636	0.1170	0.2525
0.3421	0.0870	0.2543

Variation of power coefficient with tip speed ratio at Reynolds number of 1.35×10^5 for Six Bladed S-shaped Rotor

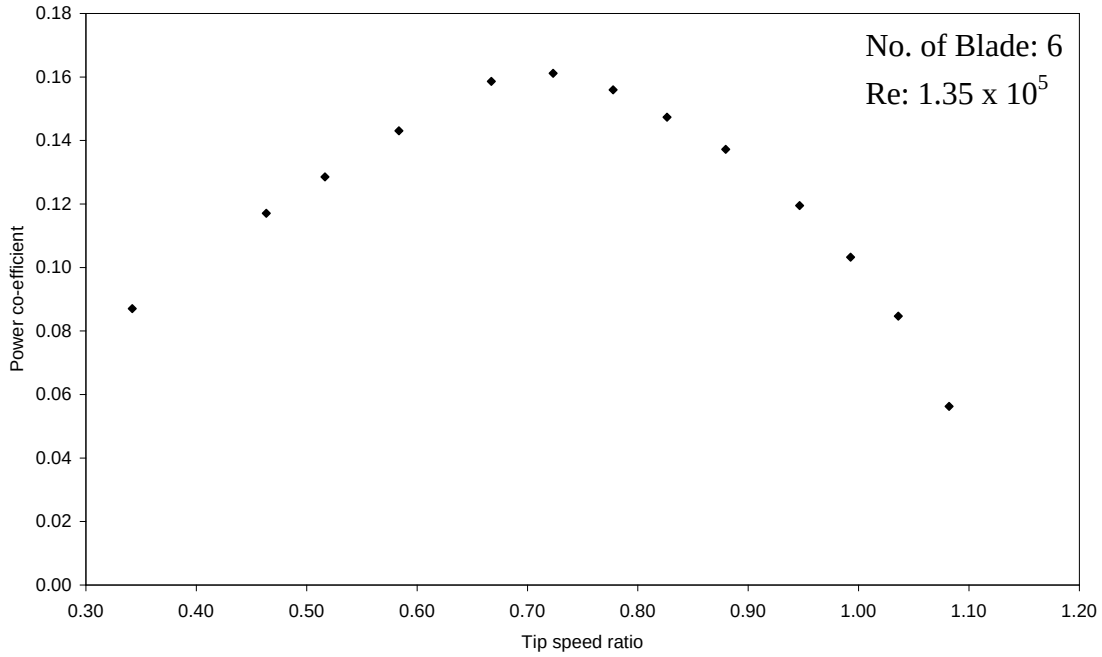

Variation of torque coefficient with tip speed ratio at Reynolds number of 1.35×10^5 for Six Bladed S-shaped Rotor

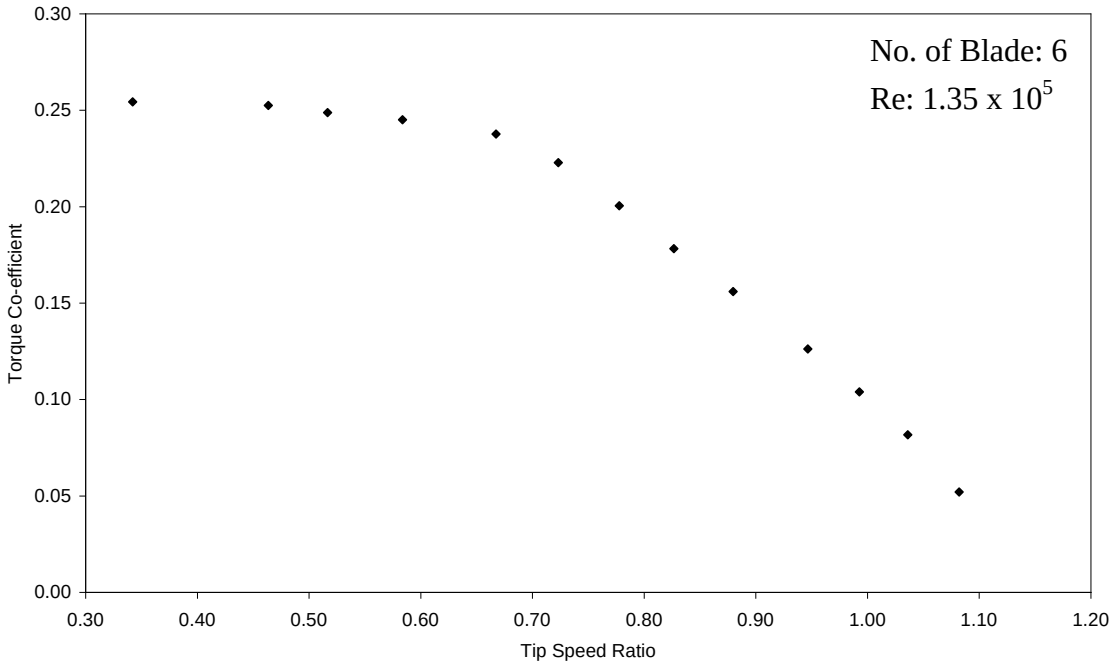

Types of wind turbines

Wind turbines can rotate about either a horizontal or vertical axis, the former being more common.[11]

Horizontal axis

Components of a horizontal axis wind turbine (gearbox, rotor shaft and brake assembly) being lifted into position

Horizontal-axis wind turbines (HAWT) have the main rotor shaft and electrical generator at the top of a tower, and must be pointed into the wind. Small turbines are pointed by a simple wind vane, while large turbines generally use a wind sensor coupled with a servo motor. Most have a gearbox, which turns the slow rotation of the blades into a quicker rotation that is more suitable to drive an electrical generator.[12]

Since a tower produces turbulence behind it, the turbine is usually pointed upwind of the tower. Turbine blades are made stiff to prevent the blades from being pushed into the tower by high winds. Additionally, the blades are placed a considerable distance in front of the tower and are sometimes tilted forward into the wind a small amount.

Downwind machines have been built, despite the problem of turbulence (mast wake), because they don't need an additional mechanism for keeping them in line with the wind, and because in high winds the blades can be allowed to bend which reduces their swept area and thus their wind resistance. Since cyclic (that is repetitive) turbulence may lead to fatigue failures most HAWTs are upwind machines.

[edit] Horizontal subtypes

Doesburger windmill, Ede, The Netherlands.

12th-century windmills

These squat structures, typically (at least) four bladed, usually with wooden shutters or fabric sails, were developed in Europe. These windmills were pointed into the wind manually or via a tail-fan and were typically used to grind grain. In the Netherlands they were also used to pump water from low-lying land, and were instrumental in keeping its polders dry.

In Schiedam, the Netherlands, a traditional style windmill (the *Noletmolen*) was built in 2005 to generate electricity.[13] The mill is one of the tallest Tower mills in the world, being some 42.5 metres (139 ft) tall.

19th-century windmills

The Eclipse windmill factory was set up around 1866 in Beloit, Wisconsin and soon became successful building mills for pumping water on farms and for filling railroad tanks. Other firms like Star, Dempster, and Aeromotor also entered the market. Hundreds of thousands of these mills were produced before rural electrification and small numbers continue to be made.[8] They typically had many blades, operated at tip speed ratios not better than one, and had good starting torque. Some had small direct-current generators used to charge storage batteries, to provide power to lights, or to operate a radio receiver. The American rural electrification connected many farms to centrally-generated power and replaced individual windmills as a primary source of farm power by the 1950s. They were also produced in other countries like South Africa and Australia (where an American design was copied in 1876[14]). Such devices are still used in locations where it is too costly to bring in commercial power.

Modern wind turbines

Three bladed wind turbine

Turbines used in wind farms for commercial production of electric power are usually three-bladed and pointed into the wind by computer-controlled motors. These have high tip speeds of over 320 km/h (200 miles per hour), high efficiency, and low torque ripple, which contribute to good reliability. The blades are usually colored light gray to blend in with the clouds and range in length from 20 to 40 metres (65 to 130 ft) or more. The tubular steel towers range from 60 to 90 metres (200 to 300 feet) tall. The blades rotate at 10-22 revolutions per minute. At 22 rotations per minute the tip speed exceeds 300 ft per second.[15][16] A gear box is commonly used to step up the speed of the generator, although designs may also use direct drive of an annular generator. Some models operate at constant speed, but more energy can be collected by variable-speed turbines which use a solid-state power converter to interface to the transmission system. All turbines are equipped with shut-down features to avoid damage at high wind speeds.

Horizontal axis advantages

- Variable blade pitch, which gives the turbine blades the optimum angle of attack. Allowing the angle of attack to be remotely adjusted gives greater control, so the turbine collects the maximum amount of wind energy for the time of day and season.
- The tall tower base allows access to stronger wind in sites with wind shear. In some wind shear sites, the wind speed can increase by 20% and the power output by 34% for every 10 metres in elevation.
- High efficiency, since the blades always move perpendicular to the wind, receiving power through the whole rotation. In contrast, all vertical axis wind turbines, and most proposed airborne wind turbine designs, involve various types of reciprocating actions, requiring airfoil surfaces to backtrack against the wind for part of the cycle. Backtracking against the wind leads to inherently lower efficiency.
- The face of a horizontal axis blade is struck by the wind at a consistent angle regardless of the position in its rotation. This results in a consistent lateral wind loading over the course of a rotation, reducing vibration and audible noise coupled to the tower or mount.

Horizontal axis disadvantages

This section **does not cite any references or sources**.
Please help improve this article by adding citations to reliable sources. Unsourced material may be challenged and removed. *(September 2009)*

Turbine blade convoy passing through Edenfield in the UK

- The tall towers and blades up to 45 meters long are difficult to transport. Transportation can now amount to 20% of equipment costs.
- Tall HAWTs are difficult to install, needing very tall and expensive cranes and skilled operators.
- Massive tower construction is required to support the heavy blades, gearbox, and generator.
- Reflections from tall HAWTs may affect side lobes of radar installations creating signal clutter, although filtering can suppress it.
- Their height makes them obtrusively visible across large areas, disrupting the appearance of the landscape and sometimes creating local opposition.
- Downwind variants suffer from fatigue and structural failure caused by turbulence when a blade passes through the tower's wind shadow (for this reason, the majority of HAWTs use an upwind design, with the rotor facing the wind in front of the tower).
- HAWTs require an additional yaw control mechanism to turn the blades and nacelle toward the wind.
- In order to minimize fatigue loads due to wake turbulence, wind turbines are usually sited a distance of 5 rotor diameters away from each other, but the spacing depends on the manufacturer and the turbine model.

Cyclic stresses and vibration

Cyclic stresses fatigue the blade, axle and bearing resulting in material failures that were a major cause of turbine failure for many years. Because wind velocity often increases at higher altitudes, the backward force and torque on a horizontal-axis wind turbine (HAWT) blade peaks as it turns through the highest point in its circle. The tower hinders the airflow at the lowest point in the circle, which produces a local dip in force and torque. These effects produce a cyclic twist on the main bearings of a HAWT. The combined twist is worst in machines with an even number of blades, where one is straight

up when another is straight down. To improve reliability, teetering hubs have been used which allow the main shaft to rock through a few degrees, so that the main bearings do not have to resist the torque peaks.

The rotating blades of a wind turbine act like a gyroscope. As it pivots along its vertical axis to face the wind, gyroscopic precession tries to twist the turbine disc along its horizontal axis. For each blade on a wind generator's turbine, precessive force is at a minimum when the blade is horizontal and at a maximum when the blade is vertical.

[edit] Vertical axis design

This section **does not cite any references or sources**.
Please help improve this article by adding citations to reliable sources. Unsourced material may be challenged and removed. *(September 2009)*

Vertical-axis wind turbines (or VAWTs) have the main rotor shaft arranged vertically. Key advantages of this arrangement are that the turbine does not need to be pointed into the wind to be effective. This is an advantage on sites where the wind direction is highly variable.

With a vertical axis, the generator and gearbox can be placed near the ground, so the tower doesn't need to support it, and it is more accessible for maintenance. Drawbacks are that some designs produce pulsating torque.

It is difficult to mount vertical-axis turbines on towers[*citation needed*], meaning they are often installed nearer to the base on which they rest, such as the ground or a building rooftop. The wind speed is slower at a lower altitude, so less wind energy is available for a given size turbine. Air flow near the ground and other objects can create turbulent flow, which can introduce issues of vibration, including noise and bearing wear which may increase the maintenance or shorten the service life. However, when a turbine is mounted on a rooftop, the building generally redirects wind over the roof and this can double the wind speed at the turbine. If the height of the rooftop mounted turbine tower is approximately 50% of the building height, this is near the optimum for maximum wind energy and minimum wind turbulence.

[edit] Vertical axis subtypes

30 m Darrieus wind turbine in the Magdalen Islands

Darrieus wind turbine

"Eggbeater" turbines, or Darrieus turbines, were named after the French inventor, Georges Darrieus.[17] They have good efficiency, but produce large torque ripple and cyclical stress on the tower, which contributes to poor reliability. They also generally require some external power source, or an additional Savonius rotor to start turning, because the starting torque is very low. The torque ripple is reduced by using three or more blades which results in a higher solidity for the rotor. Solidity is measured by blade area divided by the rotor area. Newer Darrieus type turbines are not held up by guy-wires but have an external superstructure connected to the top bearing.

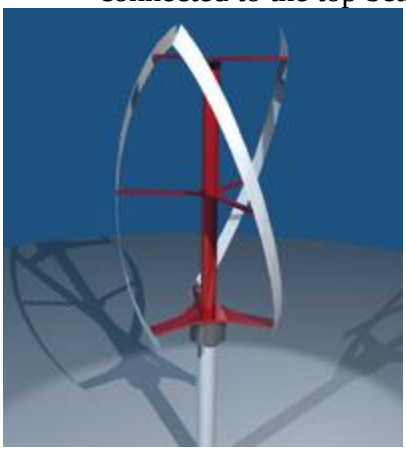

A helical twisted VAWT.

Giromill

A subtype of Darrieus turbine with straight, as opposed to curved, blades. The cycloturbine variety has variable pitch to reduce the torque pulsation and is self-starting.[18] The advantages of variable pitch are: high starting torque; a wide, relatively flat torque curve; a lower blade speed ratio; a higher coefficient of performance; more efficient operation in turbulent winds; and a lower blade speed

ratio which lowers blade bending stresses. Straight, V, or curved blades may be used.

Windmill with rotating sails
Savonius wind turbine

These are drag-type devices with two (or more) scoops that are used in anemometers, *Flettner* vents (commonly seen on bus and van roofs), and in some high-reliability low-efficiency power turbines. They are always self-starting if there are at least three scoops. They sometimes have long helical scoops to give a smooth torque.

[edit] Vertical axis advantages

- A massive tower structure is less frequently used, as VAWTs are more frequently mounted with the lower bearing mounted near the ground.
- Designs without yaw mechanisms are possible with fixed pitch rotor designs.
- The generator of a VAWT can be located nearer the ground, making it easier to maintain the moving parts.
- VAWTs have lower wind startup speeds than HAWTs. Typically, they start creating electricity at 6 m.p.h. (10 km/h).
- VAWTs may be built at locations where taller structures are prohibited.
- VAWTs situated close to the ground can take advantage of locations where mesas, hilltops, ridgelines, and passes funnel the wind and increase wind velocity.
- VAWTs may have a lower noise signature.[*citation needed*]

[edit] Vertical axis disadvantages

- A VAWT that uses guy-wires to hold it in place puts stress on the bottom bearing as all the weight of the rotor is on the bearing. Guy wires attached to the top bearing increase downward thrust in wind gusts. Solving this problem requires a superstructure to hold a top bearing in place to eliminate the downward thrusts of gust events in guy wired models.
- The stress in each blade due to wind loading changes sign twice during each revolution as the apparent wind direction moves through 360 degrees. This reversal of the stress increases the likelihood of blade failure by fatigue.
- While VAWTs' components are located on the ground, they are also located under the weight of the structure above it, which can make changing out parts very difficult without dismantling the structure, if not designed properly.
- Having rotors located close to the ground where wind speeds are lower due to the ground's surface drag, VAWTs may not produce as much energy at a given site as a HAWT with the same footprint or height.

Figure 5. A steel-bladed water pumping windmill in the American Midwest (late 1800's)

In Bangladesh, some early studies on wind energy prospects were made by Professor Muhtasham Hussain of Dhaka University and his colleagues [Hussain et. al 1986], as well as some enthusiasts from Bangladesh University of Engineering and Technologies (BUET). The Bangladesh Meteorological department has wind speed measuring stations in towns and cities . Data from earlier measurements and analysis of upper air data by CWET India show that wind energy resource of Bangladesh is not good enough (>7 m/s) for grid connected wind parks [GEF 2001]. Wind data from Bangladesh Meteorological Department and different previous and ongoing wind resource assessment projects are briefly described in the subsequent sections.

The maximum velocity obtained at St. Martins Island is 30 m/s and yearly average wind speed in 4.9 m/s. The maximum velocity obtained at Teknaf is 16 m/s and yearly average wind speed in 3.8 m/s.

Wind Speeds in the Saint Martin's Island :

Available wind speeds in the Saint Martin's Island are presented in the Table 3.7 below.

Monthly average wind speeds in the island [IFRD, 2002]

Month	V_{av} (m/s)	V_{max} (m/s)
January	5.08	23.32
February	4.71	19.78
March	4.29	18.94
April	3.58	20.03
May	5.75	26.30
June	5.96	29.80
July	5.33	24.20
August	5.96	20.40
September	4.79	17.70
October	4.17	15.90
November	3.79	14.50
December	4.08	15.20

Wind Data From Bangladesh Meteorological Department in Bangladesh:

Most of the previous wind speed data in Bangladesh is available from the Bangladesh Meteorological Department. Average values calculated from such wind data during 1961 to 1993 are presented in Table

Site	Reference height (m)	Annual average wind speed(m/s)
Teknaf	5	2.16
Cox's Bazar	10	2.42
Patenga Airport	5	2.45
Kutubdia Island	6	2.09
Sandip Island	5	2.16
Hatia Island	6	2.08
Bhola Island	7	2.44
Khepupara	10	2.36
Comilla Airport	6	2.21

A high proportion of capital cost. The estimated average cost per unit incorporates the cost of construction of the turbine and transmission facilities, borrowed funds, return to investors (including cost of risk), estimated annual production, and other components, averaged over the projected useful life of the equipment, which may be in excess of twenty years. Energy cost estimates are highly dependent on these assumptions so published cost figures can differ substantially. A British Wind Energy Association report gives an average generation cost of onshore wind power of around 3.2 pence (between US 5 and 6 cents) per kW·h (2005).[92] Cost per unit of energy produced was estimated in 2006 to be comparable to the cost of new generating capacity in the US for coal and natural gas: wind cost was estimated at $55.80 per MW·h, coal at $53.10/MW·h and natural gas at $52.50.[93] Other sources in various studies have estimated wind to be more expensive than other sources (see Economics of new nuclear power plants, Clean coal, and Carbon capture and storage).

Wind Power's Beginnings
(1000 B.C. - 1300 A.D.)

Grain grinding was the first documented wind mill application and was very straightforward. The grinding stone was affixed to the same vertical shaft. The mill machinery was commonly enclosed in a building, which also featured a wall or shield to block the incoming wind from slowing the side of the drag-type rotor that advanced toward the wind.

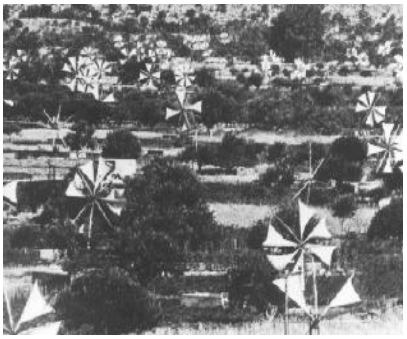

Figure 2. Water Pumping Sailwing Machines on the Island of Crete

One of the most scenic and successful applications of windpower (and one that still exists), is the extensive use of water pumping machines on the island of Crete. Here, literally hundreds of sail-rotor windmills pump water for crops and livestock.

Figure 3. An early sail-wing horizontal-axis mill on the Mediterranean coast.

Windmills in the Western World
(1300 - 1875 A.D.)

Role of Smaller Systems

For hundreds of years, the most important application of windmills at the subsistence level has been mechanical water pumping using relatively small systems with rotor diameters of one to several meters. These systems were perfected in the United States during the19th century, beginning with the Halladay windmill in 1854, and continuing to the Aermotor and Dempster designs, which are still in use today.

The first mills had four paddle-like wooden blades. They were followed by mills with thin wooden slats nailed to wooden rims. Most of these mills had tails to orient them into the wind, but some were weather-vaning mills that operated downwind of the tower. Speed control of some models was provided by hinging sections of blades, so that they would fold back like an umbrella in high winds, an action which reduced the rotor capture area to reduce thrust. The most important refinement of the American fan-type windmill was the development of steel blades in 1870 (Figure 5). Steel blades could be made lighter and worked into more efficient shapes. They worked so well, in fact, that their high speed required a reduction (slow-down) gear to turn the standard reciprocal pumps at the required speed.

Between 1850 and 1970, over six million mostly small (1 horsepower or less) mechanical output wind machines were installed in the U.S. alone. The primary use was water-pumping and the main applications were stock watering and farm home water needs. Very large windmills, with rotors up to 18 meters in diameter, were used to pump water for the steam railroad trains that provided the primary source of commercial transportation in areas where there were no navigable rivers.

In the late 19th century, the successful "American" multi-blade windmill design was used in the first large windmill to generate electricity.

First Use of Wind for "Large-Scale" Generation of Electricity

The first use of a large windmill to generate electricity was a system built in Cleveland, Ohio, in 1888 by Charles F. Brush. The Brush machine (shown at right) was a postmill with a multiple-bladed "picket-fence" rotor 17 meters in diameter, featuring a large tail hinged to turn the rotor out of the wind. It was the first windmill to incorporate a step-up gearbox (with a ratio of 50:1) in order to turn a direct current generator at its required operational speed (in this case, 500 RPM.)

Despite its relative success in operating for 20 years, the Brush windmill demonstrated the limitations of the low-speed, high-solidity rotor for electricity production applications. The 12 kilowatts produced by its 17-meter rotor pales beside the 70-100 kilowatts produced by a comparably-sized, modern, lift-type rotor.

In 1891, the Dane Poul La Cour developed the first electrical output wind machine to incorporate the aerodynamic design principles (low-solidity, four-bladed rotors incorporating primitive airfoil shapes) used in the best European tower mills. The higher speed of the La Cour rotor made these mills quite practical for electricity generation. By the close of World War I, the use of 25 kilowatt electrical output machines had spread throughout Denmark, but cheaper and larger fossil-fuel steam plants soon put the operators of these mills out of business.

By 1920, the two dominant rotor configurations (fan-type and sail) had both been tried and found to be inadequate for generating appreciable amounts of electricity. The further development of wind generator electrical systems in the United States was inspired by the design of airplane propellers and (later) monoplane wings.

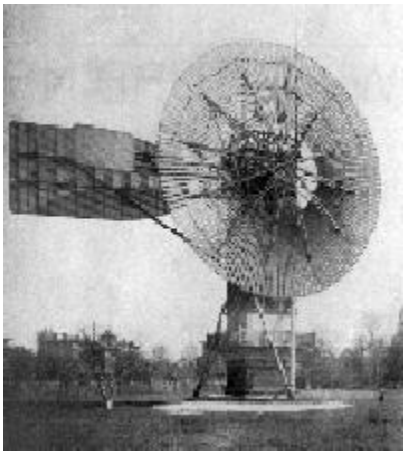

Figure 6. The Brush postmill in Cleveland, Ohio, 1888. The first use of a large windmill to generate electricity. Note the man mowing the lawn at lower right.

Small System Pioneers

The first small electrical-output wind turbines simply used modified propellers to drive direct current generators. By the mid-1920's, 1 to 3-kilowatt wind generators developed by companies like Parris-Dunn and Jacobs Wind-electric found widespread use in the rural areas of the midwestern Great Plains. (A 3-kilowatt Jacobs unit is shown at right, being adjusted by a cigarette-puffing M.L. Jacobs at Rocky Flats, Colorado in 1977.) These systems were installed at first to provide lighting for farms and to charge batteries used to power crystal radio sets. But their use was extended to an entire array of direct-current motor-driven appliances, including refrigerators, freezers, washing machines, and power tools. But the more appliances were powered by the early wind generators, the more their intermittent operation became a problem.

The demise of these systems was hastened during the late 1930s and the 1940s by two factors: the demand of farmsteads for ever larger amounts of power on demand, and the Great Depression, which spurred the U.S. federal government to stimulate the depressed rural economies by extending the electrical grid throughout those areas.

A lot is made of this development and how horrible it was for the government to intervene. (At this point in most wind energy documentaries, there's a plaintive whine of a harmonica and a shot of a rusting wind turbine hulk.) But I doubt the farmers who were helped by the new electrical grids would share this feeling. And the growing demand for electrical power created by the wind generator, combined with the inability of the technology to adapt, helped make the situation inevitable. The early success of the Midwest wind turbines actually set the stage for the possibility of more extensive wind energy development in the future.

While the market for new small wind machines of any type had been largely eroded in the United States by 1950, the use of mechanical and electrical system continued throughout Europe and in windy, arid climates such as those found in parts of Africa and Australia.

Figure 7. M.L. Jacobs adjusting the spring-actuated pitch change mechanism on a Jacobs Wind-electric in 1977.

"Bulk" Power from Wind

The development of bulk-power, utility-scale wind energy conversion systems was first undertaken in Russia in 1931 with the 100kW Balaclava wind generator. This machine operated for about two years on the shore of the Caspian Sea, generating 200,000 kWh of electricity. Subsequent experimental wind plants in the United States, Denmark, France, Germany, and Great Britain during the period 1935-1970 showed that large-scale wind turbines would work, but failed to result in a practical large electrical wind turbine.

The largest was the 1.25 megawatt Smith-Putnam machine (Figure 8, at right), installed in Vermont in 1941. This horizontal-axis design featured a two-bladed, 175-foot diameter rotor oriented down-wind of the tower. The 16-ton stainless steel rotor used full-span blade pitch control to maintain operation at 28 RPM. In 1945, after only several hundred hours of intermittent operation, one of the blades broke off near the hub, apparently as a result of metal fatigue. This is not surprising considering the huge loads that must have been generated in a structure that had a lot in common with a gigantic rotating erector set.

Figure 8. Palmer Putnam's 1.25-megawatt wind turbine was one of the engineering marvels of the late 1930's, but the jump in scale was too great for available materials.

European Development

European developments continued after World War II, when temporary shortages of fossil fuels led to higher energy costs. As in the United States, the primary application for these systems was interconnection to the electric power grid.

In Denmark, the 200 kW Gedser Mill wind turbine operated successfully until the early 1960s, when declining fossil-fuel prices once again made wind energy made uncompetitive with steam-powered generating plants. This machine featured a three-bladed upwind rotor with fixed pitch blades that used mechanical windmill technology augmented with an airframe support structure. The design was much less mechanically complex than the Smith-Putnam design. In fact, it was not that far removed from Poul La Cour's 1920-era windmill (a fact that worked to its advantage.)

Figure 9. Yes, that's an airframe holding together the three blades of the "Gedser Mollen." Fiberglass later eliminated this design requirement.

In Germany, Professor Ulrich Hutter developed a series of advanced, horizontal-axis designs of intermediate size that utilized modern, airfoil-type fiberglass and plastic blades with variable pitch to provide light weight and high efficiencies. This design approach sought to reduce bearing and structural failures by "shedding" aerodynamic loads, rather than "withstanding" them as did the Danish approach. One of the most innovative load-shedding design features was the use of a bearing at the rotor hub that allowed the rotor to "teeter" in response to wind gusts and vertical wind shear. Hutter's advanced designs achieved over 4000 hours of operation before the experiments were ended in 1968.

Post war activity in Denmark and Germany largely dictated the two major horizontal-axis design approaches that would emerge when attention returned to wind turbine development in the early 1970s. The Danes refined the simple, fixed pitch, Gedser Mill design, utilizing advanced materials, improved aerodynamic design, and aerodynamic controls to reduce some of its shortcomings. The engineering innovations of the light-weight, higher efficiency German machines, such as a teeter hinge at the rotor hub, were used later by U.S. designers.

The development of modern vertical-axis rotors was begun in France by G.J.M. Darrieus in the 1920s. Of the several rotors Darrieus designed, the most important one is a rotor comprising slender, curved, airfoil-section blades attached at the top and bottom of a rotating vertical tube. Major development work on this concept did not begin until the concept was reinvented in the late 1960s by two Canadian researchers.

U.S. efforts with the Darrieus concept at **Sandia National Laboratories** began after the 1973 oil embargo, with the entry of the U.S. Federal Wind Energy Program into the cycle of wind energy development.

Wind machines were used in Persia as early as 200 B.C.[2] The windwheel of Heron of Alexandria marks one of the first known instances of wind powering a machine in history.[3][4] However, the first practical windmills were built in Sistan, Iran, from the 7th century. These were vertical axle windmills, which had long vertical driveshafts with rectangle-shaped blades.[5] Made of six to twelve sails covered in reed matting or cloth material, these windmills were used to grind corn and draw up water, and were used in the gristmilling and sugarcane industries.[6]

By the 14th century, Dutch windmills were in use to drain areas of the Rhine River delta. In Denmark by 1900, there were about 2500 windmills for mechanical loads such as pumps and mills, producing an estimated combined peak power of about 30 MW. The first known electricity generating windmill operated was a battery charging machine installed in 1887 by James Blyth in Scotland.[7] The first windmill for electricity production in the United States was built in Cleveland, Ohio by Charles F Brush in 1888, and in 1908 there were 72 wind-driven electric generators from 5 kW to 25 kW. The largest machines were on 24 m (79 ft) towers with four-bladed 23 m (75 ft) diameter rotors. Around the time of World War I, American windmill makers were producing 100,000 farm windmills each year, mostly for water-pumping.[8] By the 1930s, windmills for electricity were common on farms, mostly in the United States where distribution systems had not yet been installed. In this period, high-tensile steel was cheap, and windmills were placed atop prefabricated open steel lattice towers.

A forerunner of modern horizontal-axis wind generators was in service at Yalta, USSR in 1931. This was a 100 kW generator on a 30 m (100 ft) tower, connected to the local 6.3 kV distribution system. It was reported to have an annual capacity factor of 32 per cent, not much different from current wind machines.[9] In the fall of 1941, the first megawatt-class wind turbine was synchronized to a utility grid in Vermont. The Smith-Putnam wind turbine only ran for 1100 hours. Due to war time material shortages the unit was not repaired.

The first utility grid-connected wind turbine operated in the UK was built by John Brown & Company in 1954 in the Orkney Islands. It had an 18 meter diameter, three-bladed rotor and a rated output of 100 kW.

[edit] Resources

Main article: Wind power

Wind turbines locations with constantly high wind speeds bring best return on investment. With a wind resource assessment it is possible to estimate the amount of energy the wind turbine will produce.

A quantitative measure of the wind energy available at any location is called the Wind Power Density (WPD.) It is a calculation of the mean annual power available per square meter of swept area of a turbine, and is tabulated for different heights above ground. Calculation of wind power density includes the effect of wind velocity and air density.

Color-coded maps are prepared for a particular area described, for example, as "Mean Annual Power Density at 50 Meters." In the United States, the results of the above calculation are included in an index developed by the National Renewable Energy Lab and referred to as "NREL CLASS." The larger the WPD calculation, the higher it is rated by class. Classes range from Class 1 (200 watts/square meter or less at 50 meters altitude) to Class 7 (800 to 2000 watts/square meter). Commercial wind farms generally are sited in Class 3 or higher areas, although isolated points in an otherwise Class 1 area may be practical to exploit.[10]

[edit] Types of wind turbines

Wind turbines can rotate about either a horizontal or vertical axis, the former being more common.[11]

[edit] Horizontal axis

Components of a horizontal axis wind turbine (gearbox, rotor shaft and brake assembly) being lifted into position

Horizontal-axis wind turbines (HAWT) have the main rotor shaft and electrical generator at the top of a tower, and must be pointed into the wind. Small turbines are pointed by a simple wind vane, while large turbines generally use a wind sensor coupled with a servo motor. Most have a gearbox, which turns the slow rotation of the blades into a quicker rotation that is more suitable to drive an electrical generator.[12]

Since a tower produces turbulence behind it, the turbine is usually pointed upwind of the tower. Turbine blades are made stiff to prevent the blades from being pushed into the tower by high winds. Additionally, the blades are placed a considerable distance in front of the tower and are sometimes tilted forward into the wind a small amount.

Downwind machines have been built, despite the problem of turbulence (mast wake), because they don't need an additional mechanism for keeping them in line with the wind, and because in high winds the blades can be allowed to bend which reduces their swept area and thus their wind resistance. Since cyclic (that is repetitive) turbulence may lead to fatigue failures most HAWTs are upwind machines.

[edit] Horizontal subtypes

Doesburger windmill, Ede, The Netherlands.
12th-century windmills

These squat structures, typically (at least) four bladed, usually with wooden shutters or fabric sails, were developed in Europe. These windmills were pointed into the wind manually or via a tail-fan and were typically used to grind grain. In the Netherlands they were also used to pump water from low-lying land, and were instrumental in keeping its polders dry.

In Schiedam, the Netherlands, a traditional style windmill (the *Noletmolen*) was built in 2005 to generate electricity.[13] The mill is one of the tallest Tower mills in the world, being some 42.5 metres (139 ft) tall.

19th-century windmills

The Eclipse windmill factory was set up around 1866 in Beloit, Wisconsin and soon became successful building mills for pumping water on farms and for filling railroad tanks. Other firms like Star, Dempster, and Aeromotor also entered the market. Hundreds of thousands of these mills were produced before rural electrification and small numbers continue to be made.[8] They typically had many blades, operated at tip speed ratios not better than one, and had good starting torque. Some had small direct-current generators used to charge storage batteries, to provide power to lights, or to operate a radio receiver. The American rural electrification connected many farms to centrally-generated power and replaced individual windmills as a primary source of farm power by the 1950s. They were also produced in other countries like South Africa and Australia (where an American design was copied in 1876[14]). Such devices are still used in locations where it is too costly to bring in commercial power.

Modern wind turbines

Three bladed wind turbine

Turbines used in wind farms for commercial production of electric power are usually three-bladed and pointed into the wind by computer-controlled motors. These have high tip speeds of over 320 km/h (200 miles per hour), high efficiency, and low torque ripple, which contribute to good reliability. The blades are usually colored light gray to blend in with the clouds and range in length from 20 to 40 metres (65 to 130 ft) or more. The tubular steel towers range from 60 to 90 metres (200 to 300 feet) tall. The blades rotate at 10-22 revolutions per minute. At 22 rotations per minute the tip speed exceeds 300 ft per second.[15][16] A gear box is commonly used to step up the speed of the generator, although designs may also use direct drive of an annular generator. Some models operate at constant speed, but more energy can be collected by variable-speed turbines which use a solid-state power converter to interface to the transmission system. All turbines are equipped with shut-down features to avoid damage at high wind speeds.

[edit] Horizontal axis advantages

- Variable blade pitch, which gives the turbine blades the optimum angle of attack. Allowing the angle of attack to be remotely adjusted gives greater control, so the turbine collects the maximum amount of wind energy for the time of day and season.
- The tall tower base allows access to stronger wind in sites with wind shear. In some wind shear sites, the wind speed can increase by 20% and the power output by 34% for every 10 metres in elevation.
- High efficiency, since the blades always move perpendicular to the wind, receiving power through the whole rotation. In contrast, all vertical axis wind turbines, and most proposed airborne wind turbine designs, involve various types of reciprocating actions, requiring airfoil surfaces to backtrack against the wind for part of the cycle. Backtracking against the wind leads to inherently lower efficiency.
- The face of a horizontal axis blade is struck by the wind at a consistent angle regardless of the position in its rotation. This results in a consistent lateral wind loading over the course of a rotation, reducing vibration and audible noise coupled to the tower or mount.

[edit] Horizontal axis disadvantages

This section **does not cite any references or sources**.
Please help improve this article by adding citations to reliable sources. Unsourced material may be challenged and removed. *(September 2009)*

Turbine blade convoy passing through Edenfield in the UK

- The tall towers and blades up to 45 meters long are difficult to transport. Transportation can now amount to 20% of equipment costs.
- Tall HAWTs are difficult to install, needing very tall and expensive cranes and skilled operators.
- Massive tower construction is required to support the heavy blades, gearbox, and generator.
- Reflections from tall HAWTs may affect side lobes of radar installations creating signal clutter, although filtering can suppress it.
- Their height makes them obtrusively visible across large areas, disrupting the appearance of the landscape and sometimes creating local opposition.
- Downwind variants suffer from fatigue and structural failure caused by turbulence when a blade passes through the tower's wind shadow (for this reason, the majority of HAWTs use an upwind design, with the rotor facing the wind in front of the tower).
- HAWTs require an additional yaw control mechanism to turn the blades and nacelle toward the wind.
- In order to minimize fatigue loads due to wake turbulence, wind turbines are usually sited a distance of 5 rotor diameters away from each other, but the spacing depends on the manufacturer and the turbine model.

[edit] Cyclic stresses and vibration

Cyclic stresses fatigue the blade, axle and bearing resulting in material failures that were a major cause of turbine failure for many years. Because wind velocity often increases at higher altitudes, the backward force and torque on a horizontal-axis wind turbine (HAWT) blade peaks as it turns through the highest point in its circle. The tower hinders the airflow at the lowest point in the circle, which produces a local dip in force and torque. These effects produce a cyclic twist on the main bearings of a HAWT. The combined twist is worst in machines with an even number of blades, where one is straight

up when another is straight down. To improve reliability, teetering hubs have been used which allow the main shaft to rock through a few degrees, so that the main bearings do not have to resist the torque peaks.

The rotating blades of a wind turbine act like a gyroscope. As it pivots along its vertical axis to face the wind, gyroscopic precession tries to twist the turbine disc along its horizontal axis. For each blade on a wind generator's turbine, precessive force is at a minimum when the blade is horizontal and at a maximum when the blade is vertical.

[edit] Vertical axis design

This section **does not cite any references or sources**.
Please help improve this article by adding citations to reliable sources. Unsourced material may be challenged and removed. *(September 2009)*

Vertical-axis wind turbines (or VAWTs) have the main rotor shaft arranged vertically. Key advantages of this arrangement are that the turbine does not need to be pointed into the wind to be effective. This is an advantage on sites where the wind direction is highly variable.

With a vertical axis, the generator and gearbox can be placed near the ground, so the tower doesn't need to support it, and it is more accessible for maintenance. Drawbacks are that some designs produce pulsating torque.

It is difficult to mount vertical-axis turbines on towers[*citation needed*], meaning they are often installed nearer to the base on which they rest, such as the ground or a building rooftop. The wind speed is slower at a lower altitude, so less wind energy is available for a given size turbine. Air flow near the ground and other objects can create turbulent flow, which can introduce issues of vibration, including noise and bearing wear which may increase the maintenance or shorten the service life. However, when a turbine is mounted on a rooftop, the building generally redirects wind over the roof and this can double the wind speed at the turbine. If the height of the rooftop mounted turbine tower is approximately 50% of the building height, this is near the optimum for maximum wind energy and minimum wind turbulence.

[edit] Vertical axis subtypes

30 m Darrieus wind turbine in the Magdalen Islands

Darrieus wind turbine

"Eggbeater" turbines, or Darrieus turbines, were named after the French inventor, Georges Darrieus.[17] They have good efficiency, but produce large torque ripple and cyclical stress on the tower, which contributes to poor reliability. They also generally require some external power source, or an additional Savonius rotor to start turning, because the starting torque is very low. The torque ripple is reduced by using three or more blades which results in a higher solidity for the rotor. Solidity is measured by blade area divided by the rotor area. Newer Darrieus type turbines are not held up by guy-wires but have an external superstructure connected to the top bearing.

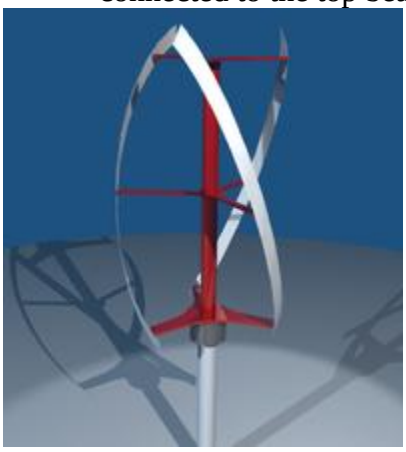

A helical twisted VAWT.

Giromill

A subtype of Darrieus turbine with straight, as opposed to curved, blades. The cycloturbine variety has variable pitch to reduce the torque pulsation and is self-starting.[18] The advantages of variable pitch are: high starting torque; a wide, relatively flat torque curve; a lower blade speed ratio; a higher coefficient of performance; more efficient operation in turbulent winds; and a lower blade speed

ratio which lowers blade bending stresses. Straight, V, or curved blades may be used.

Windmill with rotating sails
Savonius wind turbine

These are drag-type devices with two (or more) scoops that are used in anemometers, *Flettner* vents (commonly seen on bus and van roofs), and in some high-reliability low-efficiency power turbines. They are always self-starting if there are at least three scoops. They sometimes have long helical scoops to give a smooth torque.

[edit] Vertical axis advantages

- A massive tower structure is less frequently used, as VAWTs are more frequently mounted with the lower bearing mounted near the ground.
- Designs without yaw mechanisms are possible with fixed pitch rotor designs.
- The generator of a VAWT can be located nearer the ground, making it easier to maintain the moving parts.
- VAWTs have lower wind startup speeds than HAWTs. Typically, they start creating electricity at 6 m.p.h. (10 km/h).
- VAWTs may be built at locations where taller structures are prohibited.
- VAWTs situated close to the ground can take advantage of locations where mesas, hilltops, ridgelines, and passes funnel the wind and increase wind velocity.
- VAWTs may have a lower noise signature.[*citation needed*]

[edit] Vertical axis disadvantages

- A VAWT that uses guy-wires to hold it in place puts stress on the bottom bearing as all the weight of the rotor is on the bearing. Guy wires attached to the top bearing increase downward thrust in wind gusts. Solving this problem requires a superstructure to hold a top bearing in place to eliminate the downward thrusts of gust events in guy wired models.
- The stress in each blade due to wind loading changes sign twice during each revolution as the apparent wind direction moves through 360 degrees. This reversal of the stress increases the likelihood of blade failure by fatigue.
- While VAWTs' components are located on the ground, they are also located under the weight of the structure above it, which can make changing out parts very difficult without dismantling the structure, if not designed properly.
- Having rotors located close to the ground where wind speeds are lower due to the ground's surface drag, VAWTs may not produce as much energy at a given site as a HAWT with the same footprint or height.

[edit] Turbine design and construction

Main article: Wind turbine design

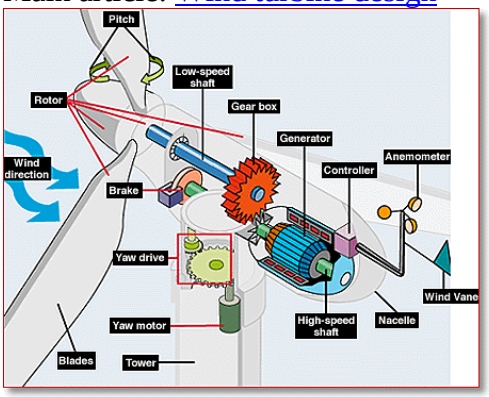

Components of a horizontal-axis wind turbine

Wind turbines are designed to exploit the wind energy that exists at a location. Aerodynamic modeling is used to determine the optimum tower height, control systems, number of blades and blade shape.

Wind turbines convert wind energy to electricity for distribution. Conventional horizontal axis turbines can be divided into three components.

- The rotor component, which is approximately 20% of the wind turbine cost, includes the blades for converting wind energy to low speed rotational energy.
- The generator component, which is approximately 34% of the wind turbine cost, includes the electrical generator, the control electronics, and most likely a gearbox

component for converting the low speed incoming rotation to high speed rotation suitable for generating electricity.

- The structural support component, which is approximately 15% of the wind turbine cost, includes the tower and rotor yaw mechanism.[19]

temperature was also kept under consideration in this experiment and the experiment was carried out at atmospheric temperature i.e. at t = 30° C.

In order to smoothen the flow, a honeycomb was fixed near the outlet of the wind tunnel. The setup had a bell-shaped converging duct at the entry. To generate the wind velocity, two axial flow fans were used, with each of the fans connected to a motor of 2.25 kW capacity and 2900 rpm. A butterfly valve was used to control the wind speed. A silencer was connected just after the butterfly valve for reduction of the noise.

The central longitudinal axis of the wind tunnel was always kept at a constant height of 990 mm from the floor. The axis of the model was also placed coinciding with the axis of the wind tunnel. The converging duct inlet was then merged into the wind tunnel so that air can enter smoothly into the tunnel and maintain uniform flow into the duct, keeping it free from any outside disturbances. The flow through the wind tunnel was induced by a two-stage axial flow fan of 18.16 m^3/s capacity with a head of 152.4 mm of water.

The Five Bladed Vane Type Rotor

The constructional detail of the test section is shown in the Figure 2. Five bladed vane type rotor was made up of five half cylinders (blade) of diameter, d = 65 mm and height, H = 340 mm. Rotor diameter, D was 200 mm. Optimum value of d/D ratio was taken as 3. The cylinders were made of PVC material. The center-to-center distance of the blade was 137.5 mm. The whole rotor was fixed on an iron frame by using two side shafts and two ball bearings.

The pressure measurements were made at 8 pressure tappings on each blade. The tappings were made with copper tubes of 1.5 mm outer diameter and 10 mm length and were press fitted to the tapping holes. The tappings were located at the mid-plane of one side of each blade and connected to an inclined multi-manometer (manometric fluid was water and had an accuracy of ± 0.1 mm of water column) through 2 mm PVC tubes.

Before measuring the pressure distribution, the mean velocity was measured in a vertical plane at 0.5 m downstream from the exit of the wind tunnel without placing the rotor by means of a pitot static tube connected to an inclined manometer with kerosene as the manometric fluid. The measured velocity distribution was found more

or less uniform.

Figure 2: Five bladed vertical axis vane type rotor.

Figure 3: Experimental setup in the laboratory.

The pressure distribution over the blade surfaces was measured step by step by using the multi-manometer bank. The experimental set-up is shown in Figure 3. At first, the vane rotor with the frame was placed 500 mm down stream of the exit section of the wind tunnel. One blade of the rotor was fixed parallel to the free stream velocity i.e. parallel to the horizontal, which was called the reference plane and from this plane angle of rotation was measured. At the beginning, the first blade was at 0° angle of rotation, exposing the convex surface in front of free stream air, so the other four blades were at 72° , 144° , 216° , and 288° angle of rotation respectively. The rotor was then made static by fixing one end of the shaft with the angle-fixing

1 Converging mouth entry 7 Diverging section
2 Perspex section 8 Converging section
3 Rectangular diverging section 9 Rectangular section
4 Fan section 10 Flow straightener section
5 Butterfly section 11 Rectangular exit section
6 Silencer with honeycomb section

Figure 1: Schematic diagram of wind tunnel.

MCDM 2006, Chania, Greece, June 19-23, 2006

THE MATERIAL SELECTION FOR TYPICAL WIND TURBINE BLADES USING A MADM APPROACH& ANALYSIS OF BLADES

1K.Suresh Babu 1N.V.Subba Raju 1M.Srinivasa Reddy 2Dr. D. Nageswara Rao
Asst. Professor Professor ME Student Professor

1. SRKR

ABSTRACT

Over the centuries, energy has been supplied by wood, coke, coal, oil and natural gas, as well as by uranium (nuclear energy). All these energy sources are limited and at the same time these energy sources create pollution problems. This has led to the focus on a sustainable energy supply, which implies optimized use of energy, minimized pollution. That is why wind energy is prominent and it is the solution to the global energy problem. The wind energy is generated by using wind turbines. The turbine blades plays very important role in the wind turbines. The efficiency of the wind turbine depends on the material of the blade, shape of the blade and angle of the blade. So, the material of the turbine blade plays a vital role in the wind turbines. The material of the blade should possess the high stiffness, low density and long fatigue life. The main objective of our topic is to discuss the different materials as candidates for turbine

blades and to select the best material for turbine blades by using one of the MADM (Multiple Attribute
Decision Making) approach with fuzzy linguistic variables. After the material selection, the turbine blades
are created by using modeling packages (CATIA V5R9) and Analysis can be done by using FEM for
different configurations, different operating conditions, in different cases were taken up to estimate the
values of deformations, stress values and different frequency sets by altering the thickness of blade and
angle of twist.
Key words: MCDM, MADM, MODM, TOPSIS, Fuzzy Linguistic variables
MCDM- Multiple criteria decision making
MADM- Multiple attribute decision making
MODM- Multiple objective decision making
TOPSIS- Technique for order preference by similarity to ideal solution
2
1. Introduction
Over the centuries, energy has been supplied by different types of energy sources like wood, coal etc. At
the same time there is an increasing concern about the pollution of the world/environment (generation of
waste). This has led to the focus on a sustainable energy supply, which (probably) implies optimized use of
energy, minimized pollution and, implicitly, reduction in energy consumption. These aspects have led to an
increasing focus on the short-time stored energy resources; among these the most developed types today are
wind energy and biomass. For wind energy a converter is needed to turn the kinetic wind energy into
operational energy, e.g., electricity and/or heat. The converter is based on a rotor driven by the wind. The
rotor needs some sort of a device, e.g., a wing or rotor blade to be able to rotate. The rotor is typically
placed on a tower, and this converter is usually called a wind turbine (in the past, a wind mill). The
development of wind turbines has made a significant contribution to human achievement and technological
advancement throughout history. Recent advances in technology and performance have resulted in current
wind turbine designs being increasingly efficient, cost effective, and reliable. The material selection of the
wind turbine blades plays an important role in the wind turbine designs. An ever-increasing variety of
materials is available today, with each having its own characteristics, applications, advantages, and
limitations. When selecting materials for engineering designs, we must have a clear understanding of the
functional requirements for each individual component. In selecting materials for an application,
technological considerations of material properties and characteristics are important. The economic aspects

of material selection, such as availability, cost of raw materials, and cost of manufacturing, are equally important. The selection of an optimal material for an engineering design from among two or more alternative materials on the basis of two or more properties is a multi criteria decision-making problem. The material selection process motivates us to develop a multi criteria decision-making method using fuzzy set theory. Fuzzy set theory was developed exactly based on the premise that the key elements in human thinking are not numbers, but linguistic terms or labels of fuzzy sets.

1.1. Wind Power Turbines

Charles F. Brush (1849-1929) is one of the founders of the American electrical industry. During the winter of 1887-88 Brush built what is today believed to be the first automatically operating wind turbine for electricity generation. After, Dane Poul la Cour, who later discovered that fast rotating wind turbines with few rotor blades are more efficient for electricity production than slow moving wind turbines. During World War II the Danish engineering company F.L. Smidth (now a cement machinery maker) built a number of two- and three-bladed wind turbines. This three-bladed F.L. Smidth machine from the island of Bogø, built in 1942, looks more like a "Danish" machine.

The innovative 200 kW Gedser wind turbine was built in 1956-57 by J. Juul for the electricity company SEAS at Gedser coast in the Southern part of Denmark. The Gedser wind turbine was refurbished in 1975 at the request of NASA which wanted measurement results from the turbine for the new U.S. wind energy programme. In 1979 they built two 630 kW wind turbines, one pitch controlled, and one stall controlled. A carpenter, Christian Riisager, however, built a small 22 kW wind turbine in his own back yard using the Gedser Wind Turbine design as a point of departure. The prototype of the NEG Micon 1500 kW Turbine was commissioned in September 1995. The prototype of the Vestas 1500 kW Turbine was commissioned in 1996. The megawatt market really took off in 1998. The prototype of the NEG Micon 2 MW turbine was commissioned in August 1999. The largest offshore wind farms in Denmark are Horns Rev by the west coast of Jutland and Nysted close to Lolland - 160 and 158 MW respectively. A tendering procedure for new offshore wind farms will be commenced in late 2003.

A wind turbine is a machine for converting the mechanical energy in wind into electrical energy. If the mechanical energy is used directly by machinery, such as a pump or grinding stones, the machine is usually also called as windmill. Wind turbines can be separated into two general types based on the axis about

which the turbine rotates. Turbines that rotate around a horizontal axis are most common. Vertical axis
turbines are less frequently used.
Horizontal Axis Wind Turbines (HAWTs) have the main rotor shaft running horizontally and generator at
the top of a tower, and must be pointed into the wind by some means. Small turbines are pointed by a
simple wind vane, while large turbines generally use a wind sensor coupled with a servomotor. Most have a
gearbox too, which turns the slow rotation of the blades into a quicker rotation that is more suitable for
generating electricity. Vertical axis wind turbines (VAWTs) have the main rotor shaft running vertically.
The advantages of this arrangement are that the generator and/or gearbox can be placed at the bottom, near
the ground, so the tower doesn't need to support it, and that the turbine doesn't need to be pointed into the
wind. Drawbacks are usually the pulsating torque produced during each revolution; and the difficulty of
mounting vertical axis turbines on towers, meaning they must operate in the slower, more turbulent air flow
near the ground, with lower energy extraction efficiency.
The rotor and its three rotor blades constitute a rather flimsy structure, consisting of cantilever-mounted
blades on a central hub. Nowadays, modern wind turbine engineers avoid building large machines with an
even number of rotor blades. The most important reason is the stability of the turbine. A rotor with an odd
number of rotor blades (and at least three blades) can be considered to be similar to a disc when calculating
the dynamic properties of the machine. A rotor with an even number of blades will give stability problems
for a machine with a stiff structure. The reason is that at the very moment when the uppermost blade bends
backwards, because it gets the maximum power from the wind, the lowermost blade passes into the wind
shade in front of the tower. So, Most of the modern wind turbines are three-bladed designs with the rotor
position maintained upwind (on the windy side of the tower) using electrical motors in their yaw
mechanism. The design life time of modern wind turbines is normally thought to be 20 years, and the
corresponding number of rotations is of the order 10^8 to 10^9. The basic design aspects for a rotor blade are
the selection of material and shape. The material should be stiff, strong, and light. The challenge for the
designers is thus to go beyond the simple plank and the shape of the blade with pre-twist into a design of
the blade structure that is optimized with respect to materials selection and cost-effective production. Older

style wind turbines were designed with wood, steel, Aluminum materials. Nowadays, composite materials
are extensively used to design the wind turbine blades.

1.2. Selection of Materials

A material is that out of which anything is or may be made. Much number of factors are affecting for the
material selection. They are properties of materials, performance requirements, material’s reliability, safety,
Physical attributes environmental conditions, availability, disposability and recyclability, and finally
economic factors. In these properties,

1) One of the most important factors affecting selection of materials for engineering design is the
properties of the materials. The important properties of the materials are mechanical, thermal,
chemical properties..,etc.
2) The material of which a part is composed must be capable of performing a part’s function (always
it must be possible or not) with out failure.
3) A material in a given application must also be reliable.
4) A material must safely perform its function.
5) Physical attributes such as configuration, size, weight, and appearance sometimes also serve
functional requirements can be used.
6) The environment in which a product operates strongly influences service performance.
7) A material must be readily available, and available in large enough quantity, for the intended
application.
8) The cost of the materials and the cost of processing the materials into the product or part. The
development and manufacture of satisfactory products at minimum cost is to make a sound, economic choice of materials.

The material selection process involves the following major operations:

□ Analysis of the materials application problem.
□ Translation of the materials application requirements to materials property values.

□ Selection of candidate materials.
□ Evaluation of the candidate materials.

And in any material selection, the following requirements are focused. They are

1) High material stiffness is needed to maintain optimal shape of performance.
2) Low density is needed to reduce gravity forces,
3) Long-fatigue life is needed to reduce material degradation.

The optimal design of the rotor blades is today a complex and multifaceted task and requires optimization
of properties, performance, and economy.

1.3. Materials

Wind energy is captured by the rotation of the wind turbine’s rotor blades. Rotor blades have
historically been made of wood, but because of its sensitivity to moisture and processing costs modern
materials such as glass fiber reinforced plastic (GFRP), carbon fiber reinforced plastic (CFRP), steel and

aluminum are replacing the traditional wooden units.
Wood is a composite of cellulose and lignin. Wood finds many engineering applications and has long been
a common construction material. Woods are potentially interesting because of their low density, but their
rather low stiffness makes it difficult to limit the (elastic) deflections for very large rotor blades. Even
wood materials with cellulosic fibers all aligned in the major load-bearing directions are close to the
maximum performance possible for wood. Furthermore, wood is a natural material and thus
environmentally attractive, but at the same time difficult to obtain in reproducible and high quality, which
is a requirement for stable and economical manufacturing of rotor blades and thus economically attractive
wind energy.
Steel is an alloy of iron and carbon. Older style wind turbines were designed with heavier steel blades or
nickel alloy steels which have higher inertia, and rotated at speeds governed by the AC frequency of the
power lines. The high inertia buffered the changes in rotation speed and thus made power output more
stable. The purpose of nickel alloy is lessens distortion in quenching and lowers the critical temperatures of
steel and widens the range of successful heat treatment. Nickel alloy possesses good corrosion and
oxidation resistance. Alloy steel was once thought to be an optimum choice for blade fabrication, but was
soon abandoned because of its high weight and low fatigue level.
Aluminium is a silvery white metal with a density about a third that of steel. Aluminum was only
implemented in testing situations because it was found to have a lower fatigue level than steel. Aluminium
is ductile and good heat conductor. Aluminium is a low price metal but it has good reliability and has a low
tensile strength. Aluminum is lightweight, but weaker and less stiff than steel.
The fibers and the matrix materials like polyesters, vinyl esters, epoxies etc., are combined into the
composites. These composites have good properties like mechanical, thermal and chemical properties.
Firstly, the glass fibers are amorphous with isotropic properties. Most glass-reinforced products are made
with E-glass (electrical glass), which has good electrical and mechanical properties and high heat
resistance. E-glass is available as chopped fiber, milled fiber, continuous roving, woven roving, woven
fabric, and reinforcing mat. Glass fibers for composites have good properties like moderate stiffness, high
strength, and moderate density.
Carbon fibers are composed of nearly pure carbon, which forms a crystallographic lattice with a hexagonal
shape called graphite. In recent years carbon fibers have become of increasing interest because of the

requirements presented by the ever-larger rotor blades and the decreasing price of carbon fibers. Carbon
fibers for composites have an excellent combination of very high stiffness, high strength, light weight and
low density.
Aramid fibers (aromatic polyamides) are characterized by excellent environmental and thermal stability,
static and dynamic fatigue resistance, and impact resistance. These fibers have the highest specific tensile
strength (strength/density ratio) of any commercially available continuous-filament yarn. Aramid5
reinforced thermoplastic composites have excellent wear resistance. Aramid fibers have low or very low
densities.

2. Decision making

In the past, engineering design of a product component is usually viewed as a problem solving
procedure. In recent years, more and more design researchers view engineering design of a product
component as a decision-making process that requires rigorous evaluation of design alternatives. A
decision is a commitment to use resources. Problem solving is generating and refining information
punctuated by decision-making.
Many decisions need to be made under conditions of lack of information. The development of statistics
and probability theory laid down the foundation of decision theory. Traditionally, the work of Bernoulli in
1738 is regarded as the beginnings of a formal decision theory under uncertainty. He proposed the idea that
decision maker might wish to maximize the expected value of something other than wealth. Later, so many
developments are happened. In those developments, Fuzzy logic also proposed by Lotfi zadeh as a
decision-making method under situation of ‘vagueness’. It was proposed in 1973. After, further
developments are happened on basis of fuzzy decision making. “Fuzzy” refers to its ability to deal with
imprecise or vague inputs. Fuzzy logic is a powerful new way to analyze and control complex systems.
Decision making theory provides a number of suggestions for how to estimate complex probabilities under
uncertainty. The use of decision making rule may facilitate a) Selection of the most desirable alternative b)
sorting of alternatives into classes arranged into a priority order c) ranking of alternatives from best to
worst. Decision rules provide on the basis for selection, sorting and ranking by integrating the data on
alternatives and Decision Maker’s preferences into an overall assessment of the alternative.

2.1. Decision making under uncertainty

One of the most important factors in decision making is the degree of uncertainty. Whenever the designer makes a decision, he is performing a prediction of the effect of future events in technical feasibility, economic viability and trade-off between them. To make a successful prediction, good information (previous experience, outcomes from the similar circumstance, design knowledge, expertise etc.), proper methods and sometime good intuition are needed. And all geometry information, material properties, manufacturing process parameters, market change, customers' preference, development and manufacturing cost etc. can be estimated exactly and the future events are perfectly predictable.

Engineering decision-making has distributed nature (linked decision-making) and involves all design stages including the selection of material, concept, configuration, geometry and process plan etc. At each stage alternatives are generated, analyzed, and selected. For Engineering Design, quality, cost and time to market are three most important objectives and they are conflicted, for example, if we want to improve the quality, the cost will increase etc. The final objective of a company's activities is to maximize the profit. All methods are based on one assumption that there is a known probability value for the future event (e.g. a product's performance). However, it may be in appropriate or impossible to assign probabilities to the future events identified for a given decision situation. There are no meaningful data available from which probabilities may be developed. Then how can people make decision under such a difficult situation?

Usually, there are two ways to solve the problem of not being able to assigning objective probability values: using subjective judgment or/and collecting new data. When there are no previous data available, decision-maker can make assessment (reasonable or not) of the probabilities of future events based on his own knowledge and experience. The result of assessment reflects his confidence level. We may have pessimist, optimist or neutral decision maker. In other instances the decision maker may be unwilling to assign such a subjective probability, as is often the case when the outcome could prove to be bad. In such a case, the decision may be deferred until enough new data have been collected to help handle uncertainties

Dept. of Energy

Technology, Stockholm, Sweden.Course “Fluid Machinery” (4A1629)
9
Reversibility of turbomachines
Reversibility of turbomachines
A propeller (axial fan rotor) and a wind turbine rotor are completely reversible. They are described by the same basic theoretical considerations.
Source: ”Energy Conversion – systems, flow physics and engineering”, Reiner Decher
Dept. of Energy Technology, Stockholm, Sweden.Course “Fluid Machinery” (4A1629)
1 0
Thrust and Torque
Thrust and Torque
Thrustis the axial force produced by a propeller (or by a jet stream) and used for driving a body immersed in a fluid.
Torqueis the load in energy terms [N.m] that delivers positive rotating motion (in turbines) or a negative braking force (in propellers). It is basically proportional to the thrust.
Torque and thrust are linked to the aerodynamic forces (lift and drag forces) created by the fluid flowing around the blades of the propeller or turbine. The productivity of a propeller is measured by the thrust, while the torque is the load that the driving engine should overcome. The productivity (but not the efficiency) of a turbine is measured by the produced torque, while the thrust is a useless axial force that the turbine casing or foundation must withstand

Energy in fluid is contained in four different forms: gravitational potential energy, thermodynamic pressure, kinetic energy from the velocity and finally thermal energy. Gravitational and thermal energy have a negligible effect on the energy extraction process. From a macroscopic point of view, the air flow about the wind turbine is at

atmospheric pressure. If pressure is constant then only kinetic energy is extracted. However up close near the rotor itself the air velocity is constant as it passes through the rotor plane. This is because of conservation of mass. The air that passes through the rotor cannot slow down because it needs to stay out of the way of the air behind it. So at the rotor the energy is extracted by a pressure drop. The air directly behind the wind turbine is at sub-atmospheric pressure; the air in front is under greater than atmospheric pressure. It is this high pressure in front of the wind turbine that deflects some of the upstream air around the turbine.

Albert Betz was amongst the first to study this phenomenon. He notably determined the maximum limit to wind turbine performance. The limit is now referred to as the Betz Limit. This is derived by looking at the axial momentum of the air passing through the wind turbine. As stated above some of the air is deflected away from the turbine. This causes the air passing through the rotor plane to have a smaller velocity than the free stream velocity. The degree at which air at the turbine is less than the air far away from the turbine is called the axial induction factor. It is defined as below.

$$U_2 = U_1 (1 - a)$$
$$U_4 = U_1 (1 - 2a)$$

U4 is introduced here as the wind velocity in the far wake. This is important because the power extracted from the turbine is defined by the following equation. However the Betz limit is given in terms of the coefficient of power. The coefficient of power is similar to efficiency but not the same. The formula for the coefficient of power is given beneath the formula for power.

$$P = 0.5\rho A U_2 (U_1^2 - U_4^2)$$
$$C_p \equiv \frac{P}{0.5\rho A U_1^2}$$

Betz was able to develop an expression for Cp in terms of the induction factors. This is done by the velocity relations being substituted into power and power is substituted into the coefficient of power definition. The relationship Betz developed is given below.

$$C_p = 4a (1 - a)^2$$

The Betz limit is defined by the maximum value that can be given by the above formula. This is found by taking the derivative with respect to the axial induction factor, setting it to zero and solving for the axial induction factor. Betz was able to show that the optimum axial induction factor is one third. The optimum axial induction factor was then used to find the maximum coefficient of power. This maximum coefficient is the Betz limit. Betz was able to show that the maximum coefficient of power of a wind turbine is 16/27. Airflow operating at higher thrust will cause the axial induction factor to rise above the

optimum value. Higher thrust causes more air to be deflected away from the turbine. When the axial induction factor falls below the optimum value the wind turbine is not extracting all the energy it can. This reduces pressure around the turbine and allows more air to pass through the turbine, but not enough to account for lack of energy being extracted.

The derivation of the Betz limit shows a simple analysis of wind turbine aerodynamics. In reality there is a lot more. A more rigorous analysis would include wake rotation, the effect of variable geometry. The effect of air foils on the flow is a major component of wind turbine aerodynamics. Within airfoils alone the wind turbine aerodynamicist has to consider the effect of surface roughness, dynamic stall tip losses, solidity, among other problems.

3.3 Angular Momentum and Wake Rotation

The wind turbine described by Betz does not actually exist. It is merely an idealized wind turbine described as an actuator disk. It is a disk in space where fluid energy is simply extracted from the air. In the Betz turbine the energy extraction manifests itself through thrust. The equivalent turbine described by Betz would be a horizontal propeller type operating with infinite blades at infinite tip speed ratios and no losses. The tip speed ratio is ratio of the speed of the tip relative to the free stream flow. This turbine is not too far from actual wind turbines. Actual turbines are rotating blades. They typically operate at high tip speed ratios. At high tip speed ratios three blades are sufficient to interact with all the air passing through the rotor plane. Actual turbines still produce considerable thrust forces.

$$\lambda \equiv \frac{R\Omega}{U_1}$$

One key difference between actual turbines and the actuator disk is that the energy is extracted through torque. The wind imparts a torque on the wind turbine. Newtonian physics dictates that for every action there is an equal and opposite reaction. If the wind imparts a torque on the blades then the blades must be imparting a torque on the wind. This torque would then cause the flow to rotate. Thus the flow in the wake has two components, axial and tangential. This tangential flow is referred to as wake rotation.

Torque is necessary for energy extraction. However wake rotation is considered as a loss. Accelerating the flow in the tangential direction increases the absolute velocity. This in turn increases the amount of kinetic energy in the near wake. This rotational energy is not dissipated in any form that would allow for a greater pressure drop (Energy extraction). Thus any rotational energy in the wake is energy that is lost and unavailable.

This loss is minimized by allowing the rotor to rotate very quickly. To the observer it may seem like the rotor is not moving fast, however it is common for the tips to be moving through the air at 6 times the speed of the free stream. Newtonian mechanics defines power as torque multiplied by the rotational speed. The same amount of power can be extracted by allowing the rotor to rotate faster and produce less torque. Less torque means that there is less wake rotation. Less wake rotation means there is more energy available to extract.

3.4 Rankine-Froude Actuator Disc Theory and Betz Limit

To begin to understand the complex physics involved in wind turbine aerodynamics, a simple one-dimensional model should be analyzed. In the one-dimensional Rankine-Froude actuator disc model, the rotor is represented by an "actuator disc," through which the static pressure has a jump discontinuity. Let us consider a control volume fixed in space whose external boundaries are the surface of a stream tube whose fluid passes through the rotor disc, a cross-section of the stream tube upwind of the rotor, and a cross-section of the stream tube downwind of the rotor. This theory is useful in the derivation of ideal efficiency of a rotor of wind turbines. A simple schematic of this control volume is given in Fig. 3.1.

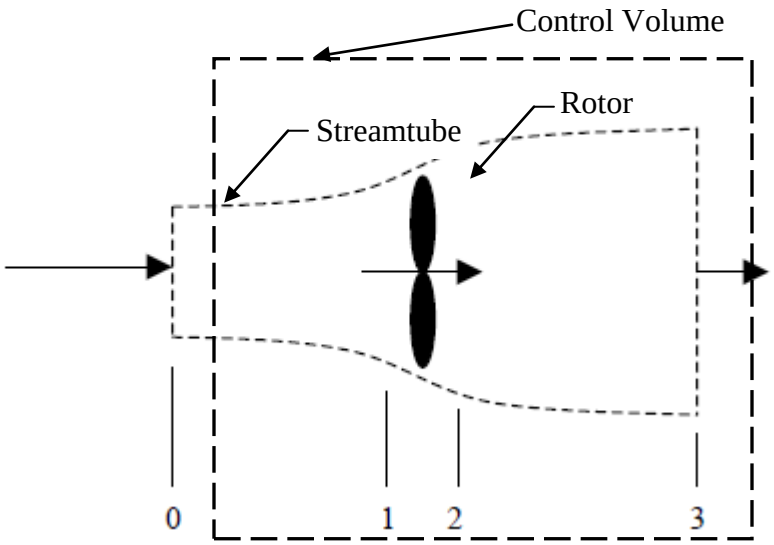

Figure 3.1: Control volume for actuator disc model

The following assumptions are made in the actuator disc model:

(1) Wind is steady, homogenous, and fixed in direction.
(2) Air is incompressible, inviscid, and irrotational.
(3) Both the flow and the thrust are uniform across the disc. The flow is uniform at the upwind (station 0) and downwind (station 3) boundaries of the control volume.
a) Uniform Wind

b) Uniform Wind Shear
c) Turbulent
(4) The upwind and downwind boundaries are far enough removed from the rotor that the static pressure at these points is equal to the unobstructed ambient static pressure. The static pressure on the stream tube portion of the boundary is also equal to the unobstructed ambient static pressure.

For a wind turbine rotor to act as an actuator disc, the rotor would have to be composed of an infinite number of very thin, drag less blades that rotate with a tip speed much higher than that of the incoming wind. Also, station 1 is designated to be slightly upwind and station 2 slightly downwind of the rotor.

Since air does not pass through the stream tube portion of the control volume boundary by definition of a stream tube, applying the conservation of mass1 to the control volume yields:

$$V_0 A_0 = V_1 A_1 = V_2 A_2 = V_3 A_3$$

where V_i is the wind speed at station i and Ai is the cross section area of station i. Since V_1 is equal to V_2 according to assumption (3), and since A_1 equals A_2 by necessity, the components of the wind speed and cross sectional area at the plane of the disc are designated without subscripts for the remainder of this analysis (i.e., $V = V_1 = V_2$ and $A = A_1 = A_2$).
$V_0A_0 = VA = V_3A_3$
(3.4.1)
The thrust at the rotor disc, *T*, can be found by applying the conservation of linear momentum to the control volume in the axial direction. This process results in:

$$T = \rho A_0 V_0^2 - \rho A_3 V_3^2$$

(3.4.2)
or equivalently, using Eq. (3.4.1):

$$T = \rho A V (V_0 - V_3)$$

(3.4.3)
where ρ is the density of the air. The thrust at the rotor disc, *T*, is also the differential pressure between stations 1 and 2 multiplied by the disc area:

$$T = (p_1 - p_2) A$$

(3.4.4)
where *pi* is the static pressure at station *i*. Since no work is done on either side of the turbine rotor, Bernoulli's equation3 can be applied to obtain the pressures incorporated into Eq. (3.4.4):

$$p_0 + \frac{1}{2}\rho V_0^2 = p_1 + \frac{1}{2}\rho V^2$$

and

$$p_3 + \frac{1}{2}\rho V_3^2 = p_2 + \frac{1}{2}\rho V^2$$

(3.4.5)

where p_i is again the static pressure at station i. Pressures p_0 and p_3 are identical by assumption

(4), so pressures p_1 and p_2 can be eliminated from the thrust Eq. (3.4.4) with the help of Eqs. (3.4.5) to obtain:

$$T = \frac{1}{2}\rho A\left(V_0^2 - V_3^2\right)$$

(3.4.6)

Eliminating thrust at the rotor disc from Eqs. (3.4.3) and (3.4.6), the velocity of the flow through the rotor disc is the average of the upwind (free stream) and downwind velocities:

$$V = \frac{V_0 + V_3}{2}$$

(3.4.7)

An axial induction (or interference) factor, a, is customarily defined as the fractional decrease in wind velocity between the free stream and the rotor plane:

$$a = \frac{V_0 - V}{V_0}$$

or equivalently:

$$V = V_0(1 - a)$$

and

$$V_3 = V_0(1 - 2a)$$

(3.4.8)

The velocity lost at the rotor plane, $V_0 - V$, in Eq. (3.4.8) is known as the induced velocity.

As a increases from zero, the downwind flow speed steadily decreases until, at a = ½, it has completely stopped and the simple theory is no longer applicable.

Substituting for V_3 from Eq. (3.4.8), Eq. (3.4.6) can be rewritten in a more useful manner:

$$T = \frac{1}{2}\rho A V_0^2 4a(1 - a)$$

(3.4.9)

The power extracted from the wind by the rotor, P, is the product of the thrust, T, from Eq. (3.4.9) and the wind velocity at the rotor plane, V, from Eq. (3.4.8):

$$P = \frac{1}{2}\rho A V_0^3 4a(1 - a)^2$$

(3.4.10)

The commonly used non-dimensional power coefficient, C_P, representing the fraction of available power in the wind that is extracted by the turbine, is defined as:

$$C_P = \frac{P}{\frac{1}{2}\rho A V_0^3}$$

(3.4.11)

Substituting the extracted power from Eq. (3.4.10) into Eq. (3.4.11) yields:

$$C_P = 4a(1-a)^2$$

(3.4.12)

The theoretical maximum power coefficient from an idealized rotor, C_{Pmax}, known as Betz limit, can be found by setting the derivative of Eq. (2.15) with respect to a equal to zero, and solving for a:

$$\frac{\partial C_P}{\partial a} = 4(1-4a+3a^2) = 0$$

which leads to an optimum interference factor,

$$a = \frac{1}{3}$$

Substituting this result into Eq. (3.4.12) yields:

$$C_{Pmax} = \frac{16}{27} \approx 0.59259$$

(3.4.13)

The maximum possible efficiency for an idealized wind turbine is roughly 59.3%. In practice, three effects prohibit a real wind turbine from achieving this efficiency:

(1) Rotation of the wake caused by the spinning rotor.
(2) Finite numbers of blades.
(3) Viscid flow causes nonzero aerodynamic drag.
All these effects will be considered in the sections that follow.

This one-dimensional model is simple and does not describe the true nature of the physical flow around wind turbines; however, it does bring to light several concepts that are key to understanding wind turbine operation. If the rotor is to extract any power from the wind, the wind must slow down as it passes through the rotor. An ideal wind turbine would have to slow the wind velocity at the rotor plane to two-thirds of the free stream value if it is to extract power at maximum efficiency. Thus, from continuity [Eq. (3.4.1)] the effective upstream area is less than the swept area of the rotor and the area of the wake downstream is greater than the swept area of the rotor. For an ideal wind turbine operating at maximum efficiency, the effective upstream area is two-thirds the swept area and the area of the wake downstream is twice the area swept by the rotor. Finally, extracting all the power available in the wind is theoretically impossible. In practice, a real wind turbine generally does not achieve a power coefficient of more than 45%.

3.4.1 Effects of Wake Rotation on Betz Limit

In the previous model, assumption (1) stated that the rotor imparted no angular momentum to the wake. However, conserving angular momentum necessitates rotation of the wake if the rotor is to extract useful torque. Moreover, the flow behind the rotor will rotate in the opposite direction as the rotor in reaction to the flow imparting torque on the rotor as shown in Fig. 3.2.

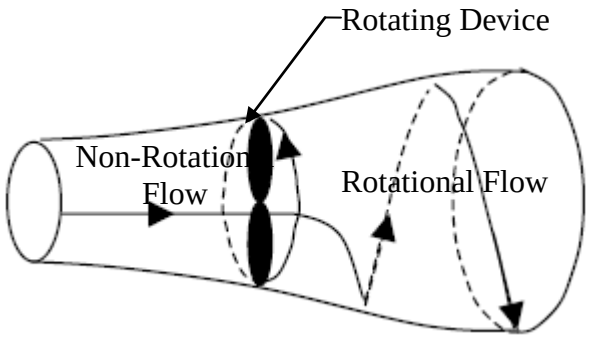

Figure 3.2: Stream Tube Model showing the Rotation of Wake

Since the wake is now rotating, it exhibits rotational kinetic energy that reduces the amount of available energy that can be extracted as useful work. As explained in the subsequent analysis, a rotor generating high torque at low speed will generate less power than a rotor generating low torque at high speed. The typical multi-bladed farm windmill is a notable example of a wind turbine whose efficiency is severely limited by wake rotation.

The Rankine-Froude actuator disc model can be easily extended to account for this wake rotation. To do this, assumptions (1) and (3) from the previous analysis can be relaxed and three supplementary assumptions added:

(1) The control volume used in the previous one-dimensional model can be split into many non-interacting annular stream tube control volumes.
(2) The flow entering the control volume(s) far upstream remains purely axial and uniform.
(3) The angular speed of the wake far downstream of the rotor is low so the static pressure far downstream can still be assumed to be identical to the unobstructed ambient static pressure.

Assumption (1) disregards assumption (3) from the previous analysis and allows for the local pressures, axial velocities (and induction factor), angular velocities, thrust, and power to all functions of the annular radius. This point of view is illustrated in Fig. 3.3:

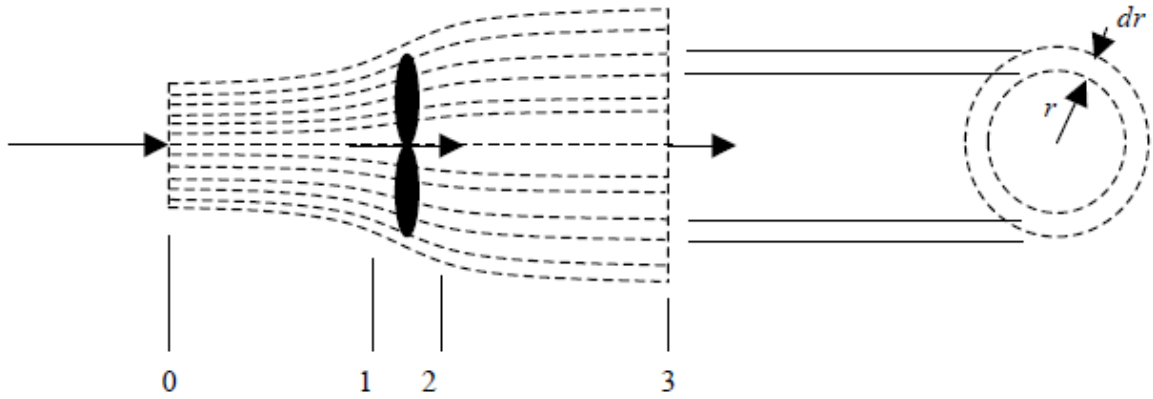

Figure 3.3: Annular stream tube control volumes

Assumption (3) in the analysis of the Rankine-Froude actuator disc model could have been relaxed in the analysis if the variables Ai, T, and P were replaced with the differentials, dA_i, dT, and dP, respectively. In this case, the differential area of an annular ring at station i, dA_i, is defined as:

$$dA_i = 2\pi r_i dr_i$$

(3.4.14)

where r_i and dr_i are the radius and differential radius, respectively, of an annular ring at station *i*.

To be precise, the radius and differential radius of the annular ring of Fig. 3.3 are shown as being the radius and differential radius, respectively, of an annular ring at station 3, or r_3 and dr_3.

Although wake rotation is now included in the analysis, the assumption that the flow is irrotational [assumption (2) from the previous analysis] has *not* been lifted. The definition of rotational flow is any flow with nonzero vorticity. A fluid particle that moves in a circular trend but always retains its original orientation has zero vorticity and is considered to be irrotational. A classic example of this type of flow is a potential vortex.

Since applying the conservation of mass is not affected by wake rotation, the conservation of mass for an annular stream tube control volume can be found by substituting dA_i from Eq. (3.4.14) in for A_i in Eq. (3.4.1) to yield:

$$V_0 2\pi r_0 dr_0 = V 2\pi r dr = V_3 2\pi r_3 dr_3$$

(3.4.15)

where the components of velocity and annular area at the plane of the disc are designated without subscripts ($V = V_1 = V_2$, $r = r_1 = r_2$, and $dr = dr_1 = dr_2$). This designation is made throughout the remainder of the analysis.

The conservation of angular momentum about an axis consistent with the control volume's axis of symmetry can be applied to obtain the differential torque at the rotor disc, dQ, resulting in:

$$dQ = \rho \omega_3 r_3^2 V_3 2\pi r_3 dr_3$$

(3.4.16)

where ω_3 is the angular velocity of the wake at station 3 defined so the differential rotor torque is positive. By assumption (1), the angular velocity of the flow stream at station i, ω_i , is also a function of the annular radius.

Since the flow entering the control volume(s) far upstream is purely axial according to assumption (2), applying the conservation of angular momentum between stations 0 and 1 necessitates that there is no mechanism to impart rotational momentum to the stream ahead of the rotor. Thus,

$$\omega_0 = \omega_1 = 0$$

Similarly, angular momentum is conserved between stations 2 and 3:

$$\omega_2 r^2 = \omega_3 r_3^2$$

(3.4.17)

The angular velocity of the flow stream is discontinuous across the rotor plane because torque is exerted onto the rotor. Also, since the downwind radius of the control volume is larger than the radius of the control volume at the plane of the rotor, the wake rotation slows with distance from the rotor. This latter outcome correlates agreeably with assumption (3).

By combining Eqs. (3.4.16), (3.4.17), and (3.4.15), the differential rotor torque can be rewritten as:

$$dQ = \rho \omega_2 r^2 V 2\pi r dr$$

(3.4.18)

In this form, as the torque of the rotor is increased, the angular speed of the wake increases accordingly.

Since applying the conservation of linear momentum in the axial direction is unaffected by wake rotation, the differential thrust at the rotor disc, dT, can be found by substituting dA_i from Eq.
(3.4.14) at station 1 (equivalently station 2) in for A in Eq. (3.4.9) to yield:

$$dT = \frac{1}{2}\rho 2\pi r dr V_0^2 4a(1-a)$$

(3.4.19)
where the induction factor, *a*, is now a function of the annular radius.

The differential thrust at the rotor disc, dT, is also governed by Eq. (3.4.4) if dA_i from Eq. (3.4.14) at station 1 (equivalently station 2) is again substituted for A. This substitution results in:

$$dT = (p_1 - p_2)2\pi r dr$$

(3.4.20)
where the local pressures at stations 1 and 2, *p1* and *p2* respectively, are now both functions of the annular radius.
To arrive at a description of the wake rotation, it is beneficial to find the difference in pressures *p1* and *p2* not by Bernoulli's equation, but:

$$p_1 + \frac{1}{2}\rho V^2 = p_2 + \frac{1}{2}\rho\left(V^2 + \omega_2^2 r^2\right) + \frac{dQ\Omega}{V 2\pi r dr}$$

(3.4.21)
The product of the differential rotor torque, *dQ*, and the angular speed of the rotor, Ω, in Eq.
(3.4.21) represents the differential power extracted by the turbine, *dP*.

Substituting Eq. (3.4.18) for dQ in Eq. (3.4.21), solving for the difference in pressure, p1 – p2, and substituting the result into Eq. (3.4.20) results in an alternative relation for the differential rotor thrust, dT:

$$dT = \rho\left(\Omega + \frac{1}{2}\omega_2\right)\omega_2 r^2\, 2\pi r\, dr$$

An angular induction factor, a', is customarily defined as:

$$a' = \frac{\omega_2}{2\Omega}$$

or equivalently:

$$\omega_2 = 2\Omega a'$$

and

$$\omega_3 = 2\Omega a'\left(\frac{r}{r_3}\right)^2$$

(3.4.22)

by virtue of Eq. (3.4.17). The ½ is used in the definition of the angular induction factor a' since the angular velocity of the flow stream at the plane of the rotor (at the jump discontinuity), ω, the average value of the angular velocity just upwind and downwind of the rotor:

$$\omega = \frac{\omega_1 + \omega_2}{2}$$

(3.4.23)

or:

$$\omega = \frac{\omega_2}{2}$$

$$a' = \frac{\omega}{\Omega}$$

and

$$\omega = \Omega a'$$

(3.4.24)

The differential rotor thrust, *dT*, and differential rotor torque, *dQ*, can now be written in terms of the two induction factors, *a* and *a'*:

$$dT = \rho \Omega^2 r^2 4a'(1+a')\pi r\, dr$$

(3.4.25)

and

$$dQ = \rho V_0 \Omega r^2 4a'(1-a)\pi r\, dr$$

(3.4.26)

Equating the differential rotor thrust from Eq. (3.4.25) with Eq. (3.4.19), the two induction factors are related:

$$\frac{a(1-a)}{a'(1+a')} = \left(\frac{\Omega r}{V_0}\right)^2$$

(3.4.27)

The local speed ratio, λ_r, is defined as the square root of the right hand side of this equation:

$$\lambda_r = \frac{\Omega r}{V_0}$$

(3.4.28)

This variable is an expanded definition of the more commonly used tip speed ratio, defined as the dimensionless number corresponding to the blade tip speed, ΩR, divided by the velocity of the free stream wind speed, V_0:

$$\lambda = \frac{\Omega R}{V_0}$$

(3.4.29)

where *R* is the radius of the turbine blades.

Substituting the local speed ratio, λ_r, from Eq. (3.4.28) into Eq. (3.4.27), and solving for *a'*, the angular induction factor is written in terms of the axial induction factor and the local speed ratio:

$$a' = \frac{1}{2}\left(\sqrt{1+\frac{4}{\lambda_r^2}a(1-a)} - 1\right)$$

(3.4.30)

As *a* increases from zero, the magnitude of *a'* (and thus the magnitude of the angular speed of the wake accordingly) also increases. The magnitude of this increase is limited

by the local speed ratio. The faster the blade spins relative to a given free stream wind speed, the smaller the angular induction factor and angular speed of the wake.
Following a procedure similar to that used when finding Betz limit in section 3.2, the equations developed thus far can be used to modify the theoretical maximum power coefficient for an idealized rotor, C_{Pmax}, accounting for wake rotation. The results of this analysis are presented graphically in Fig. 3.4:

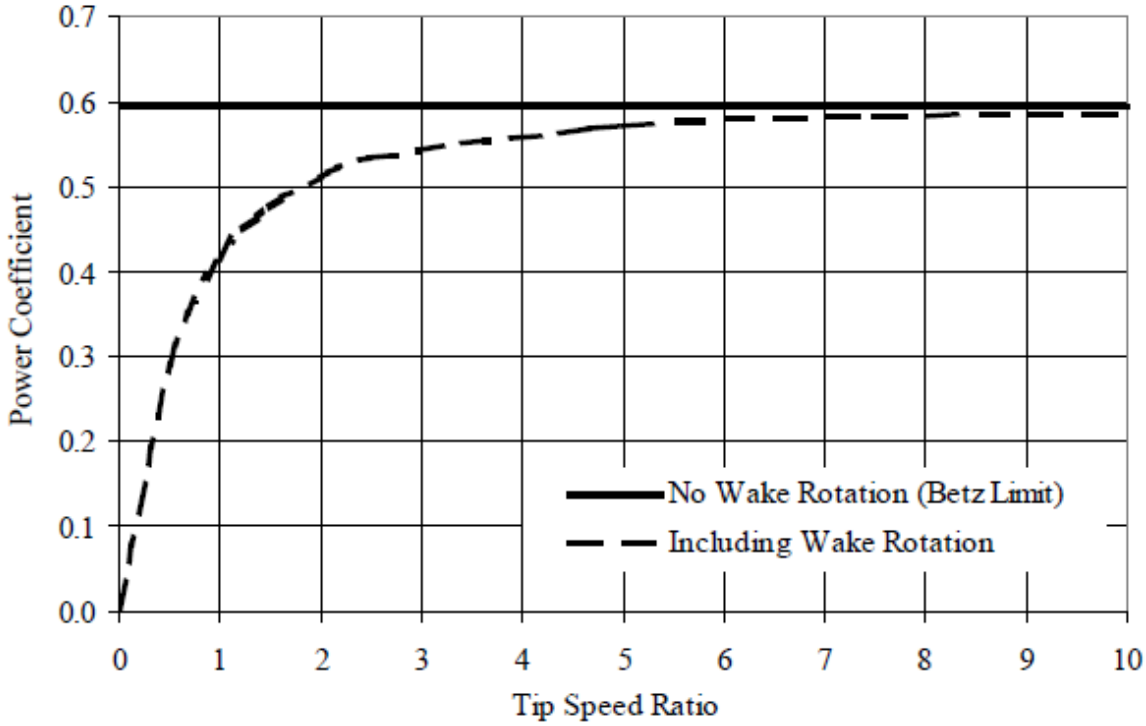

Figure 3.4: Theoretical maximum power coefficient

Strip theory

Solidity affects

Grit affects on airfoil performance

Stalling and furling

Stalling works by increasing the angle at which the relative wind strikes the blades (angle of attack), and it reduces the induced drag (drag associated with lift). Stalling is simple because it can be made to happen passively (it increases automatically when the winds speed up), but it increases the cross-section of the blade face-on to the wind, and thus the ordinary drag. A fully stalled turbine blade, when stopped, has the flat side of the blade facing directly into the wind. Furling works by decreasing the angle of attack, which reduces the induced drag from the lift of the rotor, as well as the cross-section. One major problem in designing wind turbines is getting the blades to stall or furl quickly enough should a gust of wind cause sudden acceleration. A fully furled turbine blade, when stopped, has the edge of the blade facing into the wind.

A fixed-speed HAWT inherently increases its angle of attack at higher wind speed as the blades speed up. A natural strategy, then, is to allow the blade to stall when the wind speed increases. This technique was used on many early HAWTs, until it was realized that stalled blades generate a large amount of vibration (noise). Standard modern turbines all furl the blades in high winds. Since furling requires acting against the torque on the blade, it requires active pitch angle control which is only cost-effective on very large turbines. Many turbines use hydraulic systems. These systems are usually spring loaded, so that if hydraulic power fails, the blades automatically furl. Other turbines use an electric servomotor for every rotor blade. They have a small battery-reserve in case of an electric-grid breakdown.

The variable wind speed wind turbine uses furling as its main method of rotation control. The wind turbines have three modes of operation

- Below rated wind speed operation
- Around rated wind speed operation
- Above rated wind speed operation

At above rated wind speed the rotors furl at an angle to maintain the torque. This is also known as feathering

Tip speed ratio

The ratio between the speed of the wind and the speed of the tips of the blades of a wind turbine is known as tip speed ratio. High efficiency 3-blade-turbines have design tip speed ratios of 6-7. Modern wind turbines are designed to spin at varying speeds (a consequence of their generator design, see below). Use of aluminum and composites in their blades has contributed to low rotational inertia, which means that newer wind turbines can accelerate quickly if the winds pick up, keeping the tip speed ratio more nearly constant. Operating closer to their optimal tip speed ratio during energetic gusts of wind allows wind turbines to improve energy capture from sudden gusts that are typical in urban settings.

In contrast, older style wind turbines were designed with heavier steel blades, which have higher inertia, and rotated at speeds governed by the AC frequency of the power lines. The high inertia buffered the changes in rotation speed and thus made power output more stable. The speed and torque at which a wind turbine rotates must be controlled for several reasons:

- To optimize the aerodynamic efficiency of the rotor in light winds.
- To keep the generator within its speed and torque limits.

- To keep the rotor and hub within their centripetal force limits. The centripetal force from the spinning rotors increases as the square of the rotation speed, which makes this structure sensitive to over speed.
- To keep the rotor and tower within their strength limits. Because the power of the wind increases as the cube of the wind speed, turbines have to be built to survive much higher wind loads (such as gusts of wind) than those from which they can practically generate power. Since the blades generate more downwind force (and thus put far greater stress on the tower) when they are producing torque, most wind turbines have ways of reducing torque in high winds.
- To enable maintenance; because it is dangerous to have people working on a wind turbine while it is active, it is sometimes necessary to bring a turbine to a full stop.
- To reduce noise; As a rule of thumb, the noise from a wind turbine increases with the fifth power of the relative wind speed (as seen from the moving tip of the blades). In noise-sensitive environment, the tip speed can be limited to approximately 60 m/s.

Over speed control is exerted in two main ways: aerodynamic stalling or furling and mechanical braking. Furling is the preferred method of slowing wind turbines

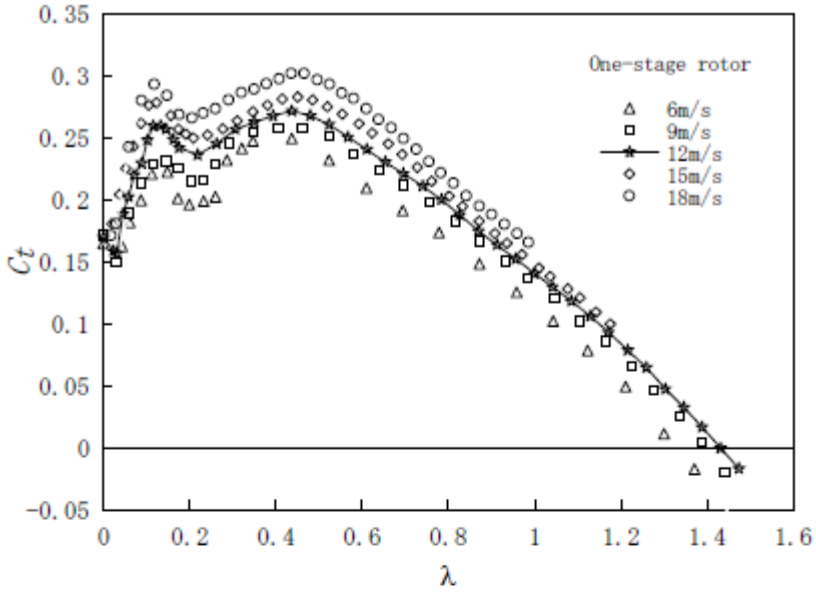

(a)

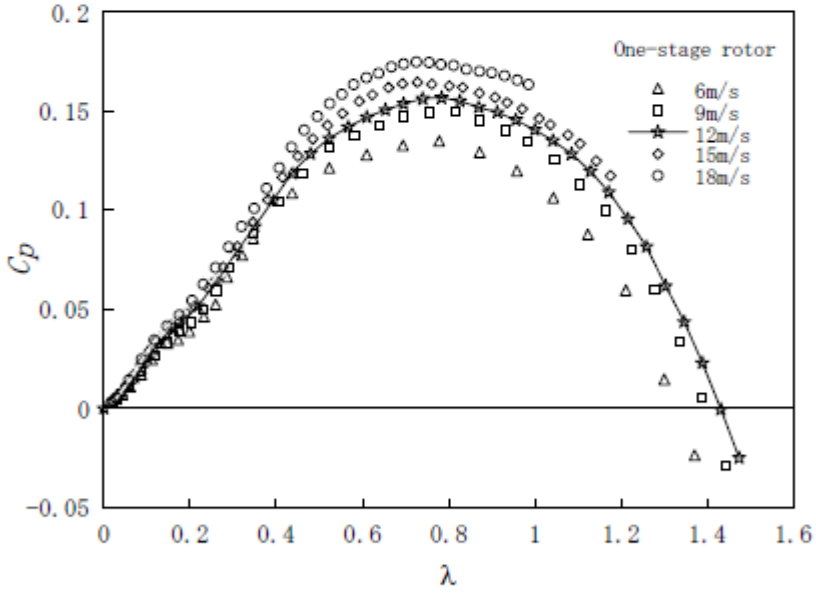

(b)

Figure 4. The torque and power characteristics of the one-stage rotor as a function of tip speed ratio: (a) torque coefficient, (b) power coefficient

Tsutomu HAYASHI[1], Yan LI[2], Yutaka HARA[3] and Katsuya SUZUKI[4]
[1] Department of Applied Mathematics and Physics, Faculty of Engineering, Tottori University, 4-101 Koyama-cho Minami,

The analysis carried out by Whitten (2002) must be viewed as preliminary for a number of reasons, including the fact that lift and drag data were not available for the symmetric blade profile used in practice. As a starting point Whitten used lift and drag data for the NACA0012H blade (Sheldahl and Klimas, 1981) and interpolated for both angle of attack and Reynolds number. Other limitations of his analysis include the fact that no tip losses were included.

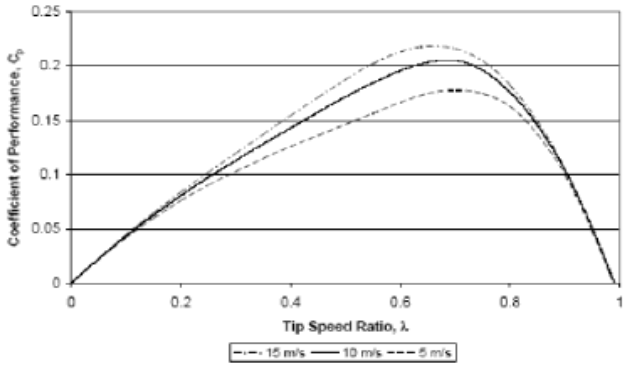

Figure 8. Performance of the Wollongong Turbine predicted for three wind speeds, assuming blade lift and drag data can be approximated by that for NACA0012H (Whitten, 2002).